Departamento de Ingeniería Química y Tecnologías del Medio Ambiente
Universidad Zaragoza

Instituto Universitario de Investigación de Ingeniería de Aragón
Universidad Zaragoza

HIGH PURITY HYDROGEN PRODUCTION FROM BIO-FUELS THROUGH 'STEAM-IRON' PROCESS

Dissertation presented by JORGE PLOU GÓMEZ for the Doctor degree in the University of Zaragoza.

Zaragoza, December 2015

D. Javier Herguido Huerta y D. José Ángel Peña Llorente

Professors at the University of Zaragoza in the Department of Chemical Engineering and Environmental Technologies and members of the Catalysis, Molecular Separations and Reactor Engineering Group (CREG) and the Aragon Institute of Engineering Research (I3A)

INFORM that:

This PhD thesis entitled:

"High purity hydrogen production from bio-fuels through 'steam iron' process"

has been developed by Mr. Jorge Plou Gómez under our supervision in the Department of Chemical Engineering and Environmental Technologies, and

AUTHORIZE

The presentation of this dissertation as papers compendium with international mention

In witness whereof, we sign this certificate in Zaragoza on December 16th, 2016

Prof. Dr. Javier Herguido Huerta

Prof. Dr. José Ángel Peña Llorente

OUTLINE

1 INTRODUCTION AND SCOPE

Nowadays, the socioeconomic state and environmental crisis have the same source of the problem: the fossil fuels. On one side, the dependence between the gross domestic product (GDP) and the oil is high due to the lack of fuel stock (Hernandez Martinez 2009). On the other side, the global warming is generated by the rise of greenhouse gases emissions (GHG). One viable solution to both problems could be the use of bio-fuels combined with hydrogen-fuel cell technology (HFC). Spain as a high agroforestry activity country offers great amount of biomass to be used as primary energy source and the hydrogen could be produced from this and other sources like solar and wind (Gómez et al. 2011).

In this work it is presented the production of high purity hydrogen through the "steam-iron" process (SIP) (Messerschmitt 1910; Hacker et al. 2000; Bleeker et al. 2007; Rydén and Arjmand 2012; Nestl et al. 2015; Sanz et al. 2015) using by-products of the biomass processing like the biogas and the bio-oil. 95% of the hydrogen produced in the US [web 1] comes from natural gas steam reforming because of the low price of the feedstock. Since it is a fossil fuel, it is preferred to avoid this kind of raw material, although it is a short-term solution waiting for a more economically attractive choice. In order to attain this goal, the hydrogen price should decrease up to 2-4 $/kg and avoid GHG emissions. At this time, the research is focused on renewables energies in a mid-log term, as it is written in the portfolio of United States Department of Energy (DOE) [web 1] and the European program Horizon 2020 [web 2].

Most of the emissions and the energy consumed are due to the industry and the transport (EIA 2013). In the first one, factories are concentrated in small areas and the gases are easily treated. But in transport, emissions are much more dispersed and the effort needed to diminish each one of them is complicated. The hydrogen and the fuel cells could help to diminish this effect being that the only product is clean water. It is necessary to promote the advancement of this technology by means of building up hydrogen filling stations. Moreover, the main sources should be renewables with a competitive price and adapted to local needs (Gómez et al. 2011; McDowall 2012). In the case of a city that generates a great amount of waste, the price

would only depend on the process of the biomass conversion. In addition, there is a second advantage of dumping site reduction.

Some of the biomass processes are gasification, combustion, torrefaction, pyrolysis or fermentative digestion (Bridgwater 2012). In the gasification a carbonaceous residue, liquid oils and mainly syngas are obtained for a subsequent use in the Fischer-Tropsch process (Tijmensen 2002; van Steen and Claeys 2008). The direct combustion generates heat but inefficiently due to the humidity of the biomass. In the torrefaction, an upgrading of the properties of the solid is made and the raw material is converted into pellets of higher heat capacity. It is similar to the traditional process of conversion of wood into charcoal. The pyrolysis consists of a high temperature process in inert atmosphere. Depending on the residence time and working temperature, it is possible to obtain an oil of high heat capacity as main product . This liquid is commonly referred to as bio-oil and is a complex mix of oxygenated hydrocarbons. The fermentative digestion of biomass produces compost and biogas (Berndes et al. 2003). This gas is a mix of methane and carbon dioxide with minor amounts of hydrogen, nitrogen, ammonia and hydrogen sulphide (Vane 2005).

In this work, the analysis of the behaviour of the SIP process for every compound of the bio-oil is presented and therefore the experiments are carried out from reactants of known composition. The synthetic biogas would be a mix of CH_4 and CO_2 with no other minority compounds. Especially hydrogen sulphide could be the most problematic because it causes deactivation of the catalysts in the decomposition reaction (Ashrafi et al. 2008). The bio-oil is a mix of a great number of species and some of the majoritarian compounds are selected as model of every fraction.

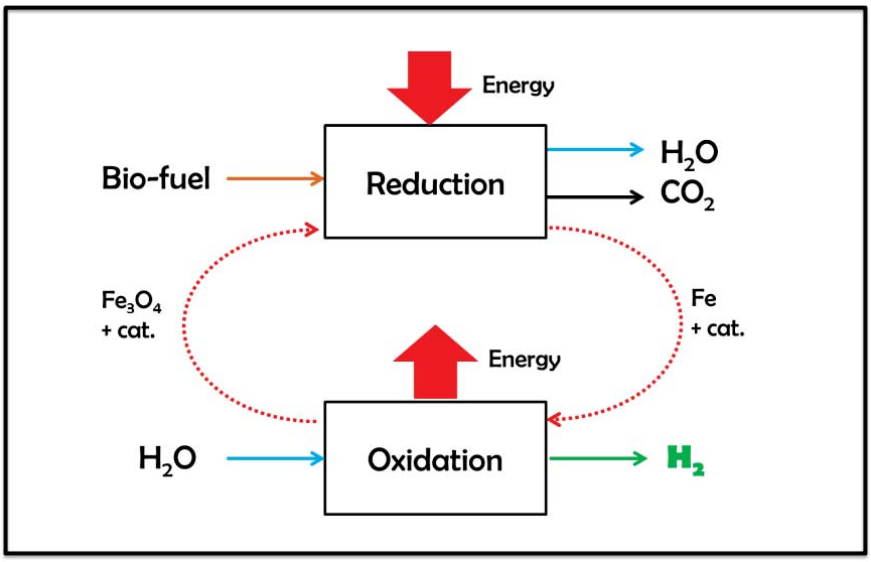

Figure 1.1 –SIP process scheme.

The SIP process is divided into two stages. Firstly, the reduction of the iron oxide into metallic iron by a gas stream, for example hydrogen, carbon monoxide or hydrocarbon able to reduce it. After obtaining metallic iron, the second stage is the oxidation, in which steam is fed into the reactor and hydrogen is produced. Moreover, the iron oxide is regenerated and the cycle begins from a slightly slower oxidation state of the iron. The unreacted water is easily condensed away from the pure hydrogen. Another concept related to the solid is that it works as an oxygen carrier between the water and the fuel. This technology is an intensification of the process of production and purification because both are carried out in the same vessel. The group of Catalysis, Molecular Separation and Reactors Engineering Group (CREG) has a wide knowledge in the processes of separation of methane/hydrogen streams coming from methane pyrolysis (Carazo 2008; Lorente 2008; Lorente et al. 2008, 2009; Herguido et al. 2014). This includes the study of reduction of iron oxides doped with low amounts of various metals. These works comprise the behaviour in different scales of reactor such as thermobalance, packed bed and Interconnected Circulating Fluidized Bed Reactor (ICFBR). Due to the optimization in nature and amount of the dopants, the redox solid has good properties: no loss of reactivity and resistance to thermal stress or sinterization. The solid composition is kept the same although the operating conditions in this work are more aggressive than the previously studied in the purification of methane and hydrogen streams.

Preliminary experiments with the doped iron oxide showed that it is not possible to reduce the solid by a sweetened biogas, so the scopes slightly

varied to use a mixture of solids instead of only iron oxide. The first scope was finding a mixture of catalyst and oxygen carrier able to be reduced by the biogas stream. In the **papers I and II** that comprise this thesis the experiments were focused on the catalyst and its elemental composition for the purpose of decomposing methane into hydrogen and carbon monoxide. Once the catalyst is able to do it, the iron oxide reduction is ensured. The ratio between methane and carbon monoxide was varied in the range described by bibliography and there is no hydrogen sulphide. The synthesis method of the catalyst and oxygen carrier was also tested and it was verified the suitability of a common synthesis or a mechanical mixture of the two solids. Apart from the exposed, the characterization of the carbonaceous residue is included.

There are two main hypotheses involving the use of hydrocarbons: the biofuel is fully decomposed in a mixture of gases according to reaction r 1.1 and the methane is the most stable specie in the operating conditions of this work. Consequently, the optimization of the catalyst using biogas (**papers I and II**) is extrapolated to any hydrocarbon, liquid or gas, used in this work.

$$Biofuel \rightarrow H_2 + H_2O + CO + CO_2 + CH_4 + C_{(s)} \qquad \text{(r 1.1)}$$

In the case of biogas, after obtaining the optimal mixture of oxygen carrier and catalyst, the scale up was increased and the behaviour of the reaction in packed bed was studied. The amount of sample increased from some milligrams to several grams. On this way, the solid reaction rate increases from a low conversion in the TGA to the highest possible conversion in the fixed bed. In the **paper III**, are shown the results at different temperatures and different composition. The scopes were to demonstrate the feasibility and to obtain the optimal operating conditions for the SIP process using biogas as feeding material. Three stages appeared in the reduction. In the case of other liquid compounds as reactants the behaviour was identical. This is due to the fact that the process is controlled by iron oxide reactions. Firstly, it starts from Fe_2O_3 and pass through Fe_3O_4 to finish in metallic iron. There exists a certain probability of FeO formation, but in all the experiments carried out there were no evidence of that. Every reaction is strongly governed by thermodynamic equilibriums and the composition is determined by these.

The liquid bio-fuel, bio-oil, is composed of a great number of oxygenated hydrocarbons. As model compounds that simulates the properties of a real bio-oil, it has been used methanol, ethanol, acetic acid, acetone and hydroxyacetone (or acetol). These are selected as representatives species of

the different fractions: alcoholic, acid and ketonic, the most abundant in a standard bio-oil (Oasmaa and Meier 2005; Bertero et al. 2012). Furthermore, in order to approximate the real behaviour of a real bio-oil, a mixture of three of them was prepared adding also water in some cases. The study was divided in three sections: iron oxide reaction without catalyst, complete mixture reduction by model compounds and complete mixture reduction by simulated bio-oils.

In order to reduce the iron oxide in absence of catalyst, it has been used methanol and ethanol. These are able to fully decompose without nickel catalyst. In these cases, the oxygen carrier is working as an active catalyst. The scopes of the **papers IV and V** were to analyse the behaviour of the reduction in absence of catalyst and identify the differences with other compounds. Some differences were found in the ability of the carbonaceous residue to appear as carbon fibres or amorphous coke.

The full mixture of oxygen carrier plus catalyst has been experimented with acetic acid, acetone and hydroxyacetone as reactants. **Congress communication I**, presents the results of the experiments with acetic acid. Among them there is some similarity in the functional groups and differences in the composition. Every one of them could be vaporized for feeding it at the reactor. In this study it is pretended to check out the existence of a common behaviour pattern in the equilibrium with any substance or any difference that depends on any characteristic of the model compound used.

Once the behaviour with every compound was known, it was necessary to study a mixture of some of them to observe if there is any crossed dependence between the reactants. Moreover, this is closer to the use of a pyrolytic oil. Mixtures of reactants have been synthesized in the range found in bibliography and the number of experiments optimised by means of a simple design of experiments (DOE). The selected species were methanol, acetic acid and hydroxyacetone as representatives of the alcoholic, acid and ketonic fractions. Moreover, the effect of water was studied because it is a major compound (the range is between 15% and 30% (Czernik and Bridgwater 2004; Oasmaa and Meier 2005)) and it could have a negative effect in the reduction of the iron oxide. The results of the experiments with the synthetic mixtures are shown in the **congress communication II**.

The work of this thesis is focused on the reduction stage because it is the limiting and characteristic step of the process. The oxidation has been extensively studied in previous works (Lorente et al. 2008).

After all the experiments carried out, the phenomena that govern the process were known and it made possible modelling the reactor. The kinetic model assumed was a shrinking core model (SCM) (Levenspiel 1999). The composition of the product stream coming from the methane dry reforming or liquid decomposition is different and it was necessary a high number of experiments to identify and quantify the reaction mechanisms. This problem was solved by the integral fitting of the data from the packed bed reactor. This is explained in the **papers VI**. Part of the algorithm written in Matlab® code was improved in a stay in the "Technische Universiteit" of Eindhoven (TUe). Moreover the validation of the code with external work was done with the data presented in the work of P. Hamers (Hamers et al. 2014). In the **congress communication III** is presented the improved code, the model validation and its use for the optimization of some variables of the process.

1.1 Scope

- Study of the catalyst in the mix of solids for the reduction stage of the SIP process with biofuels (biogas and vaporised bio-oil).
- Study of the behaviour of the optimal solid in the reduction with biogas in a packed bed.
- Study of the oxygen carrier behaviour in absence of catalyst for the reduction by alcohols.
- Study of the behaviour of the optimal mix of solids in the reduction with vapours of model compounds
- Modelling of the reactor in the reduction and oxidation and its dependency respecting to operating variables.

2 EXPERIMENTAL

The work of this thesis was carried out with two solids with different function in the process. One is the oxygen carrier based on iron oxide due to the SIP process. The other is the catalyst that favours the decomposition and reforming of the reactants. In this section are explained the properties and synthesis of each species. Moreover, the experimental setups are also detailed.

2.1 OXYGEN CARRIER: DOPED IRON OXIDE

The solid that promotes the oxygen flow between the steam and the fuel is the doped iron oxide. This is haematite, Fe_2O_3, with small amounts of dopants introduced in the synthesis. The optimised solid comes from previous works carried out in the CREG group related to the study of hydrogen storage (Lorente 2008) and separation of mixtures H_2/CH_4 (Carazo 2008; Durán 2016). It has been tested solids doped with chromium, cerium, aluminium, copper, nickel (Lorente 2008; Lorente et al. 2009), cobalt (Plou 2011) and molybdenum (Romero et al. 2012). The best results in the operating conditions of the separation of mixtures were obtained with aluminium and cerium (Escuer 2008).

The main source of reactivity loss along the cycles is specially the sinterization of the solid. This is produced over the surface above the Hüttig temperature ($0.3 \cdot T_{melting}$ (K)) and more aggressively at the Tamman temperature ($0.5 \cdot T_{melting}$ (K)) (Moulijn et al. 2001), correspondent to half the melting temperature measured in Kelvin. In the case of iron oxide, the Tamman temperature is equal to 640 °C. In order to diminish this effect, the most suitable solution is to add refractory elements to the structure of the solid. The alumina has a Tamman temperature around 900 °C, so is able to keep the micro-structure of the metallic crystal. Other advantages are the low cost and its structural properties. As disadvantages, the oxygen mobility is reduced and consequently, the reaction rate decreases. To enhance the kinetic properties, cerium is added because is a refractory element and it has been proved the benefits in the reactions in which oxygen is involved (Otsuka et al. 2003a, 2003b; Takenaka et al. 2004).

In the figure 2.1, a comparison between the fresh iron oxide and the doped iron oxide is represented. It can be observed that the optimised solid has no loss of reactivity along 7 cycles and the total conversion is reached in very short times. In the case of haematite, the solid loses its reactivity up to 25% of the initial conversion (Escuer 2008).

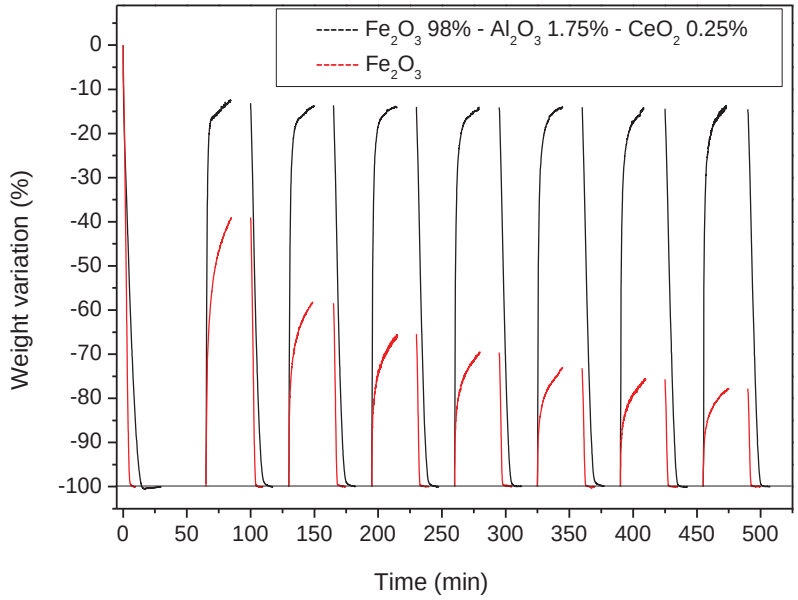

Figure 2.1 – 7 cycles of reduction with H_2 and oxidation with steam for the pure haematite and the doped iron oxide (Adapted from (Escuer 2008)). The lowest percentage corresponds to the maximum stoichiometric loss of mass.

The synthesis method is called gel-citrates and it has been found as the most repetitive and most suitable to obtain a homogeneous composition over the particle (Kirchnerova et al. 2002; Alifanti et al. 2003). In the first step, the citrate complex is prepared. Therefore, a 1M solution of the metal nitrates is made with iron ($Fe(NO_3)_3 \cdot 9H_2O$), aluminium ($Al(NO_3)_3 \cdot 9H_2O$) and cerium ($Ce(NO_3)_2 \cdot 6H_2O$) nitrates in the right proportions to obtain a final solid 98% Fe_2O_3, 1.75% Al_2O_3 and 0.25% CeO_2. Another solution with 1.1M citric acid is made and finally mixed in a vessel at 75 °C with continuous stirring. After part of the water is evaporated, the gel is formed. This liquid is disposed in flat crucibles and let in the oven at 60 °C overnight. Then it is calcined in a two ramp program: 3 °C/min up to 350 °C during 2 hours and then 3 °C/min up to 800 °C during 8 hours.

2.2 CATALYST: NICKEL ALUMINATE

Due to the oxygen carrier has no enough catalytic activity to decompose some of the reactants tested, it is mandatory to use a catalyst that favour the decomposition of hydrocarbons and reforming of the biogas. Because the biogas is the most stable species, it is used for the catalyst tests.

Previous to the nickel aluminate, bulk nickel oxide was synthesised by the same method as the oxygen carrier, gel-citrates. In the paper I, a preliminary work was carried out and the bulk NiO is not suitable for the process because the catalyst sinters with the iron oxide decreasing the reactivity of the mixture. At the same time, packed bed tests with this catalyst were done and it was found unfavourable results (Berenguer 2011).

In order to solve the sinterization problem, the research was focused on finding a catalyst that takes into account the reactions involved. In thermogravimetry analysis, the experiments were done with mixtures of methane and carbon dioxide, so the catalyst selected should be related to the dry reforming and by extension, to the steam reforming too. This is because the controlling step is the same: gradual dehydrogenation of the methane adsorbed (Verykios 2003; Fan et al. 2009). The most used catalyst is the nickel supported on alumina, but usually the deactivation is caused by solid reaction between γ-alumina and nickel forming nickel aluminate (Gayán et al. 2008). In order to avoid this problem, nickel over nickel aluminate is synthesized by co-precipitation according to the work of Al-Ubaid (Al-Ubaid and Wolf 1988). In the paper II, the active phase in the catalyst and the composition of the mixture oxygen carrier plus catalyst are optimised. One of the advantages of the catalyst in this process is that the previous activation is not necessary; it is carried out during the reaction in the very first moments.

The synthesis method is the co-precipitation at increasing pH (Al-Ubaid and Wolf 1988). The initial solution is a mixture of nickel nitrate and aluminium nitrate 1M and it is heated up to 45 °C in a heated bath. Then, a aqueous solution of ammonia (1:10 ammonia:water) is added dropwise under continuous stirring till a pH of 7.9 is reached. The precipitate has a turquoise colour and corresponds to nickel and aluminium hydroxide. This is washed three times with water, dried at 100 °C overnight and finally calcined at 900 °C during 3 hours with a previous ramp of 5 °C/min.

In the figure 2.2, it is represented the diffractogram of the solids that comprise the full mixture: doped iron oxide and nickel aluminate. In the spectrum of the iron oxide, the peaks are narrow so the crystallinity of the metal is high. In the bottom, the spectrum of the catalyst shows the nickel oxide from the excess in the synthesis.

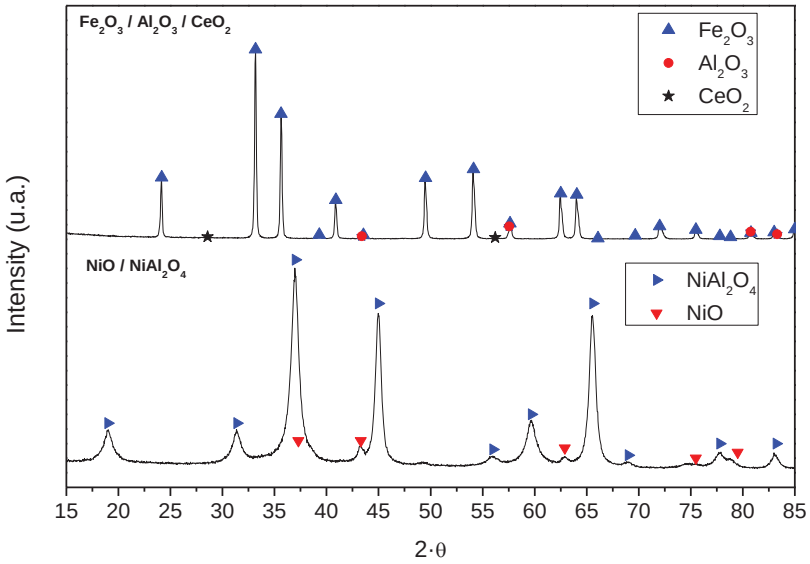

Figure 2.2 –XRD diffractogram of the doped iron oxide and the catalyst.

2.3 REACTANTS FED

In the case of feeding gases as reactants, it has been fed only methane and CO_2. For the calibration of the chromatograph, it has been used mixtures in concentrations controlled by the mass flows. The purity of the gases is of 99.5% as minimum.

The composition of the bio-oil depends on the raw material and the pyrolytic process carried out. Usually, the operating temperatures are in the range between 450 °C and 550 °C with short spatial times, around some seconds (Czernik and Bridgwater 2004; Mohan et al. 2006; Wang et al. 2013). Despite this fact, the composition and characteristics varies in a short interval (table 2.1).

Table 2.1 – Characteristics and properties of the bio-oil. (Adapted from (Czernik and Bridgwater 2004; Oasmaa and Meier 2005; Ingram et al. 2007)).

Properties (wet base)	Range
Water (% weight)	14 – 30
pH (-)	2.3 – 3.2
Realtive density (-)	1.19 – 1.22
High heat value (MJ/kg)	16.0 – 23.1
C (% weight)	45.5 – 62.6
H (%weight)	4.5 – 7.5
O (%weight)	29 – 48
N (%weight)	0 – 0.2
Ash (%weight)	0 – 0.2
Ketones (%weight)	17.6%
Acids (%weight)	9.8%
Alcohols (%weight)	4.3%
Sugars (%weight)	4.0%
Phenols (%weight)	2.3%

The model compounds used are majority components and representatives of different fractions of the bio-oil. They are based on the bibliography (Oasmaa and Meier 2005; Rioche et al. 2005; Bimbela 2009; Graça et al. 2009; Wu and Liu 2010; Xie et al. 2011; Bertero et al. 2012; Trane et al. 2012; Zhang et al. 2013; Leng et al. 2013; Remón et al. 2015). The most utilized are the acetic acid, hydroxyacetone, methanol, phenol, ethanol, acetone and some sugars, ordered by importance. In this work the sugars and the phenol was not tested because they are not able to be evaporated, essential condition in the experimental setups.

The experimentation with a pyrolytic oil in the available setups has the difficulty that when this is heated up, the components in the oil reacts between them producing a carbonaceous residue similar to the asphalt (Czernik and Bridgwater 2004; Bimbela 2009; Westerhof et al. 2011). This is solved in bigger reactors by feeding it directly inside the reactor with a spray (Bleeker et al. 2007).

Besides the use of model compounds individually, it has been studied simple mixtures similar in composition to a real bio-oil. A simple design of experiments was done in order to minimize the number of experiments and mixtures, obtaining a total of 4 mixtures (table 2.2). The composition is simplified into three fractions: acid, aldehidic and alcoholic. They are

represented by acetic acid, hydroxyacetone and methanol. In addition, water is added in an average mixture (M#4) with the purpose of analyse its effect. This is important because its concentration in a real bio-oil is high and the process changes from the decomposition of hydrocarbon to a steam reforming. Despite this, the catalyst selected is effective for both processes.

Table 2.2 – Summary of the mixtures selected.

Fraction	Acid	Aldehidic	Alcoholic	Total	
Conc. (%p)	15.1	13.4	5.4	33.9	
Majority	**Acetic acid**	**Hydroxycetone**	**Methanol**	**Water**	
Range	30-60	20-50	10-20	0-30	**Formula**
M#1	60	20	20	0	$C_{2.15}H_{4.52}O_{1.89}$
M#2	50	40	10	0	$C_{2.42}H_{4.94}O_{1.95}$
M#3	30	50	20	0	$C_{2.50}H_{5.21}O_{1.90}$
M#4	47.5	37.5	15	0	$C_{2.38}H_{4.91}O_{1.92}$
M#4+15	40.4	31.9	12,7	15	$C_{1.30}H_{3.66}O_{1.47}$
M#4+30	33.3	26.3	10,4	30	$C_{0.87}H_{3.10}O_{1.31}$

2.4 EXPERIMENTAL SETUPS

There are two types of experiments: thermogravimetry analysis in reactive atmosphere and packed bed reactions.

For the study and obtaining of the optimal mixture (oxygen carrier plus catalyst), the instrument used was a thermobalance (Neztsch® STA Jupiter 449 J3 Jupiter). The amount of sample is 20 mg and is assured that exists only kinetic control and not diffusional. Mainly, the reactants are methane and carbon dioxide for the reduction, and steam for the oxidation. The steam is fed by an evaporator coupled to the system supplied by Neztsch®. In some cases, the exhaust gases are analysed by a micro-GC (Agilent 490) in order to determine the gas conversion degree and a mass spectrometer (Pfeiffer, Omnistar Prisma model) to follow the temporal evolution of the gases with a high sampling frequency.

For the experiments in packed bed, the setup scheme is almost identical for the three setups used. There are three zones: the feeding zone, the reactor zone and the analysis zone. The feeding zone is composed of the cylinders and the mass flow controllers (Alicat or Brooks) for the gases and HPLC

pump (Water 515 or Shimadzu LC20AT) and evaporator (Topre®) for the liquids. The reaction zone is defined by the reactor and the oven. The reactor dimensions are kept in all the experiments. The ovens are common oven with electrical resistances (made by Tellsa) or one of them is configured to be used at very high temperatures (Nabertherm). The analysis systems are three: chromatograph CE instruments GC 8000, Chromatogrpah Agilent 7890A, micro-chromatogrpah Agilent 490 and mass spectrometer Omnistar Prima from Pffeiffer. In the case of the micro-GC, it is necessary to condense the steam of the stream in a Peltier module. In the figure 2.3 the general setup is presented.

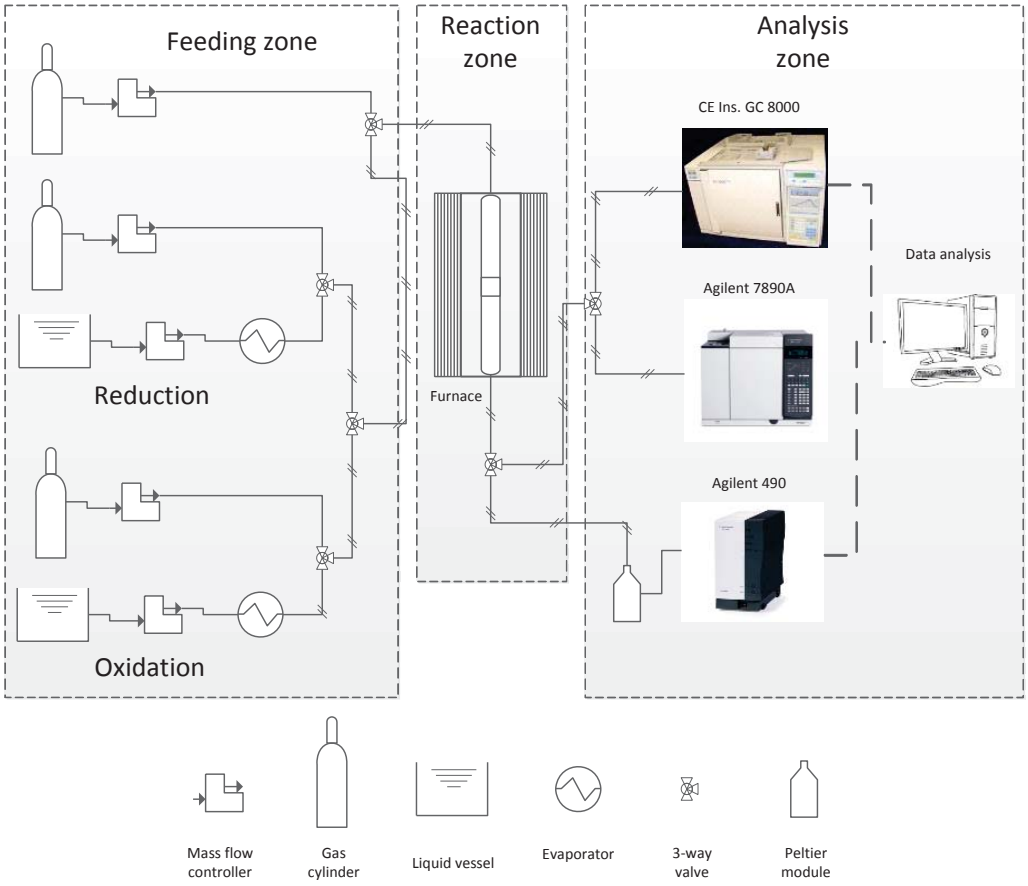

Figure 2.3 – Diagram of the lab setups.

2.4.1 Experimental conditions

The operating temperatures fluctuate between 600 °C and 850 °C. The range is suitable for the decomposition of the reactants and the reduction stage take place. These are determined by the thermogravimetry analysis. The

oxidation temperature is fixed in 500 °C due to the carbon is not gasified at this temperature (ΔG=0 above 675 °C) and favouring that the carbon monoxide is not produced (Herguido et al. 2014).

The gaseous reactants are exclusively methane and carbon dioxide. The concentration of the mixture is 25% of the total and the rest is inert gas (He, Ar or N_2). The concentration of the liquid reactants at the inlet stream is 10%, except the steam, that is 25%. With these concentrations are assured a stable feeding of the liquids.

The solid sample is composed by 67.5% of doped iron oxide, 7.5% of catalyst and 25% of chemically inert sand. Total weight is 2.5 grams. In the experiments with alcohols, the absolute amount of doped iron oxide was constant.

2.5 THERMODYNAMIC OF THE PROCESS

The reduction of the solid pass through three oxidation degrees: Fe_2O_3, Fe_3O_4 and Fe (r 2.1 and r 2.2). But in the oxidation, the iron is only able to pass to Fe_3O_4 (inverse r 2.2).

$$3Fe_2O_3 + H_2 / CO \rightarrow 2Fe_3O_4 + H_2O / CO_2 \quad \text{(r 2.1)}$$

$$Fe_3O_4 + 4H_2 / CO \leftrightarrow 3Fe + 4H_2O / CO_2 \quad \text{(r 2.2)}$$

The reactions that take place inside the reactor are very fast due to the operating conditions and the catalysts used. Therefore, the reaction extent is only restricted by the thermodynamic of the process. The most important reaction is the pass of magnetite (Fe_3O_4) to iron and vice versa because happen in the reduction and in the oxidation. Moreover, the reaction with carbon monoxide occurs at the same time.

The chemical thermodynamic dictates that if a reaction is in equilibrium, another reaction that contains one of its reactants or products is also in equilibrium between them. Extensively, a mixture of components in a phase should be in equilibrium and thus the Gibbs energy of the system is minimal.

Apart from the solid-gas reactions, the decomposition of the reactants into gases is carried out too. The products generated are H_2, H_2O, CO, CO_2, CH_4 y coke. These species are in equilibrium with the system and because the

reactions involved are numerous (dry reforming (r 2.3, methane decomposition (r 2.4), steam reforming (r 2.5), CO disproportionation (r 2.6) and water gas-shift (r 2.7)), it is necessary to calculate the final compositions by minimization of Gibbs energy. For that purpose, it has been used software (HSC®) and own code in Matlab®.

$$CH_4 + CO_2 \rightarrow 2H_2 + 2CO \quad \text{(r 2.3)}$$

$$CH_4 \rightarrow 2H_2 + C(s) \quad \text{(r 2.4)}$$

$$CH_4 + H_2O \rightarrow 3H_2 + CO \quad \text{(r 2.5)}$$

$$2CO \rightarrow CO_2 + C \quad \text{(r 2.6)}$$

$$CO + H_2O \rightarrow CO_2 + H_2 \quad \text{(r 2.7)}$$

The most restrictive reaction respect to the catalytic decomposition is that from the biogas. The dry reforming is spontaneous above 643 °C, so there is a minimum of operating temperature.

2.5.1 Baur-Glaessner diagram

In each reduction experiment, the composition of the 5 gases involved is obtained and their temporal evolution. Comparing the curves at different temperatures is complicated because of the high number of curves. The Baur-Glaessner (BG) diagram is able to reduce the number of curves to only one: hydrogen ratio or carbon monoxide ratio (Baur and Glaessner 1903). They are calculated as $[H_2]/([H_2]+[H_2O])$ or $[CO]/([CO]+[CO_2])$, respectively. In the figure 2.4, the theoretical lines of the different oxidation degrees are represented. Every zone corresponds to the stability conditions for every solid. For example, at high hydrogen ratios, the stable specie would be metallic iron. The wüstite (FeO) is only stable in specific concentrations and the temperature should be above 570 °C (Darken and Gurry 1945, 1946). The hydrogen ratio decreases and the CO ratio increases along the temperature. Because in the oxidation the hydrogen ratio is equal to the water conversion, the working temperature is low in order to achieve high conversion.

Moreover, in the figure 2.4, the dotted curve corresponds to the equilibrium of the gases in the methane dry reforming with the initial

composition equal to the thermogravimetry analysis. The gas-gas equilibrium curves changes according to the elemental composition of the hydrocarbon, the inert gas and the dilution gas.

In the section 3, it is explained how the transformation of the iron oxide into a different oxidation state is related to an specific composition of the exhaust gases and this is represented into the BG diagram.

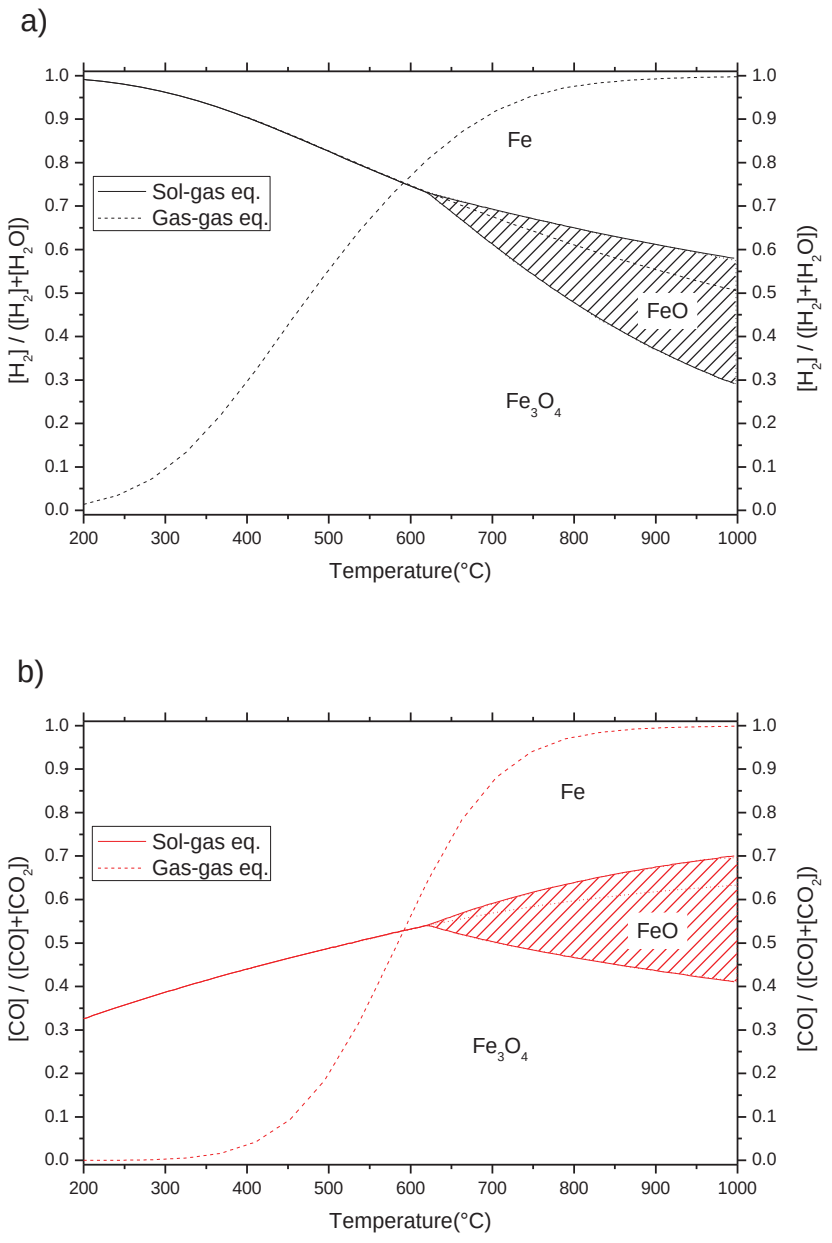

Figure 2.4 - Baur-Glaessner diagram. Top: hydrogen ratio. Bottom:carbon monoxide ratio

3 EXPERIMENTAL RESULTS

This chapter is divided into two parts: firstly the results obtained in thermogravimetry are explained and the best catalyst is selected as more suitable for the process. Then, the solid behaviour was observed when the gases or vapours pass through the mix of solid in the fixed bed reactor °.

3.1 THERMOGRAVIMETRY

At the beginning of the study, the samples tested were mixtures of doped iron oxide and nickel bulk as catalyst. The iron oxide has low amounts of ceria and alumina. This solid has been optimised according to the process of separation of hydrogen and methane at temperature around 500 °C (Escuer 2008). At this operating condition the methane acts as inert and does not react with the iron oxide. Therefore, in the SIP process, the hydrogen reacted in the reduction might appear in the oxidation step as product, free of methane. The work of E. Lorente (Lorente 2008) and P. Durán (Durán 2016) demonstrate the experimental validity in thermogravimetry and in packed bed.

The optimal amounts of dopants were determined in the work of M. Escuer (Escuer 2008) and the composition is 98%Fe_2O_3, 1.75%Al_2O_3 and 0.25%CeO_2. The goodness of the solid is presented in the figure 2.1 (experimental chapter). The reactivity does not decrease along the cycles of reduction with hydrogen and oxidation with steam at 450 °C. In the work of P. Durán (Durán 2016), the behaviour of the solid in packed bed is studied. In the reductions, there is a low solid conversion due to the equilibrium at 550 °C around 20%, but in the oxidation, the reaction is reversed and the conversion increases up to 80%. Moreover, over the cycles, it appears a loss of reactivity and consequently it is necessary longer reaction time to achieve full conversion. The main difference between thermogravimetry and packed bed experiments is the low extension of the conversion in the TG respect to the fixed bed.

Respect to the catalyst used in first place, bulk nickel oxide, the synthesis method is the same as the iron oxide, citrates-gel. So the common characteristic is that both act as oxygen carriers. Bulk catalyst is selected

because of the characteristics of carbon formation in big particles. In the work of t. Chen (Chen et al. 2005), the relation of carbon formation and nickel particles size is presented and high particle diameter could reduce the carbon produced. As the size is related to the diameter of the carbon nanofibers (CNF), there is a limit in which there is no production of them. Initially, this characteristic is supposed to favour the process and decrease the activity loss of the catalyst.

Nickel oxide has been reviewed as a good oxygen carrier in "Chemical Looping Combustion" technology in which the oxidation is made by air (Jerndal et al. 2006; Adanez et al. 2012). Thermodynamically, it is not possible to oxidize it with steam, so nickel oxide is constant among the cycles. In the same way iron oxide suffers sinterization, also nickel oxide lose part of its specific surface. In cases that it is used as catalyst over γ-alumina, it could produce nickel aluminate and lose active phase (Gayán et al. 2008).

The possibility of test a solid with iron and nickel synthesized together was also carried out creating nickel ferrite, $NiFe_2O_4$ (Plou 2011). The experiments demonstrated that the working temperature needs to be higher to achieve the same conversion as using it as a mechanical mixture. Probably, this is causing a lower mobility of the oxygen lattice and the absence of catalytic active phase for the reduction. In the work of M. A. Pans (Pans et al. 2013) is presented the same conclusion and they were forced to use the solids (oxygen carrier and catalyst) separately.

3.1.1 THERMOGRAVIMETRY WITH NICKEL OXIDE

The first series of experiments were carried out in ramp of temperature (β=5 °C/min) from ambient temperature up to 1000 °C with 12% (vol.) methane and 12% (vol.) carbon dioxide. In the figure 3.1 is shown the results of the behaviour of the iron oxide, nickel oxide, mechanical mix of both and chemical mixture. As mentioned, Fe_2O_3 is able to be reduced by methane at 550 °C, but Fe_3O_4 is not reduced by methane at the same temperature. Above 850 °C it is reduced up to wüstite ($Fe_{0.89}O$). The oxidation state is non-stoichiometric and varies from $Fe_{0.84}O$ to $Fe_{0.95}O$ (Redl et al. 2004). This reaction happens because the methane is cracked thermally and part of the hydrogen produced is the responsible of the reduction of the iron oxide.

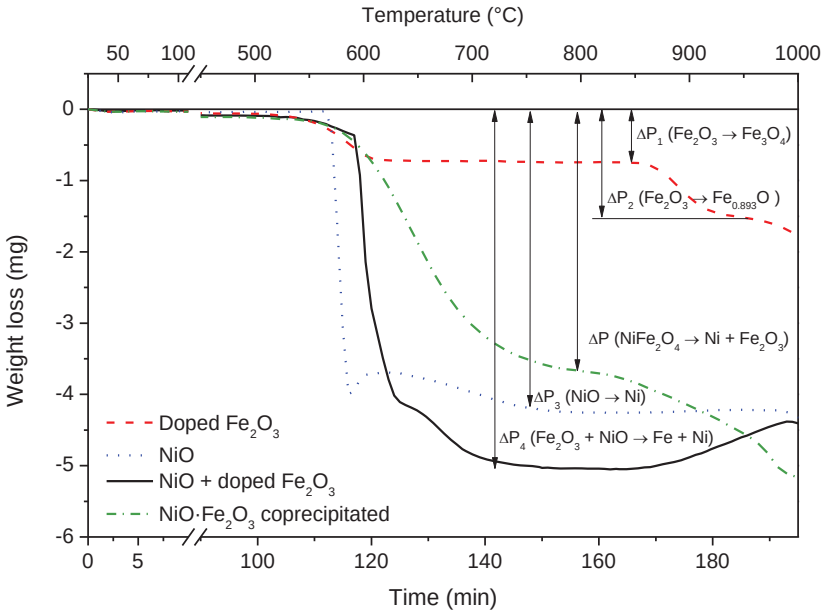

Figure 3.1 – Reduction in ramp of temperature of the solids, mechanical mixture and chemical mixture.

In the case of nickel oxide, the reaction begins at 560 °C and it loses mass till all the nickel phase appears and acts as catalyst. The methane starts to decompose and produce carbonaceous residue around the nickel particle increasing the weight. Finally, the surface is totally covered and the gasification begins, losing again weight till the temperature of 800 °C is reached. From this behaviour a conclusion comes out, the minimum working temperature is 700 °C in order to avoid high carbon deposition.

If both solids are in contact, the effect is not additive but competitive between them. Due to the reaction with the iron oxide begins before nickel oxide reaction, the temperature in which the methane is decomposed increases. After nickel oxide reduction, active phase appears and methane dry reforming starts and produces mainly hydrogen and carbon monoxide. These are able to reduce the Fe_3O_4 and just after nickel oxide is reduced the weight loss continues (there is a change in loss rate at -2mg). Before full conversion, there is a "shoulder" due to carbon deposition produced by the metallic nickel. This production-gasification behaviour lasts less time in the case of only nickel, so mixing both solids favours the fast disappearing of the carbon. Above 900 °C the weight increases because of the thermal decomposition of methane.

The chemically mixed solid needs higher temperature for its reduction than mechanical mix. Hence this solid is not selected and the mechanical mix

was studied at different temperatures in isothermal experiments. The temperature range was from 600 °C to 900 °C.

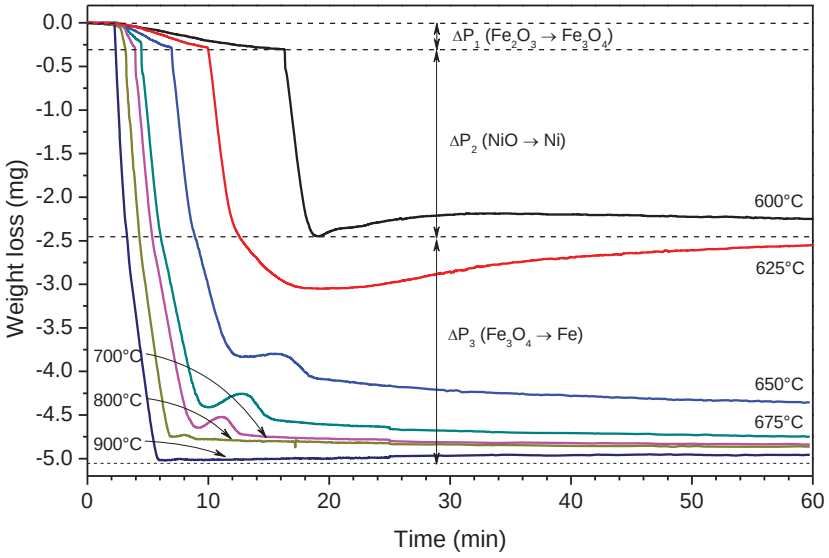

Figure 3.2 – Isothermal reduction of the mechanical mix of 50% NiO and 50% doped Fe_2O_3.

The figure 3.2 shows the results obtained of the mechanical mix of bulk nickel and iron oxide in isothermal conditions in TGA. In the transformation of Fe_2O_3 into Fe_3O_4, the duration decreases along the temperature. The next step is the nickel oxide reduction and reaction rate is similar in all of them. When the reaction rate is constant along the temperature, the reaction is controlled by the mass transfer in the particle. Then, the Fe_3O_4 is reduced to metallic iron but beside 650 °C there is no reaction. The point in which both gas-gas and solid-gas equilibriums cross is around 590 °C (figure 2.4), so the minimum working temperature is also observed experimentally. Just after the iron reduction, there is carbon deposition over the particle (increasing weight) and after some time it is gasified (loosing weight). This behaviour is repeated in all the cases and the amount of carbon deposited decreases at higher temperatures. This phenomenon is explained by a carbon deposition from the methane decomposition that saturates the surface of the particle and then the carbon dioxide is able to gasify it. The reason behind this peak is because the reaction rate of the methane decomposition changes along the time. The activity of the catalyst varies depending on the coke deposited over the surface of the particle. The reaction pathway is explained in bibliography (Verykios 2003; Fan et al. 2009).

$$CH_4 \rightarrow C + 2H_2 \qquad \text{(r 3.1)}$$

$$CO_2 + C \rightarrow 2CO \qquad \text{(r 3.2)}$$

This reaction mechanism is the same as the steam reforming (Wang 1999; Verykios 2003) (mr 3.1). First, the methane is adsorbed on the catalyst particles and the progressive dehydrogenation proceeds till producing carbon. Then, the carbon dioxide (or steam) is adsorbed in active centres near to the catalyst to generate carbon monoxide. The limiting step is the methane decomposition. The removal of carbon from the surface is also made by the solid reaction with the lattice oxygen apart from the gasification with carbon dioxide.

$$\begin{aligned} &CH_4 + Ni \rightarrow CH_4 - Ni \\ &CH_x - Ni + Ni \rightarrow CH_{x-1} - Ni + H - Ni \\ &CH - Ni + H - Ni \rightarrow C - Ni + Ni + H_2 \\ &C - Ni + CO_2 - Ni \rightarrow 2Ni + 2CO \end{aligned} \qquad \text{(mr 3.1)}$$

After reduction it is necessary oxidise the sample with steam to finish the cycle. The working temperature is fixed in 500 °C. At this condition, the water reacts with the iron letting unaltered the carbon deposited. The exhaust gases at the outlet stream of the TGA instrument were analysed by micro-GC and mass spectrometry and there is no evidence of carbon monoxide (detection limit equal to 20ppm). To summarize, using nickel oxide bulk and doped iron oxide is possible to produce hydrogen of high purity. The next step is convenient to verify the effect of the scaling up and the cycles in a packed reactor.

In the work of J. Berenguer (Berenguer 2011), the experiments in packed bed were carried out and above 700 °C the methane conversion was full in the first minutes and then decreased producing carbon over the particle that impede the reaction. Furthermore, the cleaning of the reactor showed that the solid increases de particle diameter because of the sinterization and consequently the reaction rate decreases drastically.

3.1.2 THERMOGRAVIMETRY WITH NICKEL ALUMINATE

It is found that the doped iron oxide worked properly but the catalyst was not suitable. Using same philosophy as the oxygen carrier, it is necessary to use species that increase the resistance to thermal stress. Alumina is one of the best choices and in the work of Al-Ubaid (Al-Ubaid and Wolf 1988) is presented the goodness of the nickel aluminate in the process of methane steam reforming. The synthesis used is the traditional coprecipitation and the amount of nickel is more than the stoichiometric ratio to assure the appearance of nickel as active phase. Unless nickel is in excess, it is not catalytically active because the nickel remains embedded in the aluminate. The synthesis gives us a catalyst with high dispersion and high specific surface area. Due to the high amount of alumina, it is very stable at high temperatures and it was already tested in some works as appropriate for the decomposition of bio-oil and reforming of biogas (Galdámez et al. 2005; Vagia and Lemonidou 2008; Bimbela 2009).

Once is selected a suitable catalyst, it was necessary to find the optimal operating conditions according to the amounts and proportions of oxygen carrier and catalyst. The aim is maximizing the hydrogen production with maximum methane conversion.

Firstly, the catalyst composition is optimised keeping the total amount in the mechanical mix with the value of 15%. This percentage was obtained from previous works with the bulk catalyst (Campos 2011). The excess nickel amounts tested are from 0% (stoichiometric ratio) to 40%. The TGA experiments were done in ramp of temperature from ambient to 900 °C at a rate of 5 °C/min. The gas composition is 12% CH_4, 12% CO_2 and the rest inert.

In the figure 3.3 the behaviour of the 4 catalyst tested are shown. The measure is indirect because the main variable studied is the weight loss of the iron oxide. The stoichiometric nickel aluminate (C0) has no activity in the methane dry reforming so it works as a mere support with no active phase. To confirm this hypothesis, it can be seen that the curve is identical to that in the figure 3.1 with only iron oxide. The curves identified as C10 and C20 are similar and in both there is catalytic activity. Around 510 °C starts the reduction from Fe_2O_3 and possibly nickel oxide too. Because of the amount of NiO in the sample is too low (1.5% w.), it is not possible to confirm it. Then, at 600 °C the Fe_3O_4 is reduced till 700 °C is reached with no carbon deposition. In the case of C40, the sample loses weight at 510 °C but in the second

reduction up to iron, it stops because of the carbon production. As there is more active phase, the carbon nanofibers or amorphous coke is proportional to this amount. Then the carbon is eliminated at 750 °C. Finally, the catalyst selected is C10. From now on, when the term **catalyst** is used, it is referred as the proportion **10%NiO/$NiAl_2O_4$**.

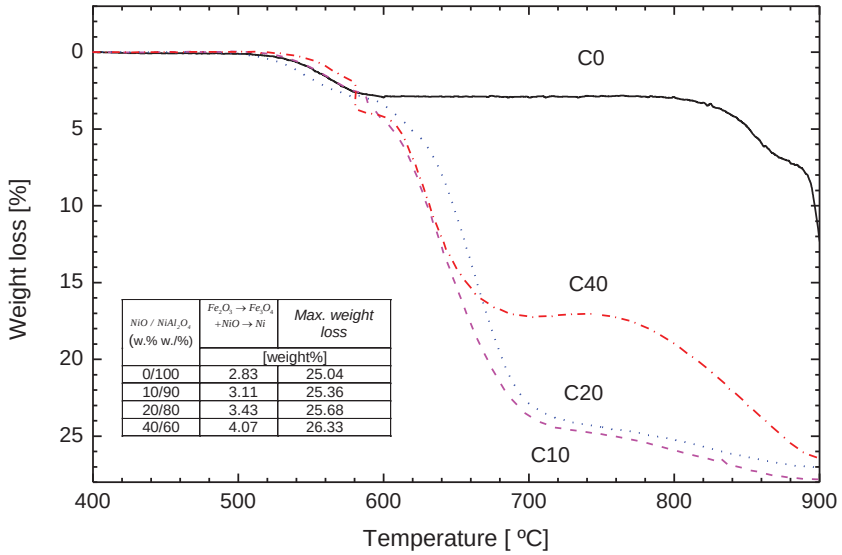

Figure 3.3 – Reduction in ramp of temperature of mixture of nickel aluminate and doped iron oxide changing the nickel oxide load.

The next step was the optimization of the ratio oxygen carrier vs catalyst. The range was between 10% and 50% of catalyst and the results are presented in the figure 3.4. As reference, the solid without catalyst is shown. In the curve associated to the highest amount of catalyst, the carbon formation is too high and then is gasified at 750 °C, quite similar as the C40 of the previous figure. The curve labelled as 70o/30c is similar but the carbon generation is lower. The decreasing in the weight loss agrees with the last curve and begins at 750 °C. In the cases in which the amount of catalyst is the lowest, the reduction duration is similar with some temperature displacement. The cause is that the hydrogen generated is not high enough for the reduction of iron oxide. Consequently, the 85o/15c mixture is selected as optimal for the production of hydrogen and carbon monoxide for the reduction of the doped iron oxide. From now, in the cases in which there is the mixture of catalyst and oxygen carrier, the term solid is referred as this mixture, **85o/15c**.

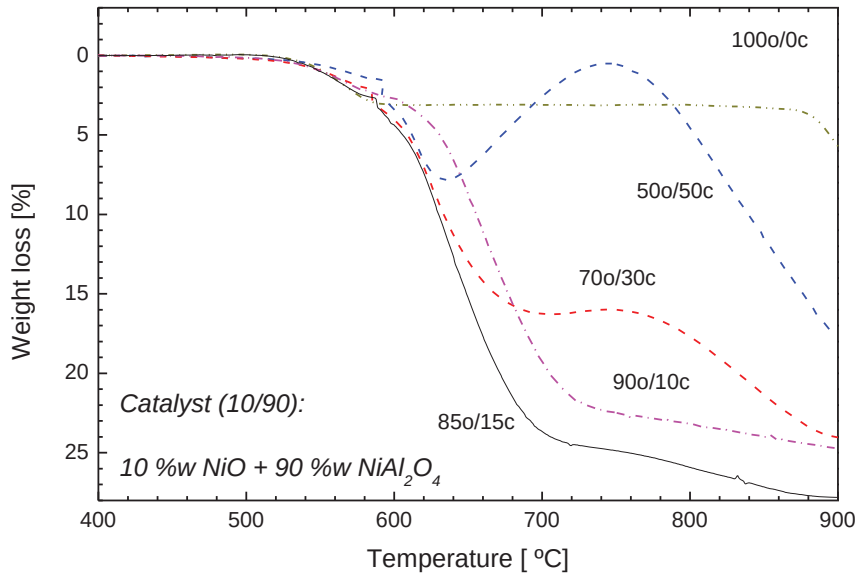

Figure 3.4 – Reduction in ramp of temperatura of the optimal mix with different oxygen carrier/catalyst ratio.

After dynamic experiments, the behaviour during cycles at isothermal conditions was tested. The number of cycles are 4, the temperature in the reduction is 700 °C and in the oxidation 500 °C. The results are shown in the figure 3.5. The reductions are fast and in less than 5 minutes all the solid is converted. After this, there is a linear grow corresponding to a carbon formation. This type of linear grow corresponds to reaction controlled by diffusion (Chen et al. 2005). The carbon deposition rate is identified as the slope in the figure and it decreases along the cycles. The particle is having more carbon over the surface of the particle and the activity is decreasing slowly because of active sites blockage. Despite this, the activity is high enough for the methane dry reforming. The hypothesis of iron as a catalyst is not possible because the range of working temperature is higher than 800 °C (Fan et al. 2009), so all the catalytic activity is related to the nickel.

In the oxidation, a weight gaining is observed and this is decreased along the cycles. The main source of this loss is the sinterization generated by thermal stress of the solid. This cause a continuous collapse of the micro-structure and a loss of specific surface area (Bleeker et al. 2009).

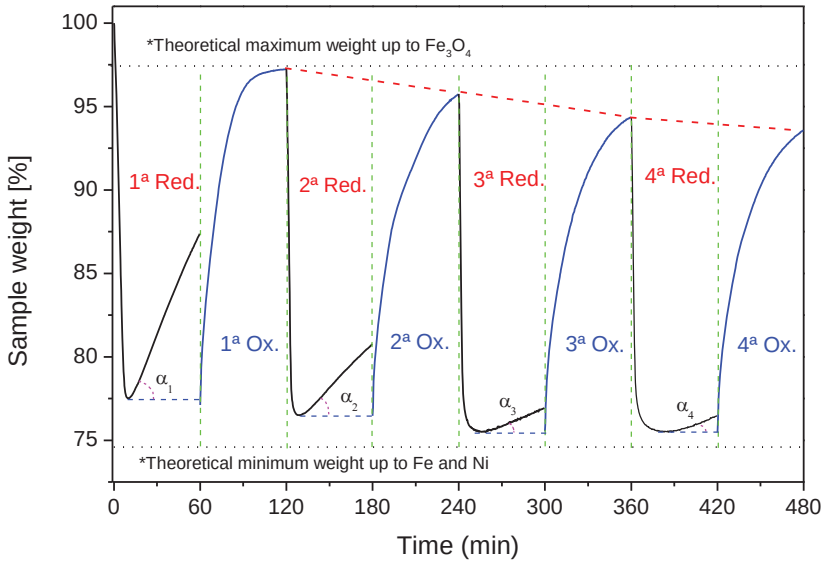

Figure 3.5 – Temporal evolution of the simple weight along 4 cycles of reduction at 700 °C and oxidation at 500 °C. (Coke weight is omitted)

In the reductions at different temperatures from 650 °C to 800 °C (figure 3.6a), it is possible to identify how the reduction rate increases and the carbon production decrees along the temperature. At 650 °C, the solid is not able to loss all the oxygen and the rate is too low compared to the reduction time at 800 °C. But in the oxidation, the effect is the opposite and at higher reduction temperatures, the rate decreases. As all of the oxidations were carried out at the same conditions, the responsible of the reactivity loss is the thermal stress suffered in the reductions. It is supposed that the macro and microstructure has changed in some way because of the sinterization.

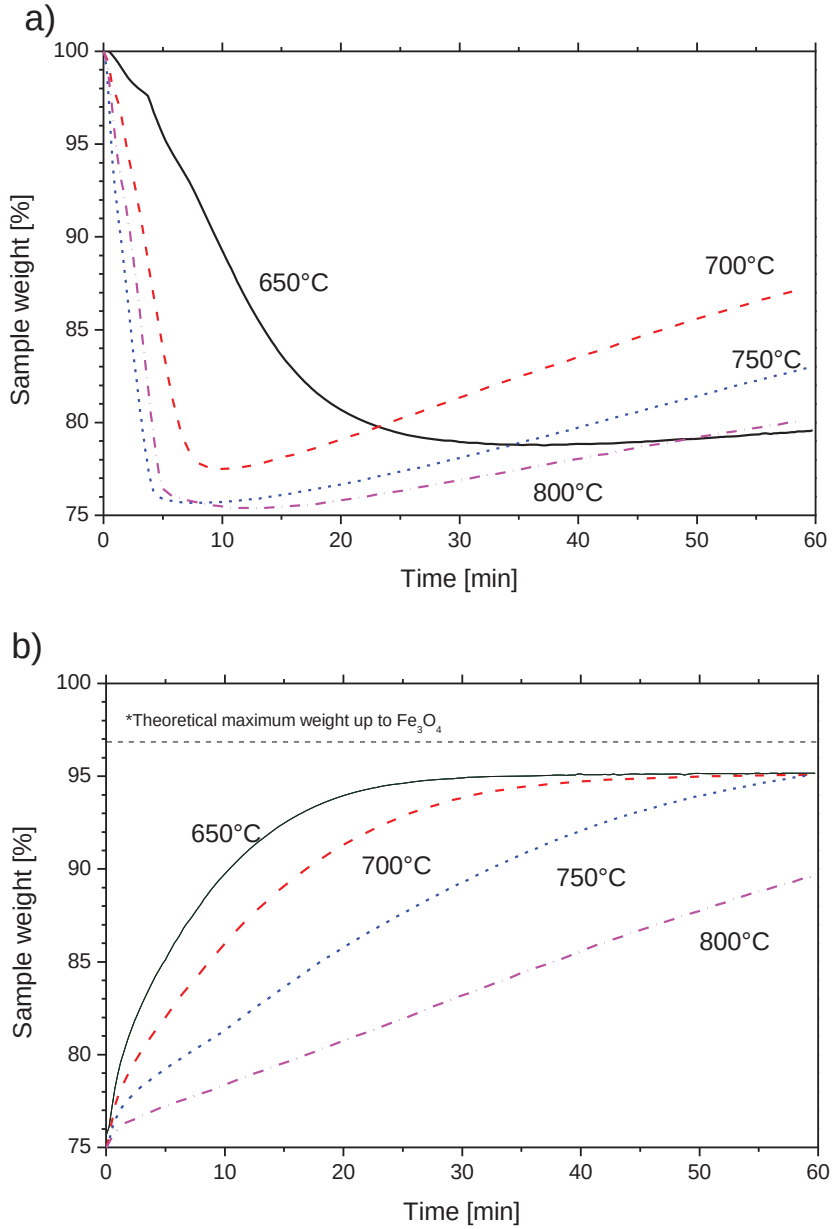

Figure 3.6 – Reductions at different temperatures (a) and oxidations at 500 °C (b) with the optimal solid in isothermal conditions.

During inertization between steps, set temperature increases from 500 °C to reduction temperature. After oxidation there is the possibility of solid reaction between carbon depositions and the lattice oxygen above 750 °C. Usually in other works, they have operated at constant temperature in reduction and oxidation (Hacker et al. 2000; Adanez et al. 2012; Thaler and Hacker 2012), but in this manner, part of the efficiency is lost. At lower temperatures the steam conversion is higher and the demanded energy is lower.

It has been analysed the solid after a reduction in order to favour the deposition of carbon. The aim is to verify where the decomposition is and according to figure 3.7, the carbon is found over the nickel particles. The iron oxide particles are identified by an outer layer of Fe_2O_3 that comes from reaction with ambient. Nickel particles do not present peaks in the Raman spectroscopy. Despite this finding in the iron particle, it is not likely a solid reaction of the carbon at ambient conditions.

The spectrum of the carbonaceous residue shows two characteristics bands: D band (1350 cm^{-1}) that is related to the defects of the carbon and a G band (1580cm^{-1}) that is correlated with the degree of graphitization. According to the figure 3.7, the degree of disorder is high and the amount of amorphous carbon is high.

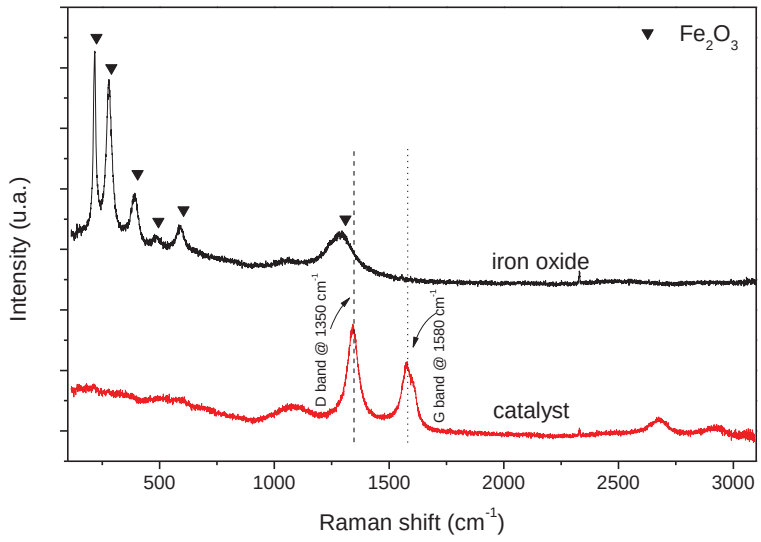

Figure 3.7 – Raman spectra of the optimal mixture after 4 cycles in the reduction at 700 °C and 500 °C in the oxidation

3.1.3 Overview of the thermogravimetry results

To summarize the chapter related to the TGA experiments, it could assures that:

- The NiO bulk catalyst does not fulfil the necessary characteristics for the SIP process due to a high carbon deposition and consequently a encapsulation of the particles, causing a loss of activity.
- The nickel aluminate catalyst obtained with 10% excess of NiO phase is the most suitable for the process of methane dry reforming. It is able to produce hydrogen and carbon monoxide for the iron oxide reduction.
- The carbon deposited over the particle has the preferential path in the nickel surface due to the decomposition of the methane over it.
- There is a middle point between a low reduction temperature that assures high conversion of the metallic iron but high carbon deposition and a high reduction temperature in which the reaction rate in the reduction is high but the oxidation is greatly affected by the thermal stress suffered.

3.2 PACKED BED EXPERIMENTS

After finding the best operating conditions and the solid most suitable for the process SIP, the next step was the scaling up in a lab-scale packed bed. In this section the behaviour with different reactants is explained.

The first reactant was a synthetic biogas that corresponds to a sweetened biogas with the full solid mixture. Then, the alcoholic fraction represented by methanol and ethanol with the doped iron oxide. After this, the full mixture with different model compounds. Finally, a liquid mixture similar to a bio-oil was tested.

3.2.1 SYNTHETIC BIOGAS

The biogas comes from the anaerobic fermentation of waste and its composition is mainly a mixture of methane and carbon dioxide. It has some traces of hydrogen sulphide, nitrogen and hydrogen. Methane varies from 50 to 70 % and the rest is CO_2. In the TGA experiments, the methane acted as inert when there is no catalyst, so the full solid is used with biogas as reactant.

In the setup used, the exhaust gases were analysed by the chromatograph CE Instruments 8000. The sampling frequency is 20 minutes, so it was necessary to enhance the analysis with a mass spectrometer. Both instruments work in parallel and the mass signal is quantified by the chromatograph. By this method, it is possible to obtain a real time signal of the gases evolution. It is necessary to measure the concentration with the chromatograph because the mass signal varies overnight (Turner et al. 2004). The feeding zone and the reactor zone are common to other setups and it is explained in the previous chapter.

The experiments without catalyst are not shown because there is no reaction. The three stages of the reduction appear through the different oxidation states of the iron: hematite, magnetite and metallic iron. The temperatures tested were from 600 °C to 750 °C. The methane and carbon dioxide conversion with the molar flow of hydrogen and water are presented in the figure 3.8. At the lowest temperature, the methane conversion has an induction time. The catalyst is not in its active phase because the solid reaction between methane and nickel oxide is slow (r 3.3) (Tokuda et al. 1973;

Piotrowski et al. 2005). Moreover, there is Fe_2O_3 that competes (r 3.4) for the methane consumption.

$$4\,NiO + CH_4 \rightarrow 4\,Ni + CO_2 + 2\,H_2O \qquad \text{(r 3.3)}$$

$$4/3\,Fe_2O_3 + CH_4 \rightarrow 8/3\,Fe + CO_2 + 2\,H_2O \qquad \text{(r 3.4)}$$

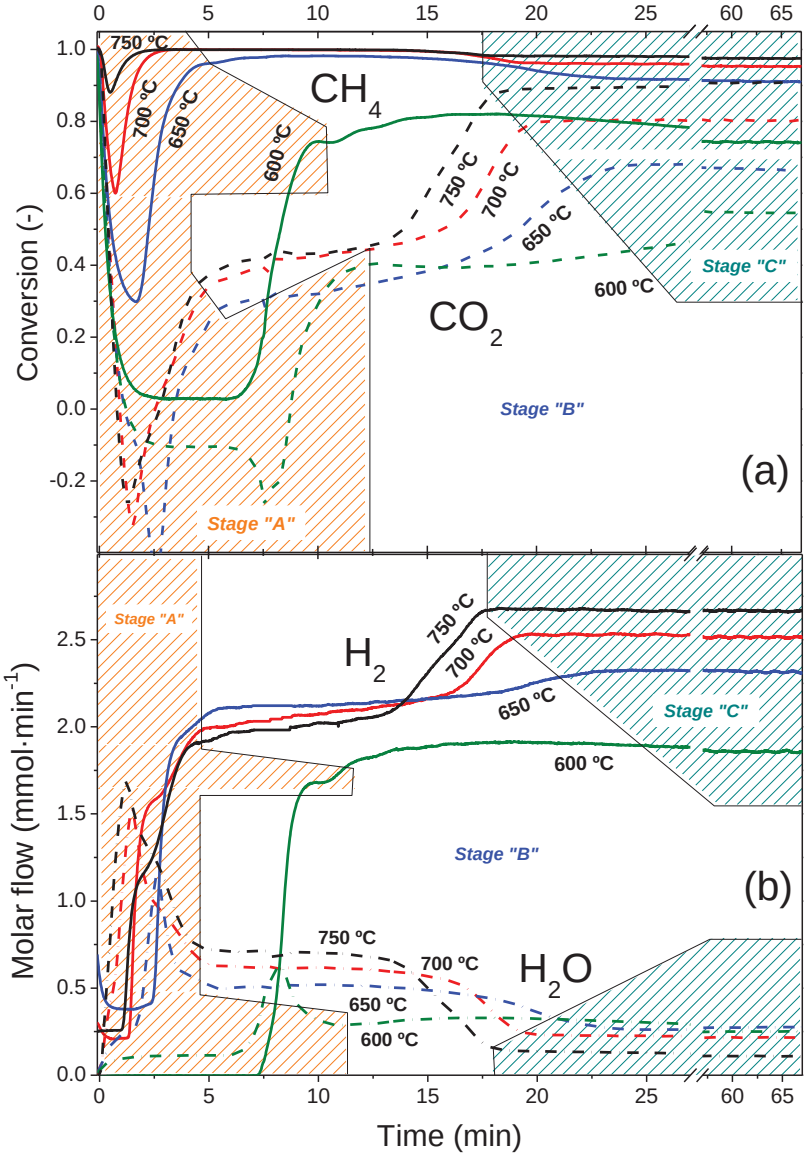

Figure 3.8 – Reactant conversion (a) and molar flow of H_2 and H_2O (b) in the reductions with biogas at different temperatures

Above 650 °C, the activation is almost immediate and the methane conversion increases till almost the maximum. The production of hydrogen and carbon monoxide increases and consequently Fe_2O_3 is reduced. Then, in

the stage B, Fe_3O_4 begins to react with the gas. As it was expected, at high temperatures the reduction times decrease. At 750 °C the duration is 17 minutes while at 650 °C is 23 minutes. In the last stage (stage C), the composition is principally the methane dry reforming and corresponds in almost every case to the gas-gas equilibrium. At lower temperatures it is not reached but is not important because the best conditions are found at higher temperatures in which there is equilibrium.

The equilibrium points are represented in the BG diagram (figure 3.9). At lower temperatures, they are separated slightly from the theoretical equilibrium because the catalyst is not active enough. Above these temperatures, the points agree well with the theoretical curve in the gas-gas equilibrium. In the case of the points related to the solid-gas equilibrium, the points are separated almost a constant gap from the theoretical (represented as a band in the figure 3.9). This is due to the diffusional restrictions of the gases to pass through the iron oxide layers of the particle.

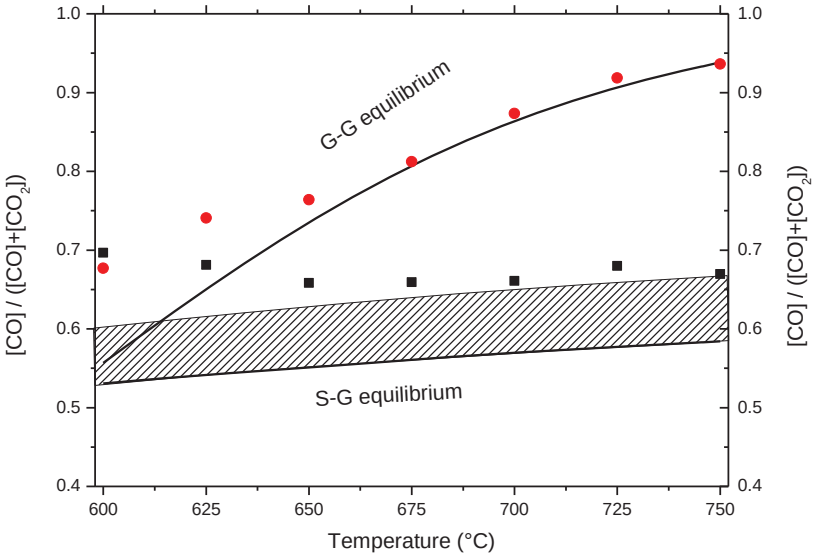

Figure 3.9 –BG diagram with the results of biogas in the reduction.

The variable tested in the next experiments was the composition in the gas stream (figure 3.10). The reaction time decreases because the methane is able to produce more moles of reductants ($2H_2$ + C(s)) than the carbon dioxide. Unfortunately, the carbon deposition increases. In the stage A, there is no difference between them because of the velocity of the reaction. Then, in the stage B, the time varies but the shape of the curve are very similar. Finally in the stage C, every composition has its own gas-gas equilibrium.

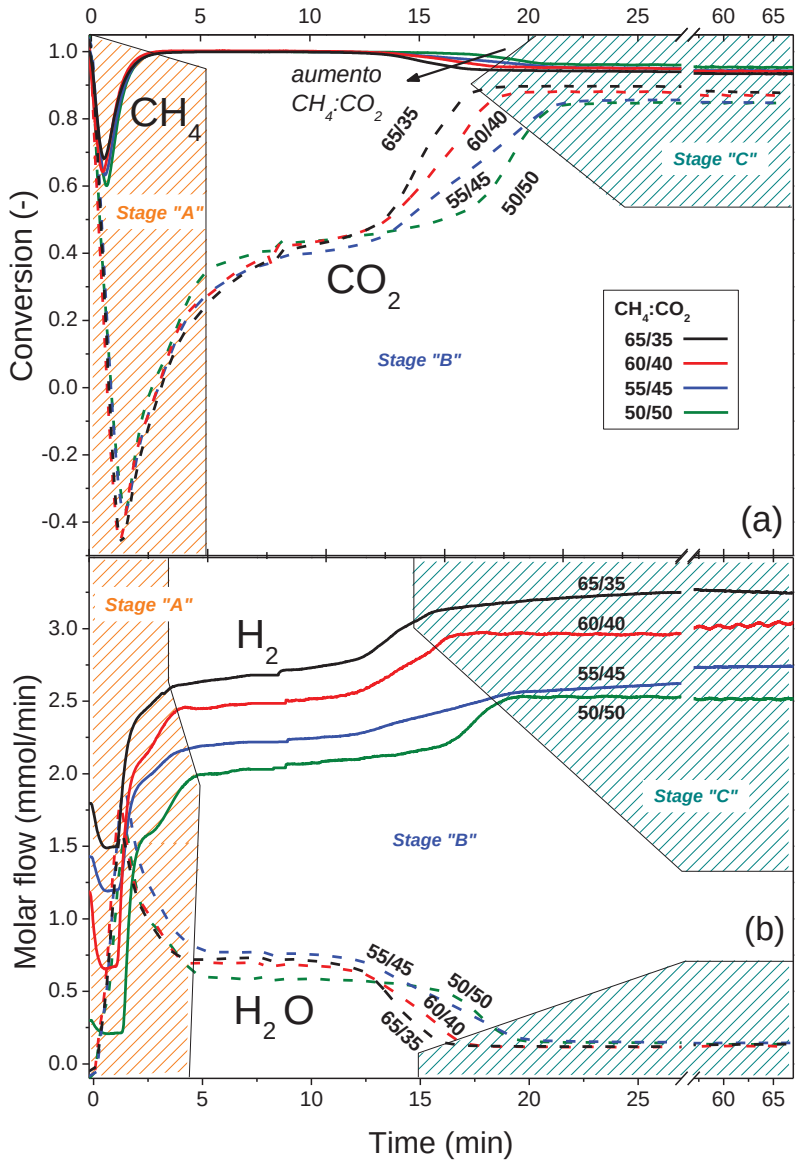

Figure 3.10 – Reactants conversion (a) and molar flow of H_2 and H_2O (b) in the reductions with biogas at different feed compositions.

During the temporal evolution along the cycles (figure 3.11), there is a significant loss of reactivity due to the sinterization. After the first cycle, the methane conversion is maximum because the nickel is not oxidised in the previous oxidation. In the CO_2 conversion at the first cycle, the value passes through 0% because there is more production from the methane combustion with the Fe_2O_3. After the first cycle, the reduction starts from Fe_3O_4 and the conversion is equal to 45%, equivalent to the equilibrium conversion between species.

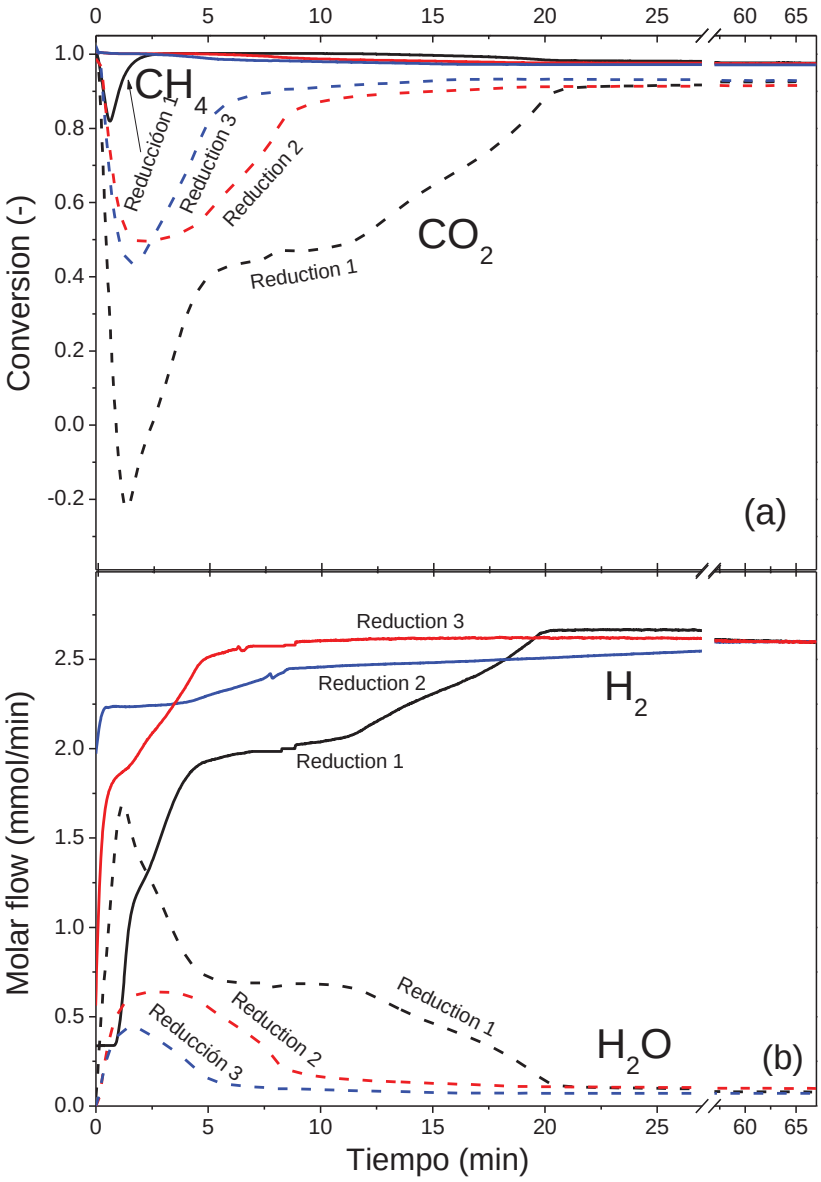

Figure 3.11 – Reactants conversion (a) and molar flows (H_2 and H_2O) (b) in the reductions with biogas along the cycles at 750 °C.

Respect to the oxidation, an example is shown in the figure 3.12. Due to the oxidation is not the controlling step of the process, there is no emphasis in this reaction. The CO_2 and CO concentrations are assured below the detection limits of the instrument ([CO_2] <0.28% y [CO] < 0.21%). So the purity of the hydrogen is high but is not known if it is suitable for a fuel cell because the poisoning limit is around 20 ppm of CO.

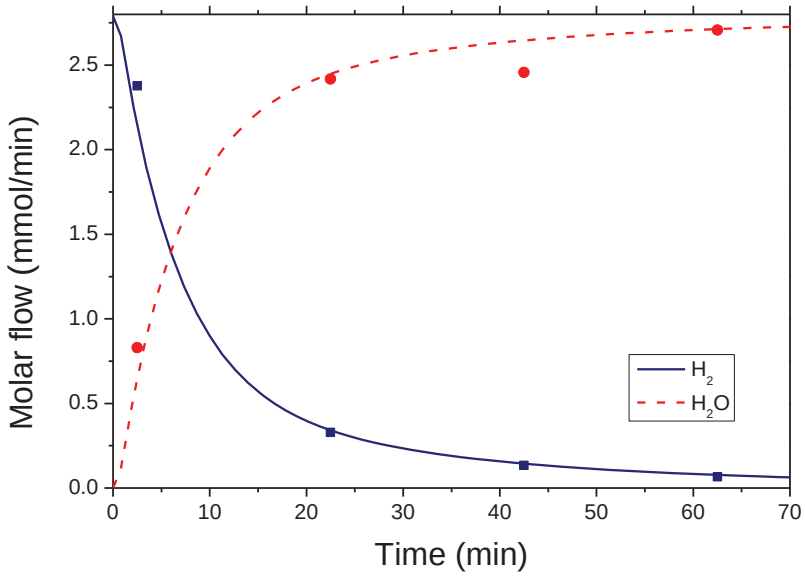

Figure 3.12 – Oxidation at 500 °C after the reduction at 700 °C

It has been taken a sample before and after first oxidation for Raman spectroscopy analysis (figure 3.13). The spectra show that the carbon deposited remains as inert during the oxidation because of the operating conditions. Moreover, this with the previous Raman spectra from the TGA experiments could confirm that the carbon is just produced over the nickel particles as a structured carbon with some disorder. The disorder depends on the D band.

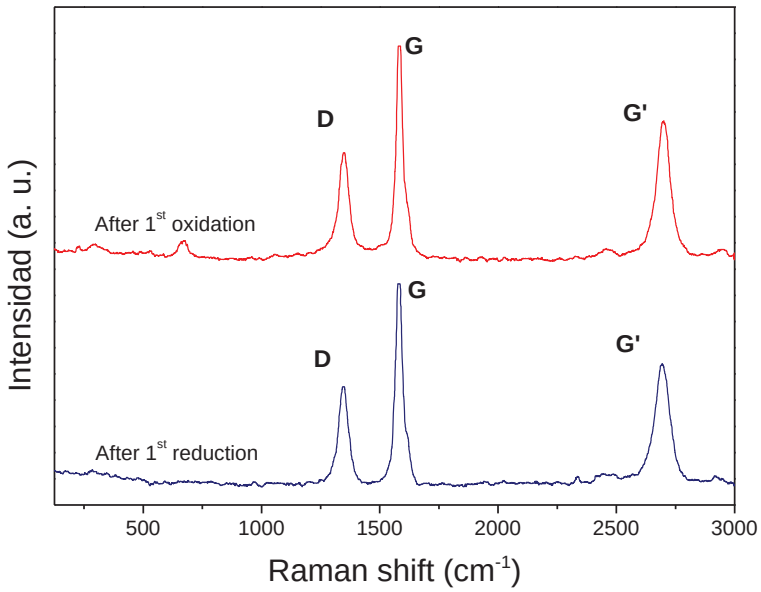

Figure 3.13 –Raman spectra of the sample before and after first oxidation in the reduction at 700 °C.

3.2.2 METHANOL

The methanol is the simplest alcohol and its production comes from the reaction between hydrogen and carbon monoxide at mid temperature (250 °C) and high pressure (100 bar). In our reactor is going to happen just the opposite reaction in order to produce H_2 and CO, they are the responsible of reduce the iron oxide.

In the experimental setup, the exhaust gases are analysed by an Agilent 7890A chromatograph. The main characteristic is that is possible to quantify steam and gases with no previous condensation. The sampling frequency is around 6 minutes. As the decomposition of the reactant occurs at low temperatures, a strict control of temperature is necessary over the whole setup to avoid carbon formation in the tubes.

The experimental temperatures were from 600 °C to 800 °C in the reduction and 500 °C in the oxidation. Initially, blank tests were carried out with and without iron oxide trying to figure out the behaviour of the thermal and catalytic decomposition. The thermal decomposition was done with an inert sand bed in order to keep the spatial time. The conversion of methanol was around 10% producing mostly methane and water, that is, the preferential path is the dehydration. When iron oxide is used, the conversion is total and the main products are hydrogen and carbon monoxide. The yield to another species as water, carbon dioxide and methane are less than 10%. The rate of carbon deposition is 18% (calculated from the elemental balance). It is important to notice that this composition is near to the theoretical decomposition.

As reference, the temporal evolution of the experiment at 700 °C is presented in the figure 3.14. It is represented the molar flow of the products and the elemental balance of C, H and O ($(C_{out}-C_{in})/C_{in}\cdot100$). The three stages of the reduction are present: from Fe_2O_3 to Fe_3O_4 in the first 6 minutes (stage A), from Fe_3O_4 to metallic iron up to 36 minutes (stage B) and finally the catalytic decomposition when all the lattice oxygen is depleted (stage C).

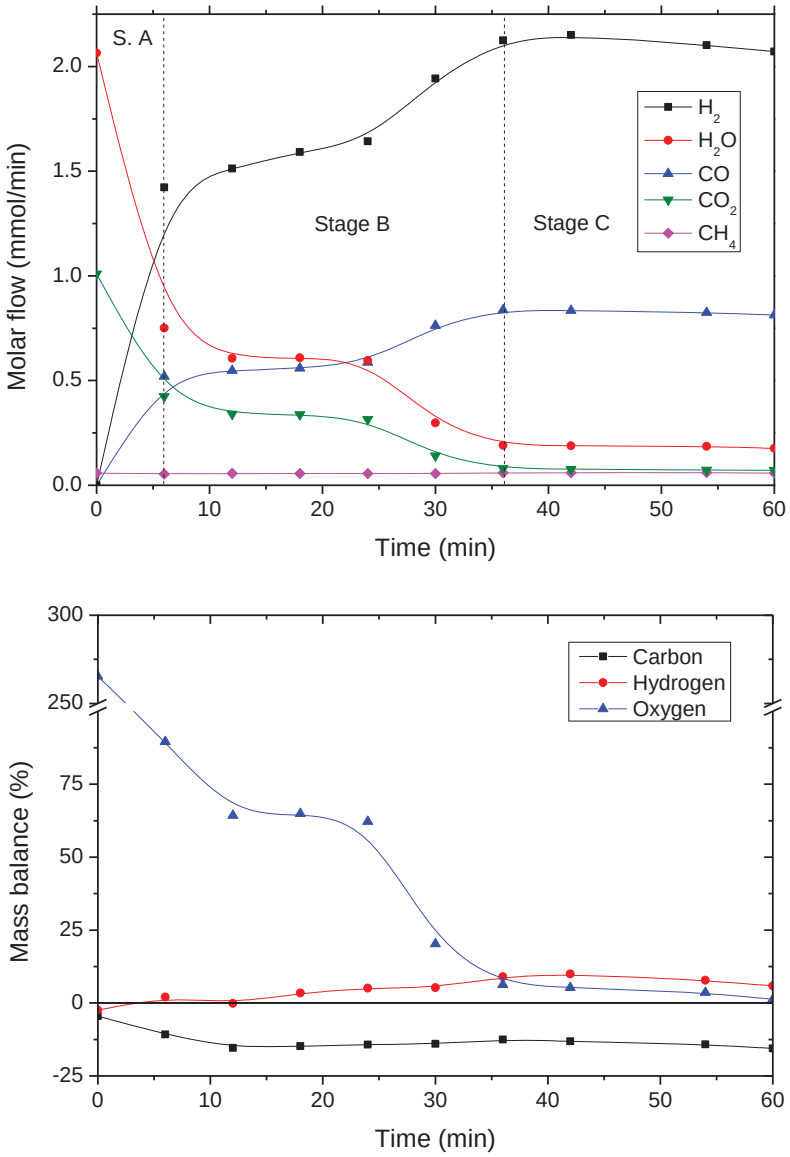

Figure 3.14 – Top: Molar flows of the reduction at 700 °C. Bottom: mass balances (out – in)

In the stage B, the solid and the gases are in equilibrium and part of the oxygen goes with the gas stream as it can be seen in the mass balances. The gases leave the reactor with 65% more oxygen. Finally, the methanol decomposition is full because the iron acts as catalyst. The carbon mass balance is constant after the stage A because the decomposition is full from the beginning despite the active phase (metallic iron) appears later. In the stage A, because of a high reactivity of the Fe_2O_3, the carbon balance is lower due to a possible solid-solid reaction between them.

Figure 3.15 shows the evolution of the CO ratio at different temperatures. The higher the temperature, the higher the hydrogen and carbon monoxide produced and consequently the reduction times are decreased. The reaction time is proportional to the difference between the equilibrium gas-gas (composition after decomposition) and solid gas equilibrium (composition of the exhaust gases). While it lasts 60 minutes at 600 °C, it does only 30 minutes at 800 °C. The carbon deposited is also less at high temperatures: at 600 °C the deficit in the carbon mass balance is 30% and at 800 °C is 7.5%.

In a first view, it is possible to think that the best conditions is at high temperatures in order to avoid carbon deposition, but the sinterization is too high and the average conversion in the oxidation decreases (figure 3.16). After reduction at high temperatures, the steam conversion is low and constant. But at low temperatures, the conversion is higher and the iron is oxidised in less time, around 35 minutes.

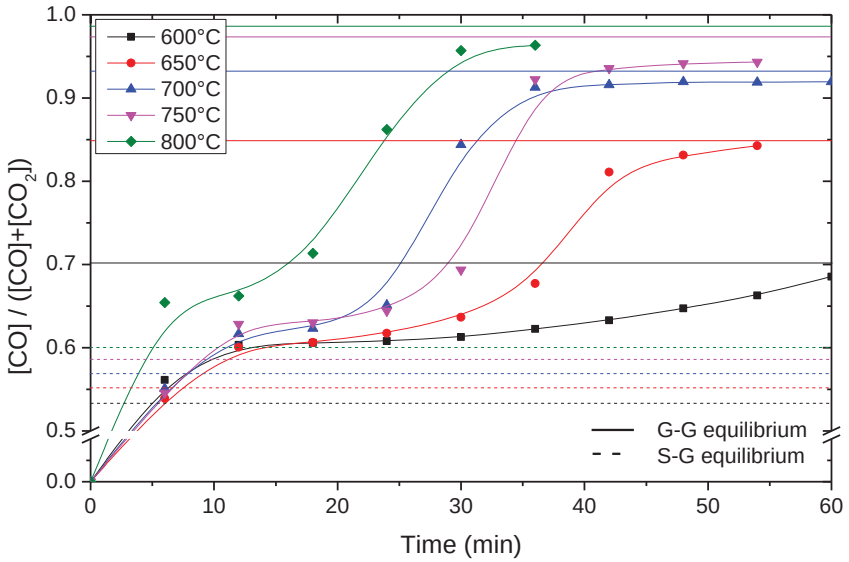

Figure 3.15 – Temporal evolution of the CO ratios in the reductions at different temperatures. Theoretical lines in gas-gas equilibrium (straight line) and solid-gas equilibrium (dotted line) are included.

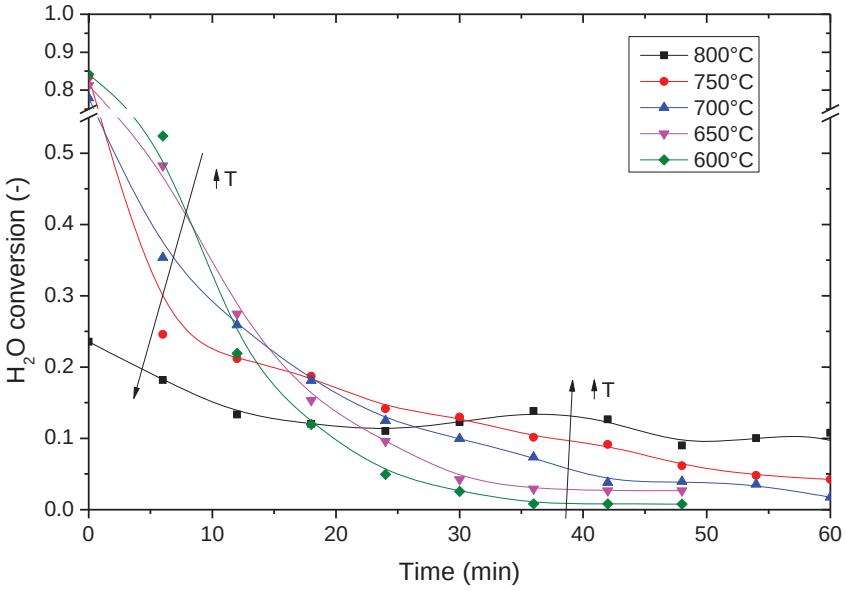

Figure 3.16 – Temporal evolution of the water conversion in the oxidation (500 °C) at different reduction temperatures.

If the experimental and theoretical values are compared in the BG diagram, it is possible to see how close they are (figure 3.17). In the gas-gas equilibrium (stage C), the points agree with minor displacements. But in the solid-gas equilibrium (stage B), all the points are separated from the theoretical by a constant gap. It is known that the reaction of iron and hydrogen is related to reaction pathways controlled by diffusion (Tokuda et al. 1973; Pineau et al. 2007). In addition, the carbon deposited over the surface and the slower reaction with carbon monoxide could increase the resistance to diffusion. So the main hypothesis for this gap is that there is a diffusional restriction in the mass transfer from outer layers to the reaction zone, which it is found near to the core of the particle.

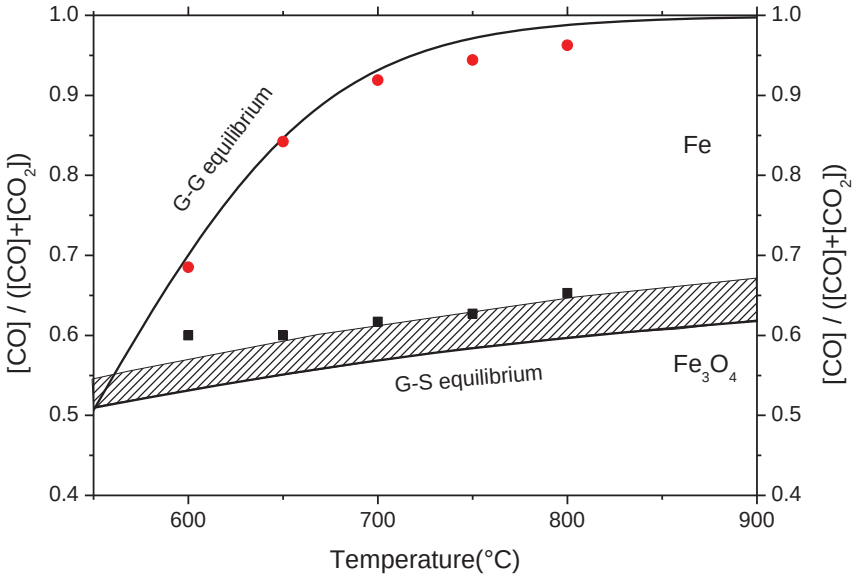

Figure 3.17 –BG diagram for the reductions at different temperatures

At high reduction temperatures, the water conversion is around 15%, very far from the theoretical value that is 83% ($X_{eq,500\,°C}$), but at 600 °C, it is possible to reach it. This is due to the thermal stress or thermal history. If it is worked cyclically, this increases in every cycle and consequently the suitability decreases. The hydrogen yield is represented in the figure 3.18 and there is a maximum because there are two counter effects: low conversion of water at higher temperatures and high carbon deposition at low temperatures. Despite the carbon deposition, the purity of the hydrogen is assured by the detection limit of the instrument, CO < 50 ppm. During the oxidations there is no detection of carbon monoxide because of the inert character of the carbon at operating conditions (500 °C).

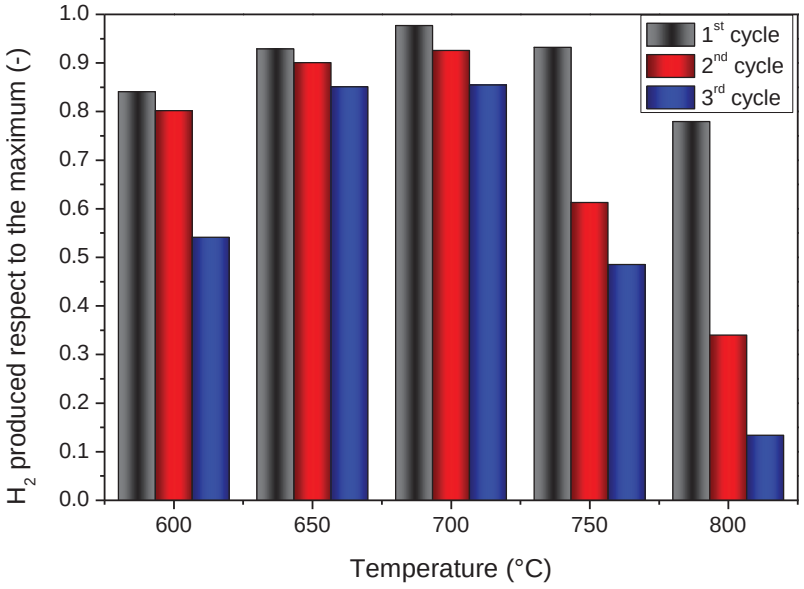

Figure 3.18 – Hydrogen produced in the oxidations normalised respect to the theoretical maximum.

At 600 °C the hydrogen produced in the cycle decreases because the limit pressure is reached before convert the iron oxide. The oxidation time is fixed in 60 minutes and thus the yields are comparable. The best conditions are a reduction working temperature of 700 °C in which the carbon deposition is moderated and the capacity for producing hydrogen is not severe.

When the carbon deposited could be a problem, a cleaning step is advisable, for example, burning of the coke with air. With the purpose of rise the efficiency of the process, feeding inert and using the carbon to pre-reduce the iron oxide at high temperatures is an alternative. Part of the fuel converted into carbon could be reused. Moreover, both solutions involve exothermic reactions that could increase the efficiency by pre-heating the reactor for the reduction.

The micrographs of the carbon by SEM and TEM are shown in the figure 3.19. The carbon deposited is a mix of amorphous carbon and carbon nanotubes of 20 and 50 nanometres. The mechanism of formation begins with the decomposition of the reactant over the surface of the particle, then the carbon diffuse through the particle to the base of the catalyst crystallite. In this point, the carbon precipitates continuously. The nanofiber type depends on the shape of the catalyst base. The growing of the carbon from the base is the responsible of the separation between the support and the crystallite.

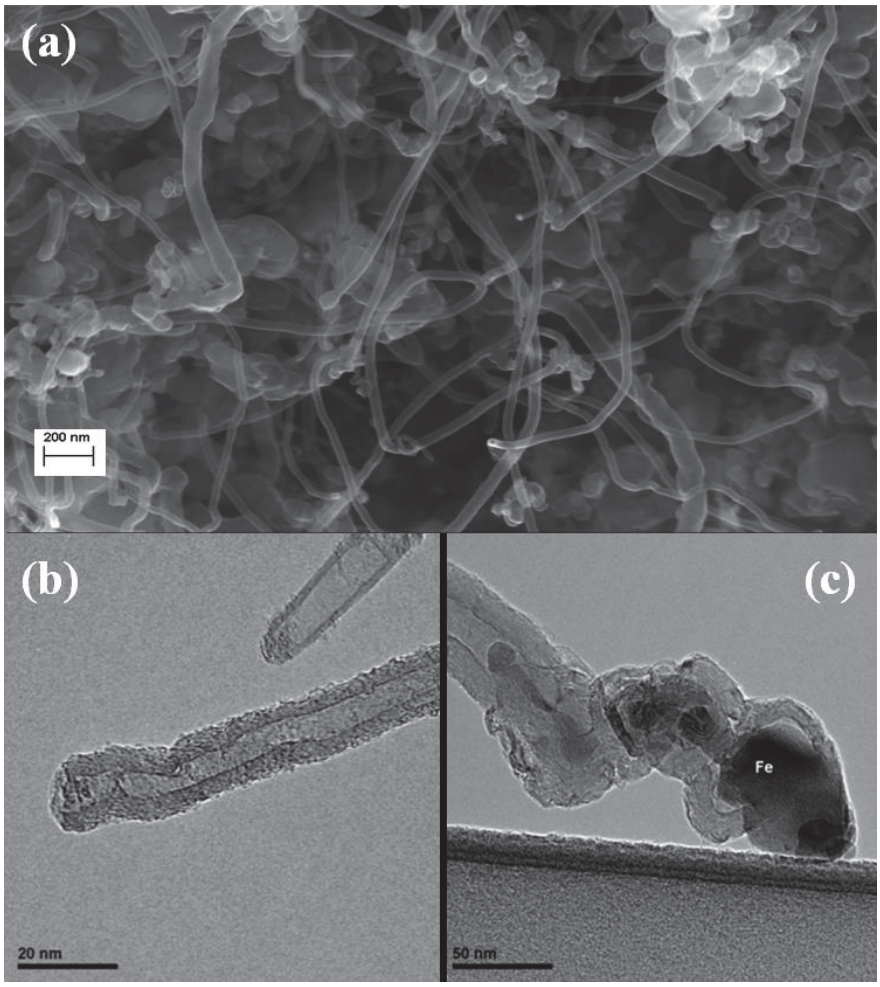

Figure 3.19 –TEM micrograph of the carbon residue.

The explanation to find crystallites of different size than the iron oxide particles (160-200 micrometres) is that it has cohesive properties and it is possible that the sieving is not enough to avoid finer particles stuck to the surface. The advantage of produced structured carbon is that is more inert than the amorphous one (Bartholomew 2007). Consequently, the purity of the hydrogen in the oxidation might be higher.

3.2.3 ETHANOL

The ethanol is the next alcohol in terms of length chain respect to the methanol. The main production comes from biological processes of fermentation of the sugars due to its use in food. Also, it comes from the hydration of the ethylene at 300 °C and 80 bar (Ramachandran and Dao 1996).

Other source is the Fischer-Tropsch synthesis like the methanol (Spivey and Egbebi 2007).

Besides the fact that it is one of the components of the bio-oil, also is final product from the fermentation from diverse plants. There is a rise in the production of bio-ethanol as alternative fuel (Kim and Dale 2004). The problem is the speculation of the product because of the double use as food and fuel. Consequently, it is probable a price war that provokes instability in the food supply. It is fundamental a political regulation to distinguish energy crops from that to farm basic food as the flour. Nowadays, the research routes are focused on energy crops and increasing the efficiency of the energy production [web 3].

From the ethanol decomposition is possible to obtain hydrogen and carbon monoxide in a ratio 3 to 1 (r 3.5) and thus a reductant stream is created for the SIP process. Due to secondary reactions there is less than these 4 moles of reductants. According to the low ratio C/O, a high carbon formation is expected.

$$CH_3CH_2OH \rightarrow 3H_2 + CO + C \qquad \text{(r 3.5)}$$

The experiments were carried out in the same experimental setup as the methanol experiments. The sampling frequency is 5 minutes and there is the possibility of quantify the water concentration. Moreover, it is analysed the methanol and ethanol present in the exhaust gases.

The solid used was doped iron oxide without catalyst due to the easy decomposition of the ethanol. The tested temperatures were from 600 °C to 750 °C. For the lowest temperature, there are no results because the carbon deposited over the bed clogged the reactor.

The thermal decomposition was tested without solid at 700 °C. The main products were methanol and hydrogen, then CO and H_2O. The ethanol conversion was around 46%. There were minor amounts of ethane and ethylene. The main reactions are the thermal decomposition and the dehydration (r 3.6 and r 3.7).

$$CH_3CH_2OH \rightarrow H_2 + CO + CH_4 \qquad \text{(r 3.6)}$$

$$CH_3CH_2OH \rightarrow CH_2 = CH_2 + H_2O \rightarrow 2H_2 + H_2O + 2C \qquad \text{(r 3.7)}$$

It is assumed that the specific surface of the porous plate is low and in the case of using a packed bed with a higher surface, a total conversion can be likely reached.

In the reduction with ethanol, the three stages are repeated according to the consecutive reduction of the doped iron oxide: Fe_2O_3 to Fe_3O_4 in the stage A, Fe_3O_4 to Fe in the stage B and finally, in the stage C, the ethanol decomposition. In the figure 3.20, the results at 675 °C are represented. During the stage B there is a decreasing in the molar flows of the oxidants and an increasing in the reductants due to a lower conversion of the solid. Since there is a high yield to carbon, the surface is covered and the solid-gas reaction could be unfavourable. This behaviour is repeated in all the temperatures.

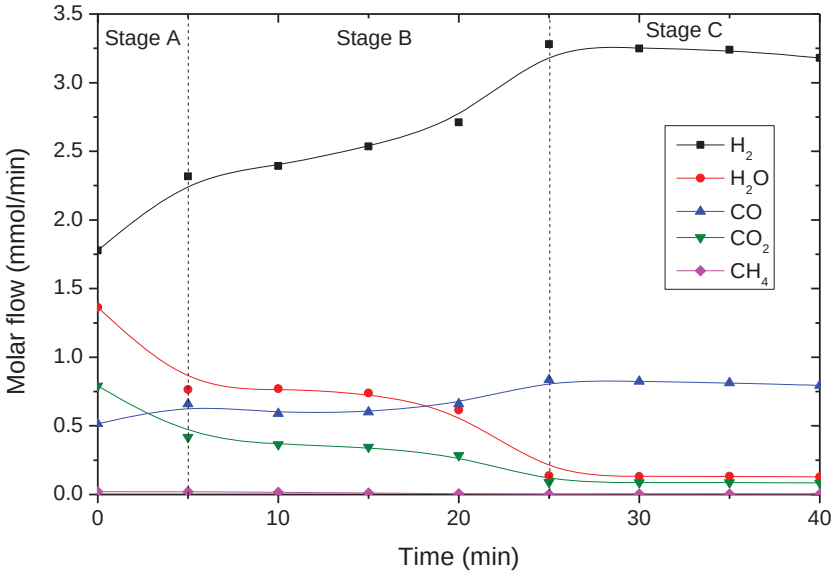

Figure 3.20 – Molar flow of the exhaust gases at 675 °C.

The mass balances of C, H and O along the time are represented in the figure 3.21. The oxygen depleted from the iron oxide are calculated and is a positive value because there is more molecular oxygen in the exhaust gases than in the reactant. The hydrogen balance corresponds only to error in the instrument. The carbon balance has negative values because is deposited over the bed and in the first stage part of the carbon is reacted with the Fe_2O_3. In the second stage, there is a deposition of around 50% of the elemental carbon that pass through the reactor, quite near to the theoretical value, 56%.

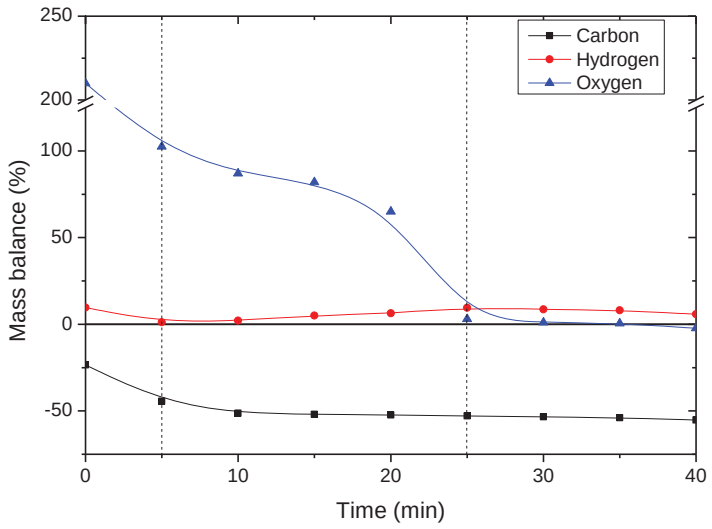

Figure 3.21 – Mass balances in the reduction at 675 °C (out – in).

The reactant composition was varied from 5% to 15% and the flows of H_2 and H_2O are represented in the figure 3.22. In all the cases the total conversion is reached but the duration are proportional to the concentration. When 5% of ethanol is fed, the reaction time is 15 minutes, but at 15% it is around 40 minutes.

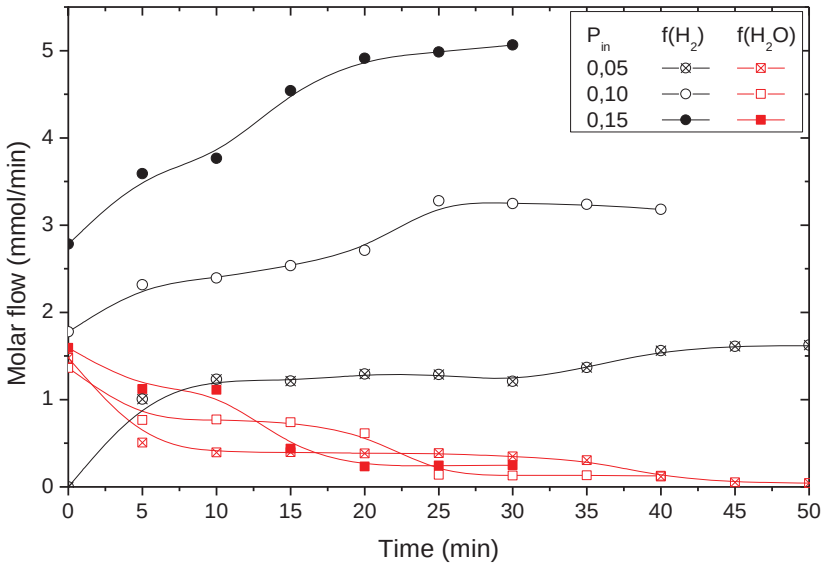

Figure 3.22 – Reduction at 675 °C at different reactant concentration.

Depending on the reduction temperature, the temporal evolution of the CO ratio is shown in the figure 3.23. In the stage A, the reduction is fast and the solid conversion duration decreases along the temperature. As in the previous experiments, at higher temperature the main products are hydrogen

and carbon monoxide, while the carbon deposited decreases. The reaction time decrease along the temperature because of the higher difference between equilibriums (lines in the same colour).

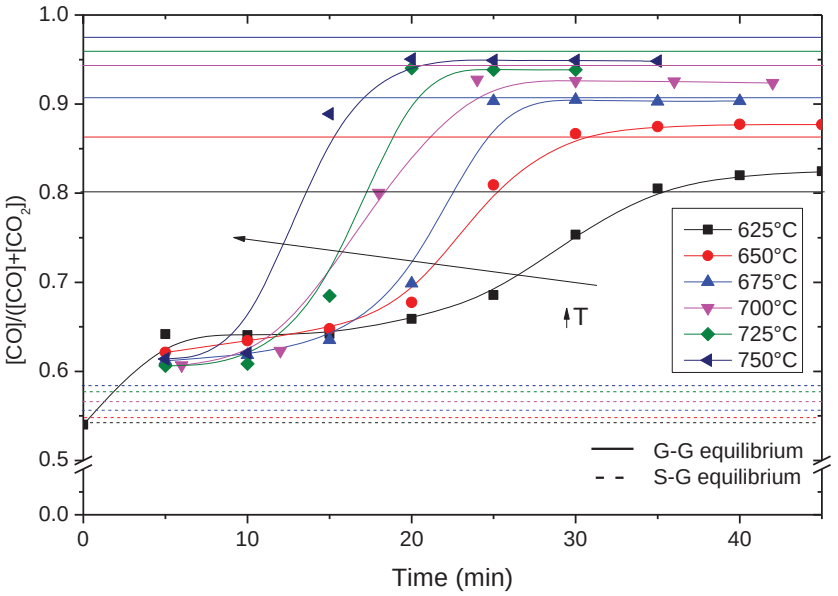

Figure 3.23 – Temporal evolution of the CO ratios in the reduction of ethanol at different temperatures. Theoretical lines in gas-gas equilibrium (straight line) and solid-gas equilibrium (dotted line) are included.

The counter effects of high carbon deposition at low temperatures and low steam conversion at high temperatures also occur with this reactant. In the figure 3.24, the molar flow of H_2O in the oxidation is shown when the reduction temperature varies. At the lowest reduction temperature, the highest steam conversion is reached but at the highest temperature tested, the conversion is below 35%. There is a mark, t*, that corresponds to the theoretical minimum time to convert the solid at maximum equilibrium conversion. The smoothing shown in the conversion is due to the limitation offered by chemical reaction and this behaviour is quite similar to the theory of time distribution in real reactors.

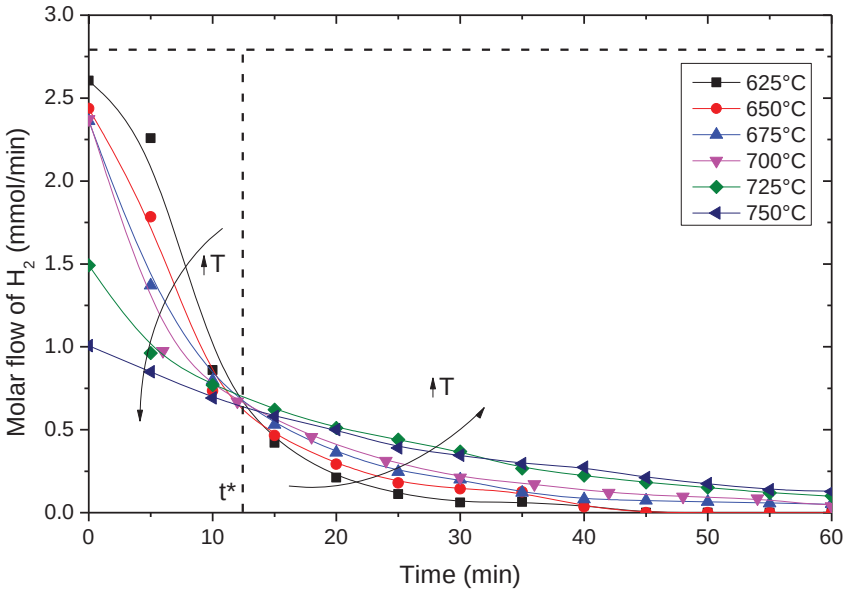

Figure 3.24 – Molar flow of hydrogen in the oxidations at 500 °C at different reduction temperatures.

The equilibrium points are represented in the BG diagram (figure 3.25). In the gas-gas equilibrium (stage C), the values agree with the theoretical, but in the case of solid-gas equilibrium (stage B), at lower temperatures the gap is further from the theoretical curve. This happened in the same way with the biogas experiments and the main hypothesis is that there is no full conversion of some of the reactants or reductants. Due to the high amount of carbon deposited, this is the most probable responsible, so at lower temperatures, the carbon layer is thicker and the gases suffer diffusional restrictions. Despite at higher temperature the carbon deposited is minimum, the gap is kept due to the diffusional restrictions of the gases through the iron oxide layers.

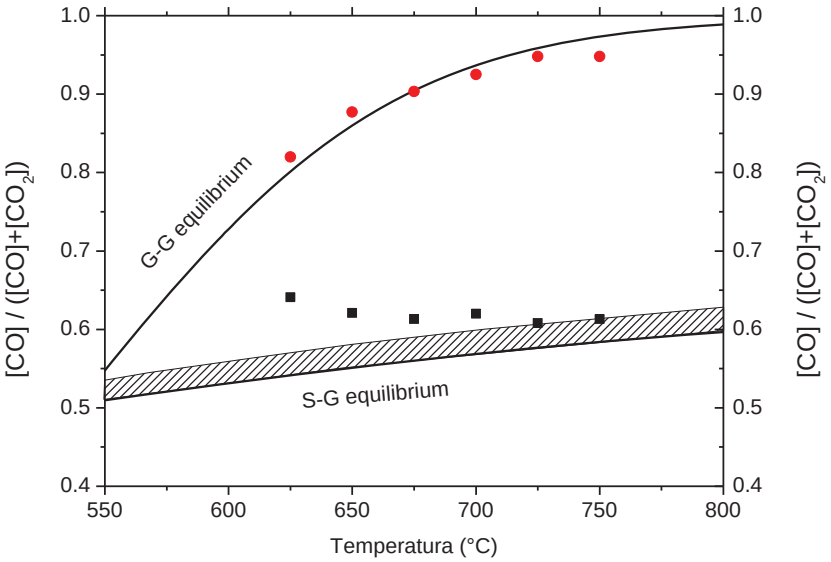

Figure 3.25 – CO ratio at different reduction temperatures.

The study of the ethanol experiments were completed with the hydrogen yield in the oxidation at different reduction temperatures and cycle number (figure 3.26). The same conclusions that in the methanol experiments were found: there is a maximum in hydrogen yield due to the carbon formation that clogs the reactor at low temperatures, and a low steam conversion at high temperatures due to a severe thermal stress. In all the oxidations is assured a concentration of CO below of the limit detection, [CO] < 50ppm.

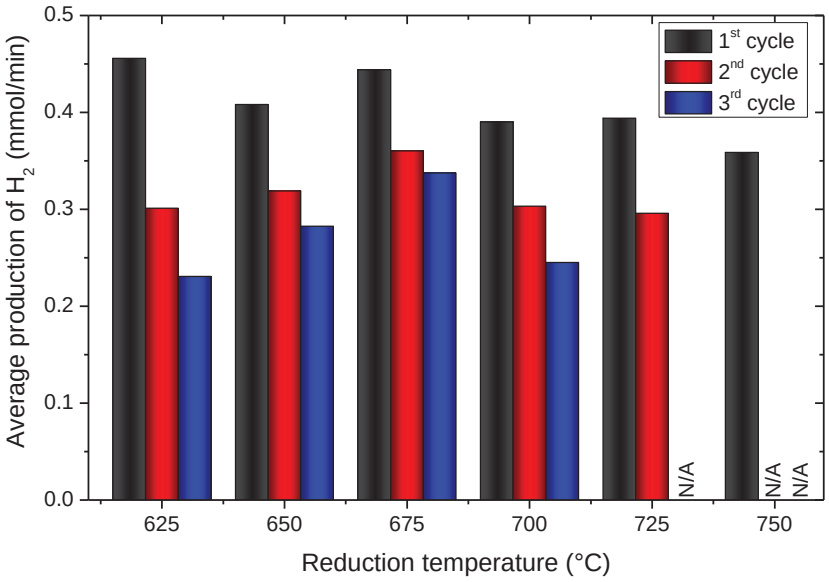

Figure 3.26 – Hydrogen production in the oxidation according to reduction temperature and cycle number.

Finally, the carbon depositions were characterised by TEM micrographs (figure 3.27). The sample selected was after 3 redox cycles at 700 °C. In this case the carbon nanotubes are better defined and it is possible to see the crystallite detached from the iron oxide surface. The nanofiber diameter is 20 nanometres and these are hollowed. The structured carbon assures an inert carbon in the oxidation and consequently the high purity of the hydrogen.

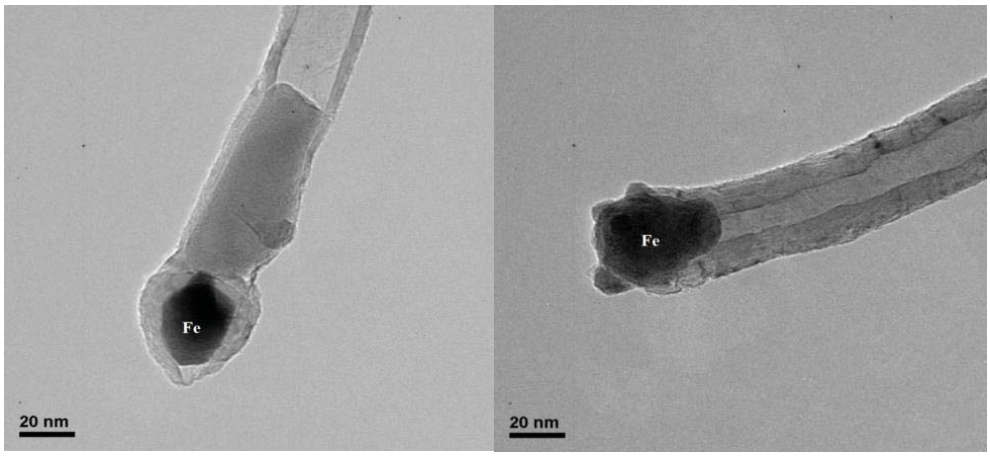

Figure 3.27 –TEM micrographs of the carbon nanotubes produced in the reduction at 700 °C after 3 cycles

3.2.4 Acetic acid

The next reactant is one of the majority components of the bio-oil. It is the most used as model compound because its characteristics. The elemental composition and the acidity are similar to pyrolysis oil (Wang et al. 1996, 2014; Takanabe et al. 2004; Hu and Lu 2007; Vagia and Lemonidou 2007; Gil et al. 2015; Li et al. 2015). The production is through methanol or biological processes in which vinegar is generated. Acetic acid comes from a higher degree of oxidation of the sugars passing through ethanol.

This reactant does not decompose as easy as the alcohols, so in this case it is mandatory the full mixture, oxygen carrier and catalyst. The experimental setup is composed of the same feeding and reactor zone, but the chromatograph that analyses the exhaust gases is a micro-GC Agilent 490. The sampling frequency is 2 minutes but is not possible to quantify the water because it is forbidden to feed water to the instrument. The steam is condensed in a Peltier module. In this way, the temporal evolutions of the

gases are slightly smoothed because the module has a death volume with a spatial time around 2 minutes.

Blank experiments were carried out: no solid, only iron oxide and only catalyst. In the first one the thermal decomposition was tested and in the second one the catalytic decomposition. The working temperatures were 700 °C and 800 °C. In the case there is no solid, the main products in order of composition were methane, carbon dioxide, ethane, ethylene, acetone and unreacted acetic acid. At higher temperature, the conversion increased somewhat more. As methane and carbon dioxide are abundant, the catalyst for the biogas is mandatory in order to obtain more conversion to hydrogen and carbon monoxide. The results without catalyst are shown in the figure 3.28. The methane produced is higher at higher temperatures, the opposite as expected from a favoured thermal decomposition. This is explained by the sinterization that leads to a lower reactivity (solid-gas reaction) and lower activity (catalytic effect).

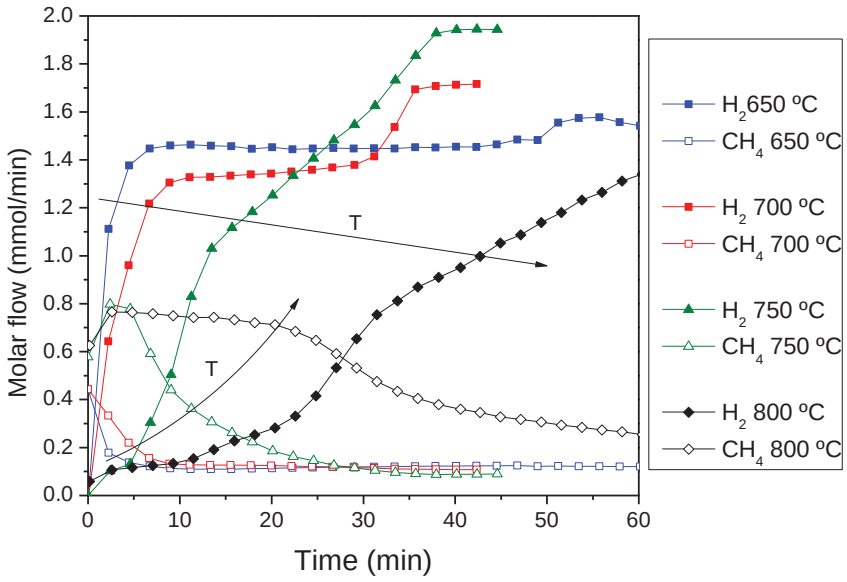

Figure 3.28 – Molar flow of hydrogen and methane at different reduction temperatures in the experiments with no catalyst.

In order to compare the differences between the use of catalyst or not, both results are represented in the figure 3.29. As it is expected, the methane conversion was maximum and consequently the hydrogen and carbon monoxide produced was higher than with no catalyst. The main result is that the reduction time decreases from 36 minutes to 27 minutes.

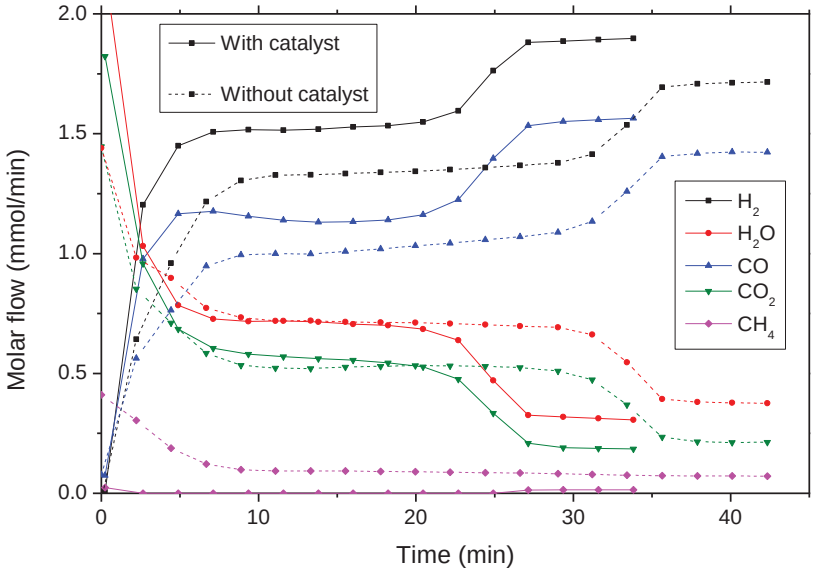

Figure 3.29 – Comparison of the molar flows between the experiments with catalyst (straight line) and without catalyst (dotted line).

The results obtained with the full solid mixture are represented in the figure 3.30. The stage A is very fast and it lasts 5 minutes. Then, the stage B varies from 25 minutes at high temperature to 45 minutes at the lowest temperature, 650 °C. The methane generated was almost negligible and the hydrogen and carbon monoxide follows the theoretical trend. At higher temperatures the reductants generated, H_2 and CO, are higher. An undesired effect is that the change of the composition between second (B) and third (C) stage is slow and this corresponds to lower reaction rates.

According to the BG diagram (figure 3.31), the behaviour is similar to the previous experiments with other reactants. In the stage B, the equilibrium solid-gas is separated from the CO ratio a constant value of 10% and in the stage C, the gas-gas equilibrium matches the theoretical line. This gap is explained by the diffusional restrictions of the gases to reach the core of the particle where the reaction occurs.

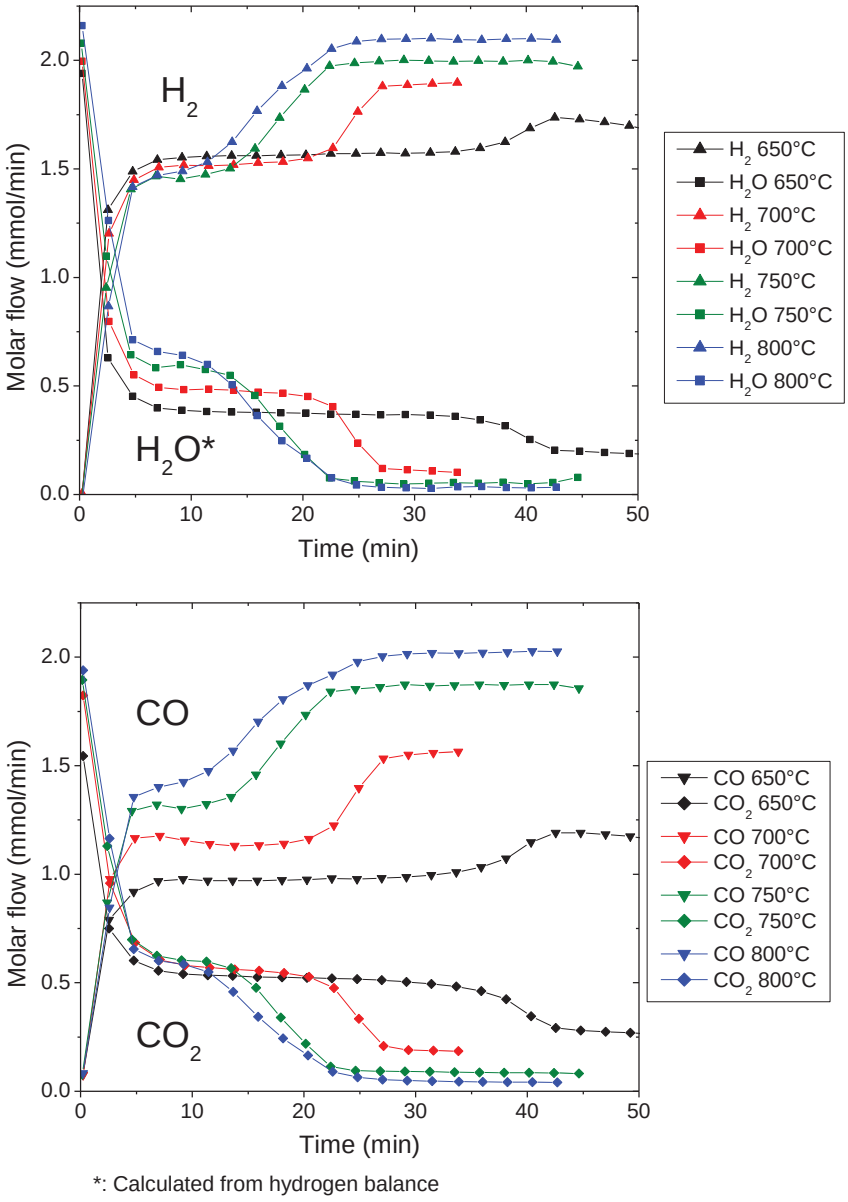

Figure 3.30 – Molar flows in the reductions at different temperatures with catalyst.

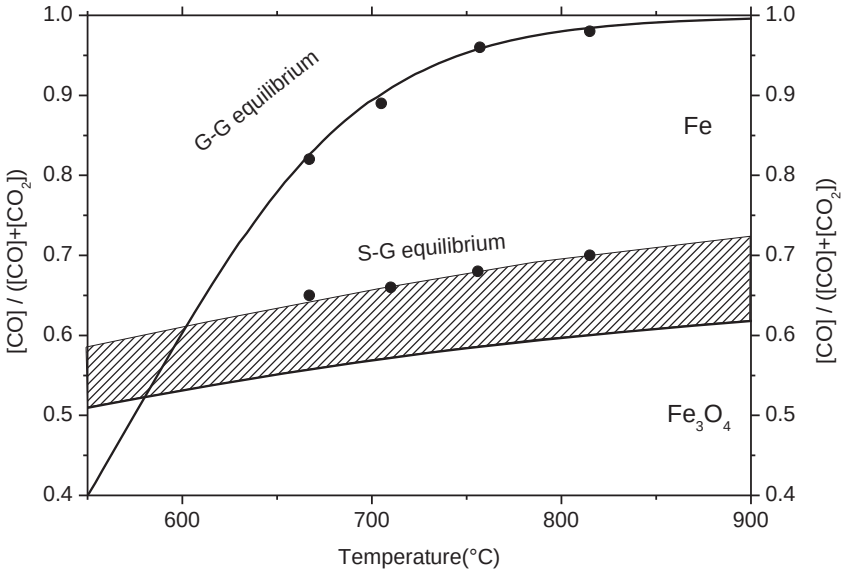

Figure 3.31 – Experimental CO ratios in the BG diagram at different reduction temperatures.

The reactant composition was varied from 5% to 15% and is represented in the figure 3.32. The shape of the CO ratio curves remain, but the duration of the stages changes. In the case of the higher concentration, the solid conversion lasted less than 20 minutes and when 15% of acetic acid was fed, the reaction time increased to around 40 minutes. The solid-gas equilibrium is constant at any composition because the temperature is the same and the reaction related to the equilibrium is equimolar. But the gas-gas equilibrium in the stage C changes because the Gibbs free energy varies depending on the concentration of inert. Summarizing, the gap is constant in the stage B and do not depend on the concentration of reactants and in the stage C the gas-gas equilibriums are reached in all the cases.

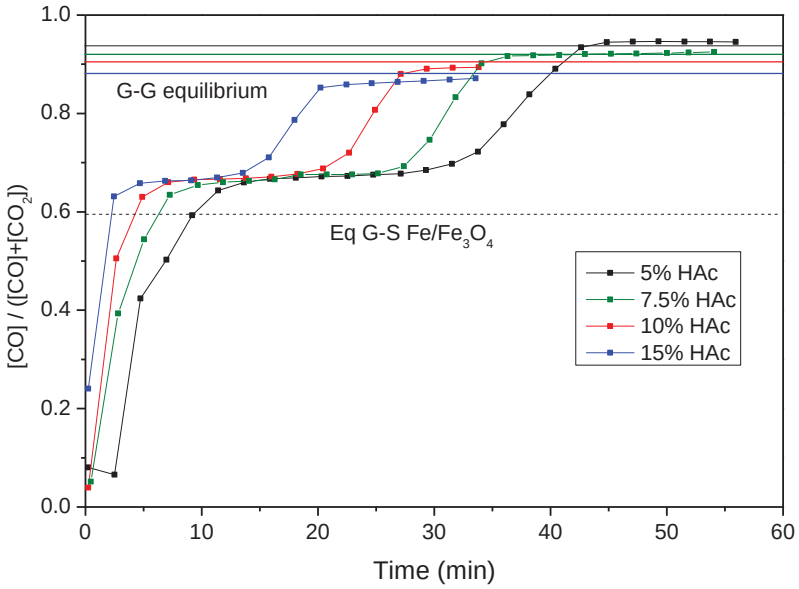

Figure 3.32 – Experimental CO ratio at different acetic acid concentration in the inlet stream. Theoretical lines in gas-gas equilibrium (straight line) and solid-gas equilibrium (dotted line) are included.

In the oxidations, the temperature was changed to 550 °C and the results are shown in the figure 3.33. The shape of the curve is similar to previous experiments. At higher temperatures the average conversion decreases greatly. But at lower temperatures the conversion begins from the equilibrium maintaining a high conversion. While in 30 minutes, it is possible to convert the solid into Fe_3O_4 at 650 °C, the conversion of solid is not total after 60 minutes at 850 °C. Thus, using acetic acid does not avoid thermal stress and the sinterization causes reactivity loss at high temperatures.

Figure 3.34 shows the hydrogen yield at different operating temperature, number of cycles and presence of catalyst. There is a maximum between 700 °C and 750 °C that corresponds to the mentioned counter effects of carbon deposition and thermal stress. In all the cases the use of catalyst is recommended because the hydrogen yield is higher.

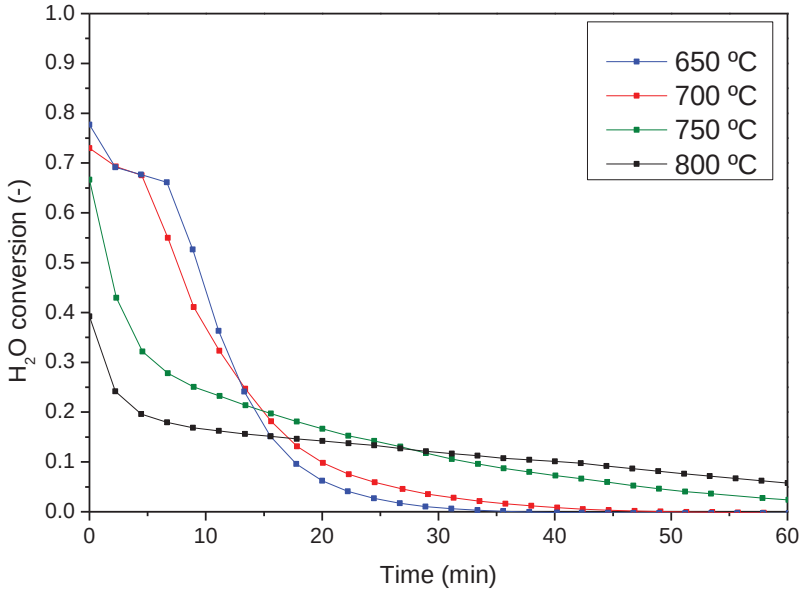

Figure 3.33 – Oxidations at 550 °C at different reduction temperatures.

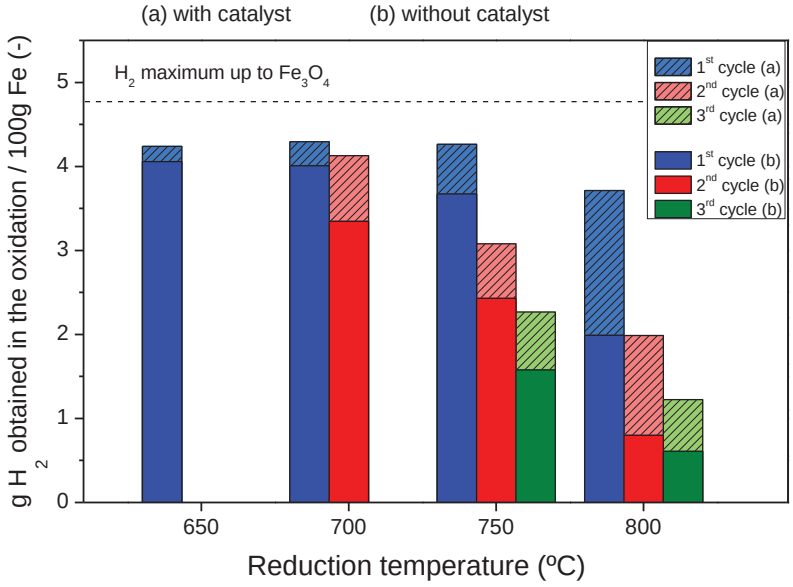

Figure 3.34 – Hydrogen yield at different operating conditions (temperature, number of cycle and presence of catalyst).

The carbon depositions were analysed by TEM micrograph and Raman spectroscopy (figure 3.35). The catalyst produces carbon nanofibers with an average diameter of 11 nanometres. As the methane is an intermediate during the reaction, there is extensive bibliography that corroborates carbon nanotubes production from methane decomposition (Chen et al. 2005; Li et al. 2011). The catalytic activity is constant with no deactivation despite the fact that during the tubes growing, the crystallite is pulled up from the surface.

Indeed, the constant activity is assured during at least 6 hours, time correspondent to 3 redox cycles. In the Raman spectra, the samples are before and after an oxidation and they are almost identical, corroborating the inert role of the carbon in the oxidation. If it is compared with the alcohol samples, the disorder degree is higher.

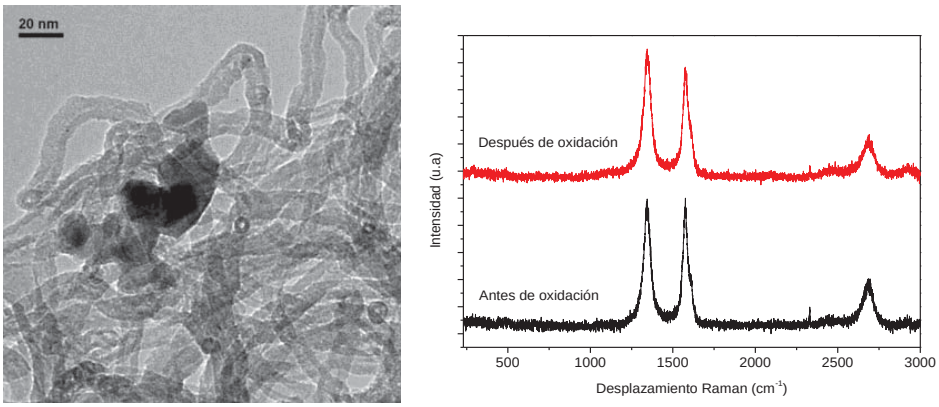

Figure 3.35 – (Left) TEM micrograph of the carbon depositions. (Right) Raman spectra of the carbon before and after oxidation (T_{red}= 650 °C)

3.2.5 HYDROXYACETONE

The hydroxyacetone, or acetol, is not stable and could change its composition at long time in ambient conditions. It is very hydrophilic and the purity from commercial supplier is 96.1%. It is one of the majority components according to bibliography (Oasmaa and Meier 2005; Bertero et al. 2012; Remón et al. 2015).

The control temperature is restricted to a short range because of the evaporation and decomposition temperatures are close, so the optimal value is 175 °C. When the temperature is increased above the decomposition, the hydroxyacetone polymerises into oil.

The chromatograph used is the Agilent 7890A and the sampling frequency is 5 minutes. The vapours are also analysed and in this case is important because the thermal decomposition presents a lot of secondary liquid products.

The thermal decomposition was tested at 700 °C to know the conversion degree and the selectivity to methane, the most stable product. In the figure 3.36 is exhibited the different species appeared after the reaction. The first

compound in concentration is the carbon monoxide. This could give an idea of the high reductant capacity of the stream. Then, the products ordered by concentration are methanol, methane, acetaldehyde and unreacted hydroxyacetone, with a conversion of 62%. Due to methane is one of the main products, it is mandatory the catalyst.

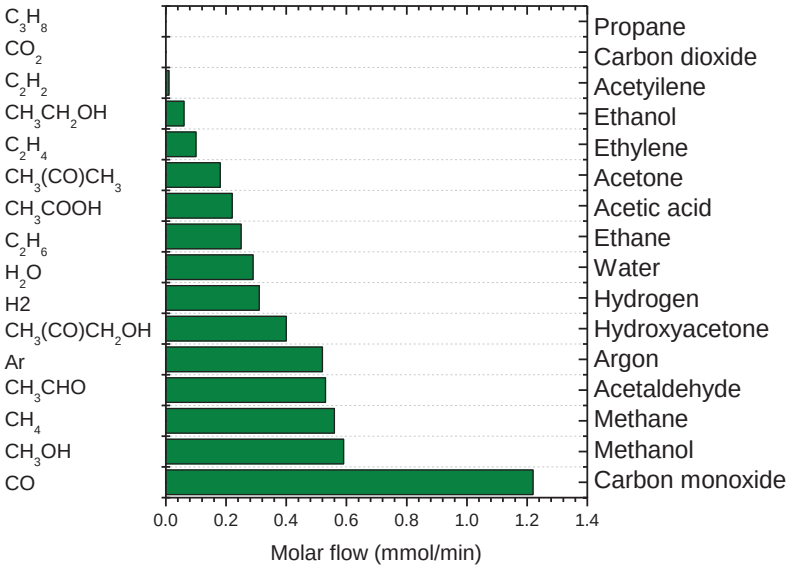

Figure 3.36 – Thermal decomposition in absence of solids.

Although the catalyst is necessary, tests have been carried out with only iron oxide. The results (not shown) indicate a total conversion of hydroxyacetone and a high amount of methane. So the iron oxide is able to decompose the acetol but the equilibrium is not reached.

The results with the full solid mixture are presented in the figure 3.37. The stage A lasts 5 minutes and the conversion of the solid is finished in only 25 minutes. Then up to 40 minutes, the catalytic decomposition of hydroxyacetone goes without any deactivation.

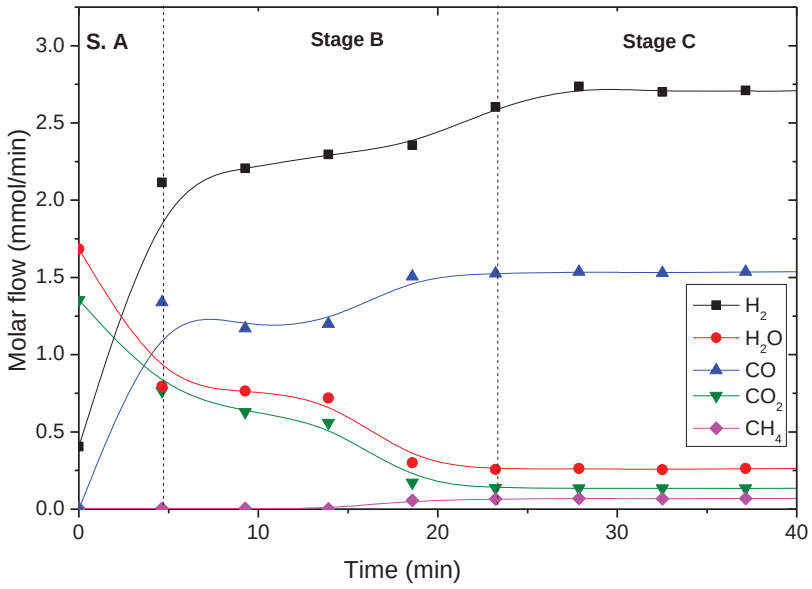

Figure 3.37 – Molar flows of the reduction with hydroxyacetone at 700 °C.

In the figure 3.38 is observed the temporal evolution of the CO ratio and its transition between the stages. At 600 °C, there is no reaction because the composition in both equilibriums is near and the reducing capacity is low. At 800 °C the time to convert the solid should be less than the rest, but due to the sinterization, the rate between the stage B and stage C is slower than the rest.

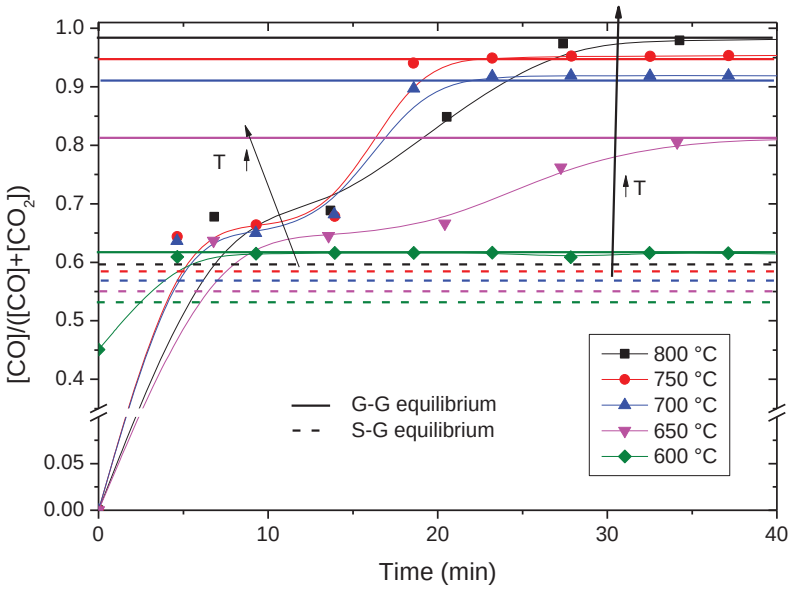

Figure 3.38 – Temporal evolution of the CO ratio at different reduction temperatures. Theoretical lines in gas-gas equilibrium (straight line) and solid-gas equilibrium (dotted line) are included.

In the BG diagram (figure 3.39), the gas-gas equilibrium (stage C) agrees with the theoretical and in the solid-gas equilibrium (stage B), the gap appears as in the previous experiments. In this case the coincident point at 600 °C is important to notice why the experimental points follow a parallel line.

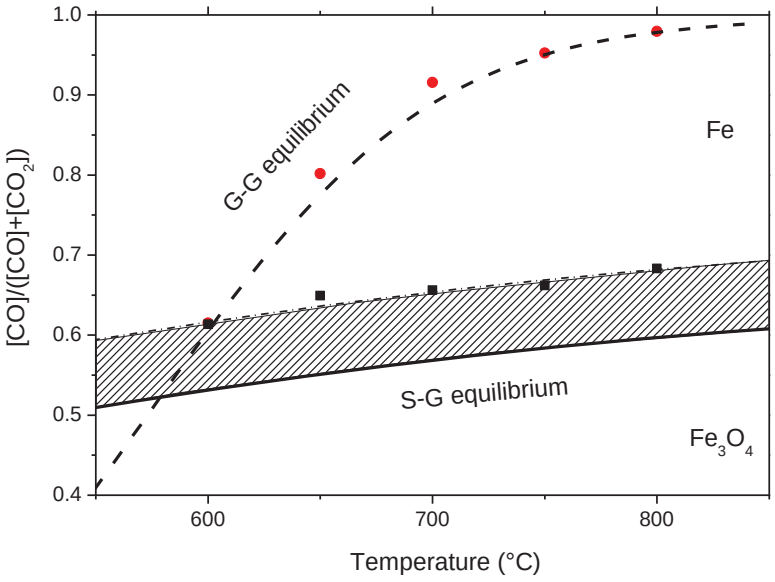

Figure 3.39 –BG diagram with the experimental values at different reduction temperatures.

In the figure 3.40 is represented the oxidations at 500 °C when the reduction temperatures were varied. The behaviour is maintained and at higher temperatures the average conversion greatly decreases. So, increasing the size of the hydrocarbon, the thermal stress is high.

The carbon residue was characterised by TEM micrograph (figure 3.41). Two types of carbon tubes were observed associated to different solids. In this analysis is firstly observed nanofibers from iron and nickel simultaneously, so in this case the catalytic effect of the iron is confirmed. In the alcohols without catalyst, carbon nanofibers are produced, thus it is possible to say that there is catalytic effect in both solids and the activity of the nickel is higher than the iron because is able to decompose the existing methane. The diameter of the nanofibers are similar.

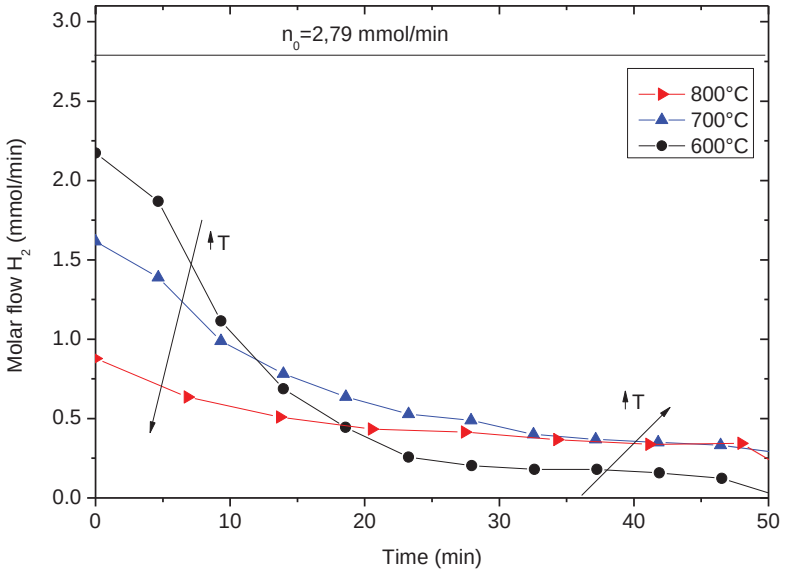

Figure 3.40 – Oxidations at 500 °C after different reduction temperature.

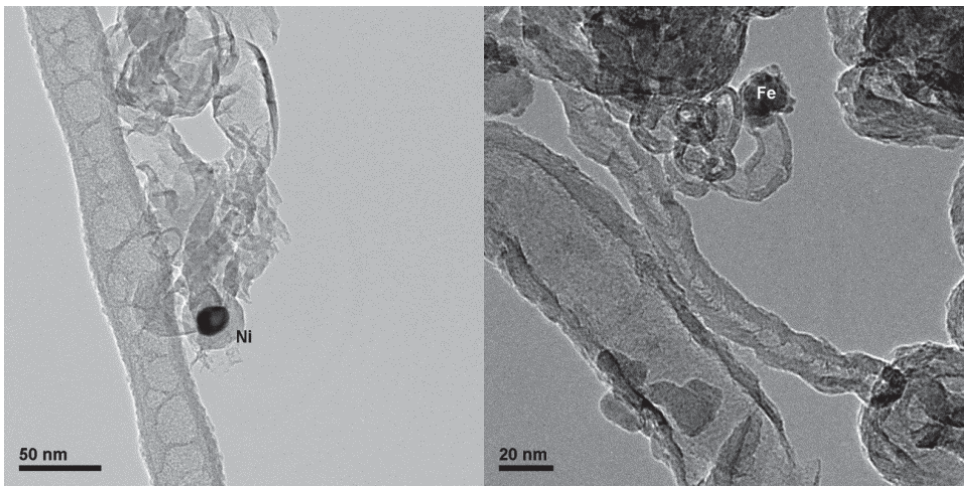

Figure 3.41 – TEM micrograph after the reduction at 650 °C. (Left) Zoom of a catalyst particle. (Right) Zoom in an oxygen carrier particle.

As the three reduction stages, the high reactant conversions and the behaviour of the oxidations are similar to previous results, the analysis by Raman spectroscopy seems unnecessary.

3.2.6 ACETONE

The acetone is a component that is not majority in the bio-oil but is the ketone with the shortest chain length, so it is representative of this functional group. Usually, this is used as solvent of organic compounds and in chemical synthesis. Its production is from the cumene process (Hock and Lang 1944). One of the main characteristics is the high volatility.

The analysis system is the Agilent 7890A in which is possible to quantify vapours at a sampling frequency of 6 minutes. There is no problem in the feeding because its high volatility but the ratio C/O is higher than the previous experiments and the carbon deposition increases causing a clog.

With this reactant, it has been tested directly with the full solid mixture of oxygen carrier and catalyst. The temperature was varied from 650 °C to 800 °C in the reduction and in the oxidation is 500 °C. It has been tested at 600 °C but the amount of carbon clogged the reactor and the maximum pressure of the experimental setup (1.5 bar) was exceeded. In the figure 3.42, the molar flows of the experiment at 700 °C are represented and the three stages are present. Despite some error in the first point, the behaviour is similar to previous experiments. The time for full conversion is around 27 minutes and finally the composition during catalytic decomposition appears.

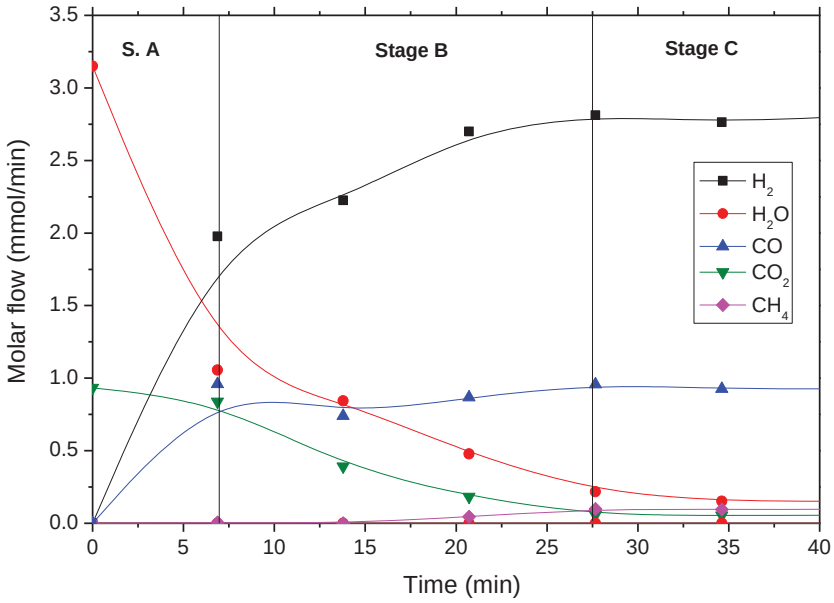

Figure 3.42 – Molar flows in the reduction at 700 °C with acetone as reactant.

In the reductions at different temperatures (figure 3.43), it is possible to observe the same phenomena than the rest of reactants. In the stage C the equilibrium are close to the theoretical values and in the stage B the gap between experimental and theoretical is similar to previous. The two experiments at low temperature and the two at high temperatures are grouped. This is the unique experiment in which this phenomenon is observed, so it is considered casual. In the BG diagram (figure 3.44) is shown how this gap depends on the temperature. The separation is explained by the diffusional restriction of the gases to pass through the layers of the iron particle.

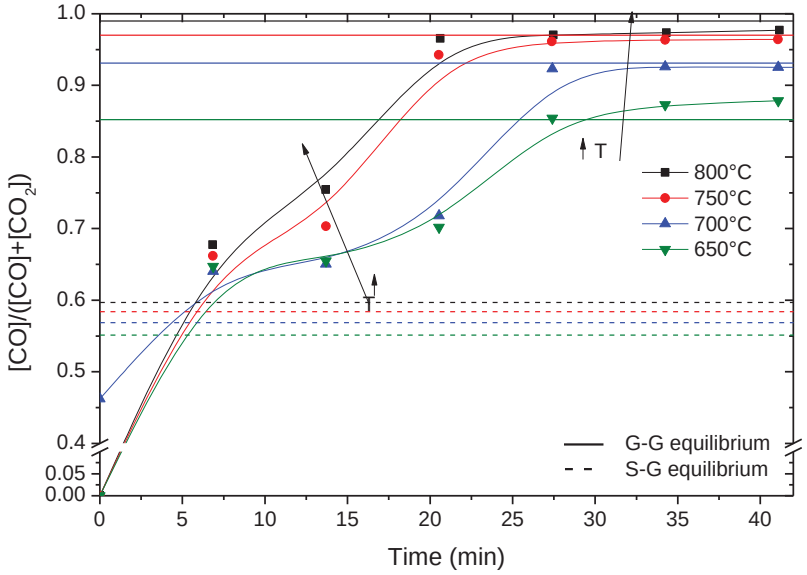

Figure 3.43 –CO ratio at different reduction temperatures. Theoretical lines in gas-gas equilibrium (straight line) and solid-gas equilibrium (dotted line) are included.

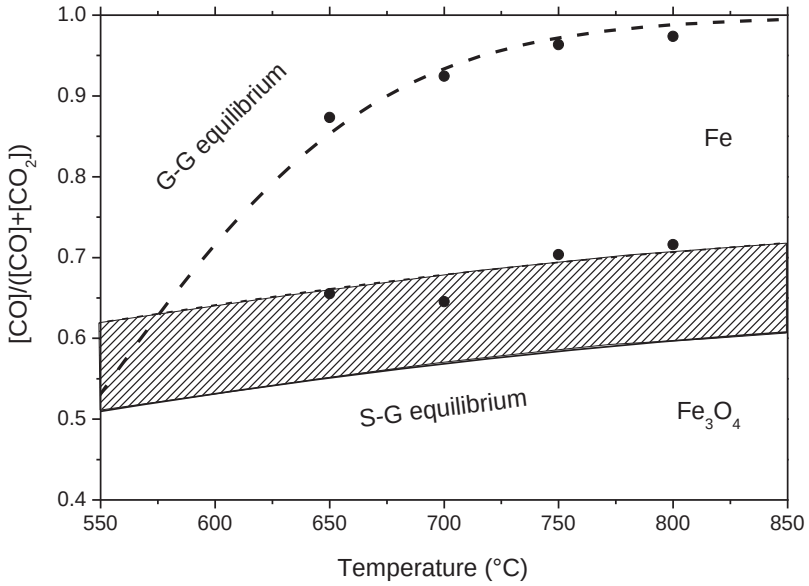

Figure 3.44 –BG diagram at different reduction temperatures.

The reactant flow was varied to obtain different concentrations from 5% to 15%. The CO ratios are represented in the figure 3.45. The theoretical G-G ratios in the three experiments are almost identical, so is represented only one theoretical value. In the stage B, the points are separated the same value from the theoretical and follows the same trend as other experiment: the gap is constant along the temperature. The full solid conversion is proportional to the flow of reactant and it is observed in the curves.

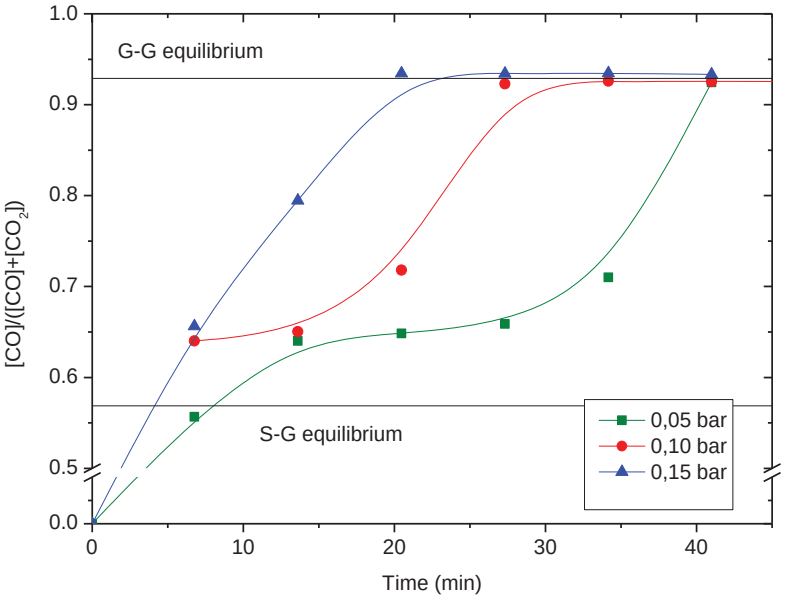

Figure 3.45 –CO ratio in the reduction at different reactant flow.

The oxidation results after the reduction with acetone is observed in the figure 3.46 and there are two groups at low and high temperatures as in the previous reduction. In the group of high temperatures, the conversion is higher than at low temperature. In the figure 3.47, the oxidations at the same temperature but different reactant flow in the reduction are compared. Because the temperature is the same, the thermal stress is identical and the curves are similar. From this result is possible to conclude that the reactivity loss has as main cause the temperature and not the reactant used.

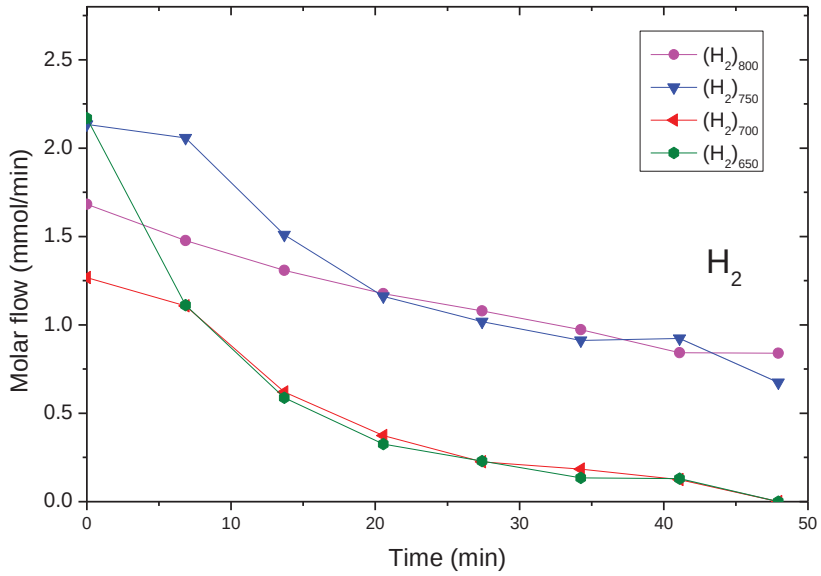

Figure 3.46 – Oxidations at 500 °C after reductions at different temperatures.

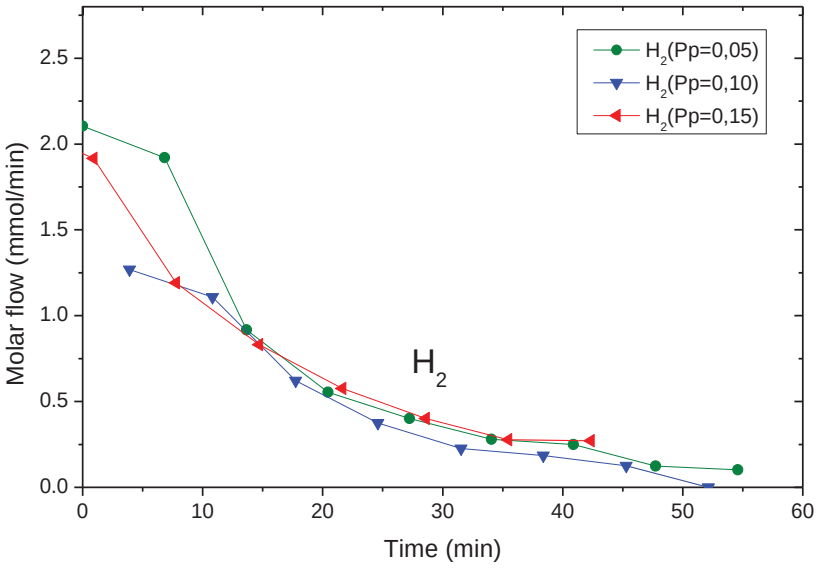

Figure 3.47 – Oxidations at 500 °C after reductions at different reactant flow.

The carbon depositions were analysed by TEM micrograph (figure 3.48) and it has been found carbon nanofibers from iron and nickel particles. The diameter is around 15 nanometres, the same size as the nickel crystallite. In the upside part of the image, there is a piece of nickel aluminate catalyst and is possible to distinguish the nickel over the particle as black points, so the dispersion is high as it can be seen.

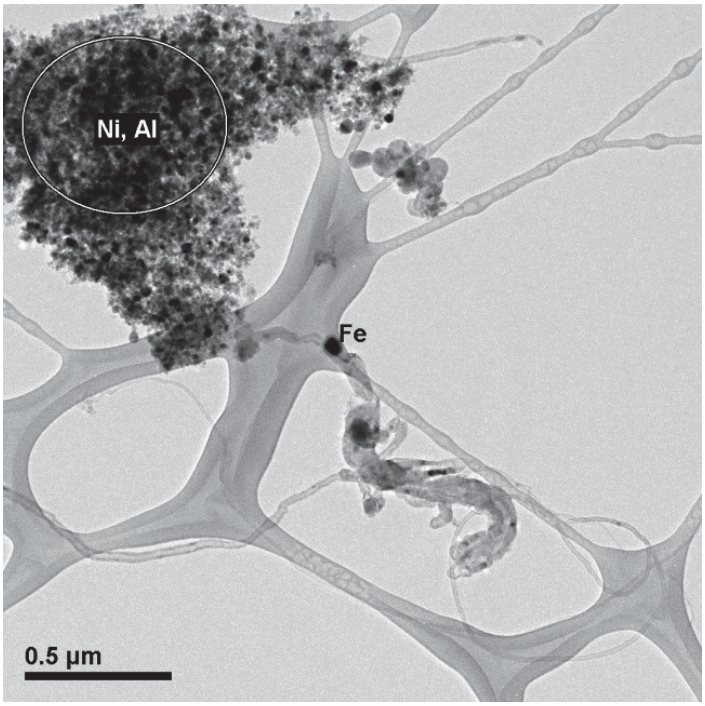

Figure 3.48 –TEM micrograph of the solid after reduction at 650 °C and oxidation at 500 °C.

3.2.7 SYNTHETIC BIO-OIL

The bio-oil is a complex mixture, mainly oxygenated hydrocarbons in which is included every tested compound. The individual behaviour were analysed but it is unknown the crossed effects between them.

The mixture used in the next experiments contained methanol, acetic acid and hydroxyacetone. Moreover, the effect of adding water into the mixture was tested but it is necessary to say that is a different reaction. It changes from catalytic decomposition to steam reforming of the reactant. Because the catalyst is used for the steam reforming, the expected behaviour should not be different when water was used in the mixture.

One of the main necessary characteristics of the reactant should be that it has to be evaporated with no residue because of the experimental setup configuration. Consequently, the sugars and hydrocarbons that polymerize are discarded. The synthetic mixtures were heated overnight and no residue was present. As it is commented in the experimental section, the elemental composition of the bio-oil does not vary substantially according to the process used in the pyrolysis, but the amount of the different compounds changes. The compositions of the mixtures were described in the table 2.2 and they agree to the concentration ranges found in bibliography.

The design of experiments consisted of 6 reactant mixtures and three temperatures (650 °C, 750 °C and 850 °C). The oxidation temperature is fixed in 500 °C. The exhaust gases are analysed by the micro-GC Agilent 490 and the vapours are condensed in the Peltier module. As this section is an extension of the previous tests, the blank experiments are not carried out and it has been used the full solid mixture: oxygen carrier and catalyst.

In the figure 3.49, the results at the lowest temperature, 650 °C and with the mixtures M#1, M#2 and M#3 are shown. In this case, the amount of carbon deposited is so high that is not possible to finish the first cycle. The carbonaceous residue is 34.4%, 40.2% and 43.4% of the carbon fed, respectively for M#1, M#2 and M#3. In the stage B is possible to observe that the equilibrium points are near and separated from the equilibrium, the same gap that appears in all the previous reactants. The reason because they are not identical is due to the high pressure in the reactor that causes some minor error in the GC analysis.

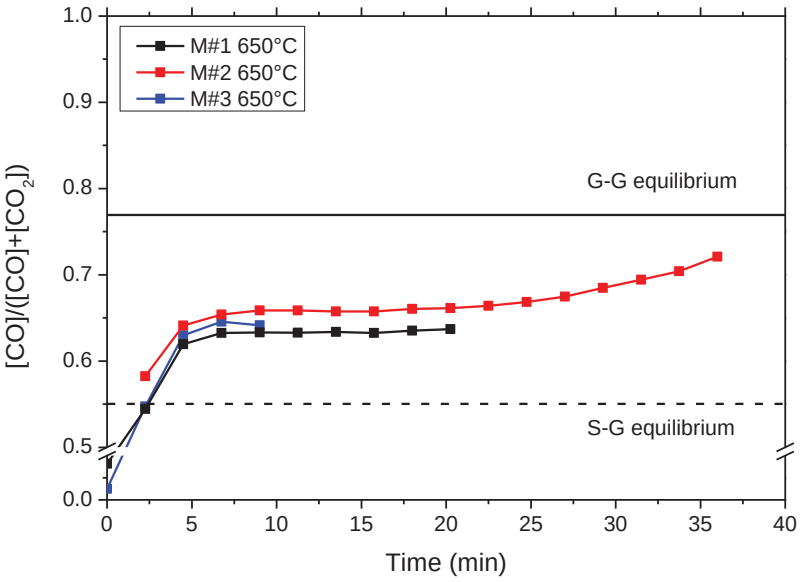

Figure 3.49 –CO ratio in the reductions at 650 °C with different bio-oil compositions (M#1, M#2 and M#3).

At 850 °C, the observed behaviour was coincident in the mixtures M#1, M#2 and M#3 (figure 3.50). The solid conversion in the first cycle finishes in 30 minutes. The stage A is fast and lasts 5 minutes. Then, the stage B has no constant conversion over the solid reaction caused by the high temperature used and the thermal stress suffered at 850 °C. The separation from the theoretical equilibrium is the gap observed in all the reactants and has a value of around 0.1 units of ratio. The time to full conversion decreases in every cycle from 25 minutes to 15 and finally 7 minutes in the third cycle, so it is patent the reactivity loss of the solid. Despite the three mixtures has different species composition but similar elemental composition, the curves are coincident and it is possible to conclude that the behaviour of the reduction depends on the elemental composition of the reactant and not the functional groups. According to the catalyst, in all the cycles and mixtures, the equilibrium is reached and there is no deactivation.

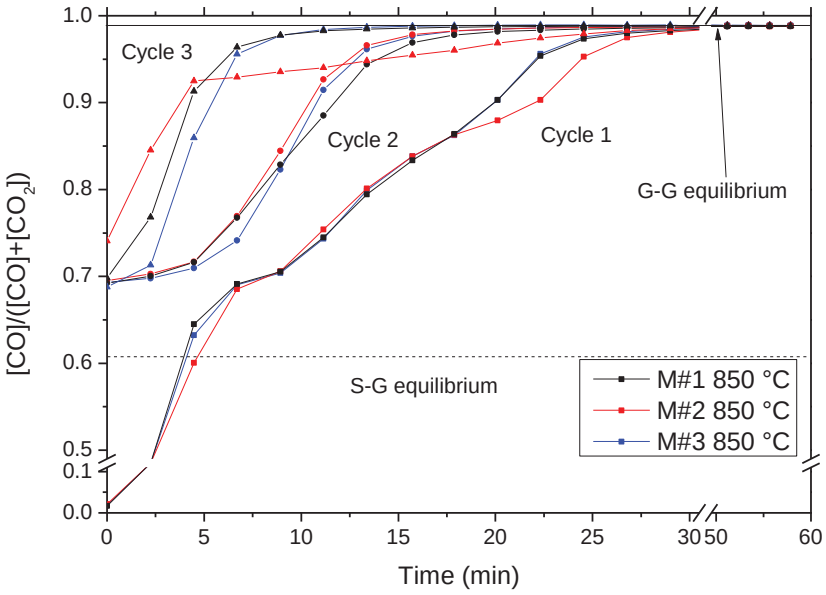

Figure 3.50 – Temporal evolution of the CO ratios in the reductions at 850 °C with different compositions of synthetic bio-oil.

At mid temperature, 750 °C, the average mixture from M#1, M#2 and M#3, numbered as M#4 is tested beside the M#4 with 15% (M#4+15) and 30% (M#4+30) of water. As the water is an oxidant, the reductant capacity is decreased and consequently the gas-gas theoretical equilibrium is found at lower hydrogen and carbon monoxide ratios. The difference between the two theoretical equilibriums is reduced and the rate of oxygen depleted is diminished. In the figure 3.51, the reductions with these mixtures at 750 °C are presented. The M#4 mixture is able to reduce the solid in only 25 minutes, the M#4+15 mixture around 35 minutes and the M#4+30 mixture lasts 100 minutes to reduce it. In the other way, the higher the amount of elemental oxygen in the inlet stream, the carbon deposition is reduced or even avoided. Indeed, the samples with water do not produce carbonaceous residue and the M#4 mixture has a carbon mass balance of 25%. This fact permits to work up to 3 cycles in the wet mixtures. A common effect is that along the cycles the reactivity was decreasing and the reaction rate too. The sinterization and the thermal stress are unavoidable at this temperature. At this point, the crossed effects of the model compounds were not observed

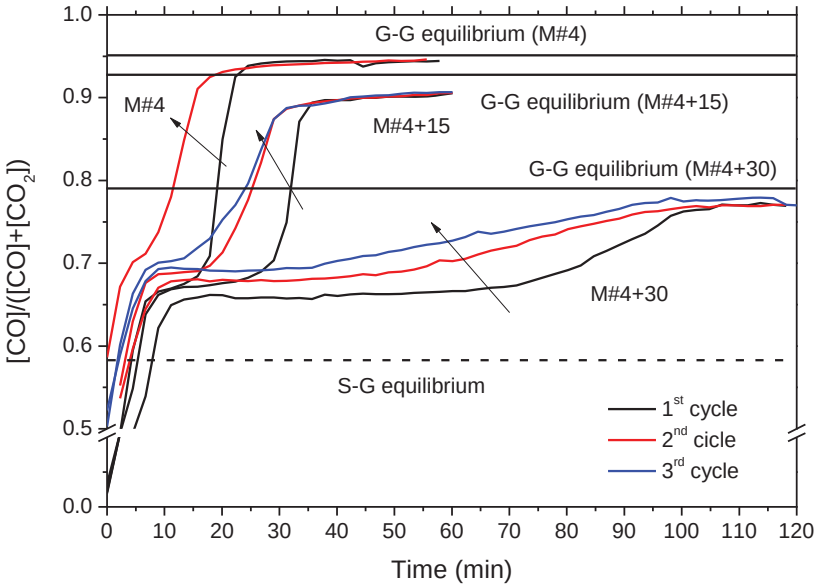

Figure 3.51 – Temporal evolution of the CO ratios in the reductions at 750 °C with different wetness in the synthetic bio-oil.

The behaviour along a higher number of cycles is shown in the figure 3.52. The mixture selected was the M#4 and the time of experiment was decreased to exclusively the conversion of the solid, trying to avoid extra time that deposits more coke in the stage C. In a scaling up, the carbon should be burn with air every some cycles to avoid the clog. In the figure the CO ratio of ten cycles is represented and is shown how the reactivity is lost along the cycles without regeneration step. In the stage B, the solid-gas equilibrium begins with a gap that increases over the cycles due to lower reaction rates. In the third cycle, the gas-gas equilibrium is reached in all the reductions and confirms that the catalyst is not deactivated after 4 hours of reduction and 10 hours of oxidation.

The oxidations are represented in the figure 3.53 and the loss of reactivity caused by the thermal stress is observed along the cycles. In this case, above the third cycle, the curve is similar in which the maximum conversion reached is 35%. It was found in the exhaust gases CO_2 with a concentration of around 0.5% as maximum, but no carbon monoxide was detected.

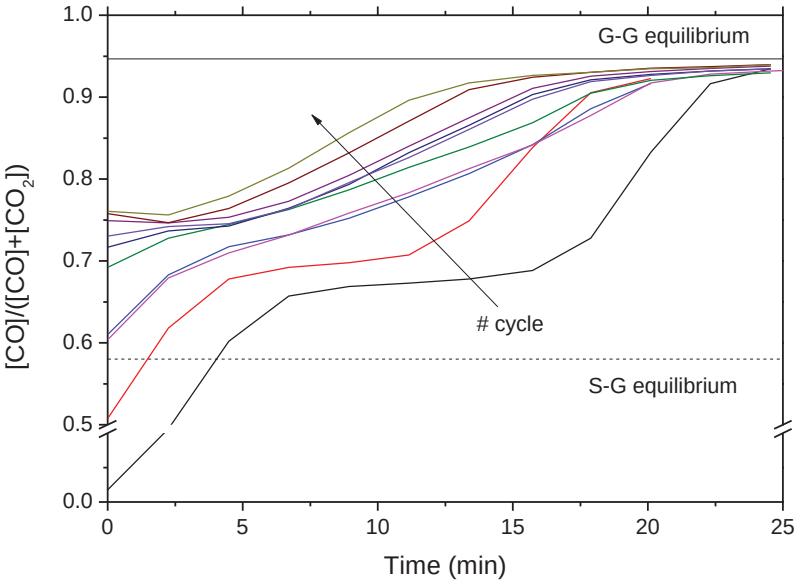

Figure 3.52 – Temporal evolution of the CO ratios in the reduction at 750 °C with the mixture M#4.

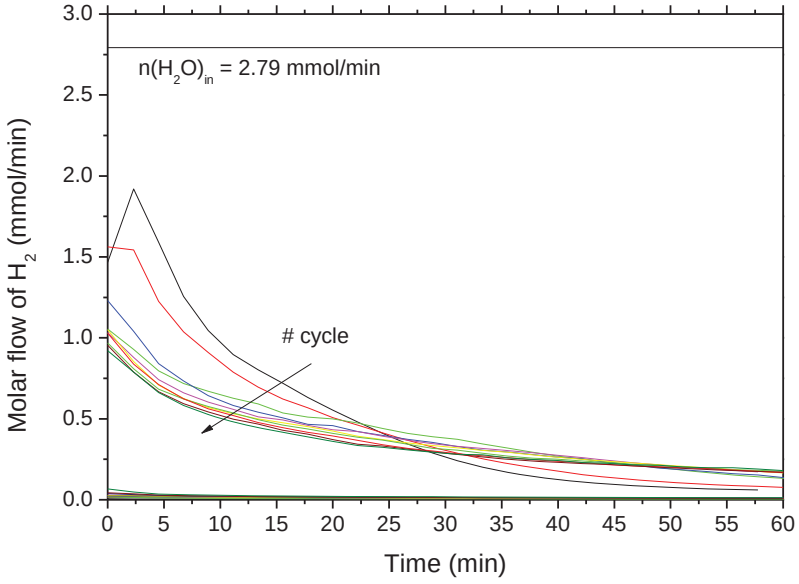

Figure 3.53 – Oxidations at 500 °C after the reductions at 750 °C along 10 cycles

To summarize, the hydrogen yield with every mixture at different temperatures and number of cycles is represented in the figure 3.54. At low temperatures, the carbon deposition is too high for completing more than one cycle, and the hydrogen generated in the next oxidation is proportional to the conversion of solid in the reduction. At high temperatures, it is possible to work during 3 cycles but the amount of hydrogen generated in 60 minutes

(fixed time in all the oxidations) is less than at mid temperatures because the low average solid conversion. The effect of varying water in the mixture on hydrogen yield is compared at mid temperatures. The best yields are obtained in the case of no water addition, but due to the carbonaceous residue, the number of cycle reached is only two. In other mixtures with water, a third cycle is reached with slightly lower hydrogen yield. The best results are obtained in the case of M#4+15 that corresponds to a low water content bio-oil (15% water) but it is still in the limits of real pyrolytic oil according to bibliography.

Regarding the 10 cycle results (when reduction lasts until stage B ends), the loss of reactivity is around 3% per cycle. Despite the increase in the number of cycles, the reduction capacity greatly decreases. On the other side, the catalyst has been suitable to be used continuously without any deactivation during 14 hours, time of the 10 redox cycles.

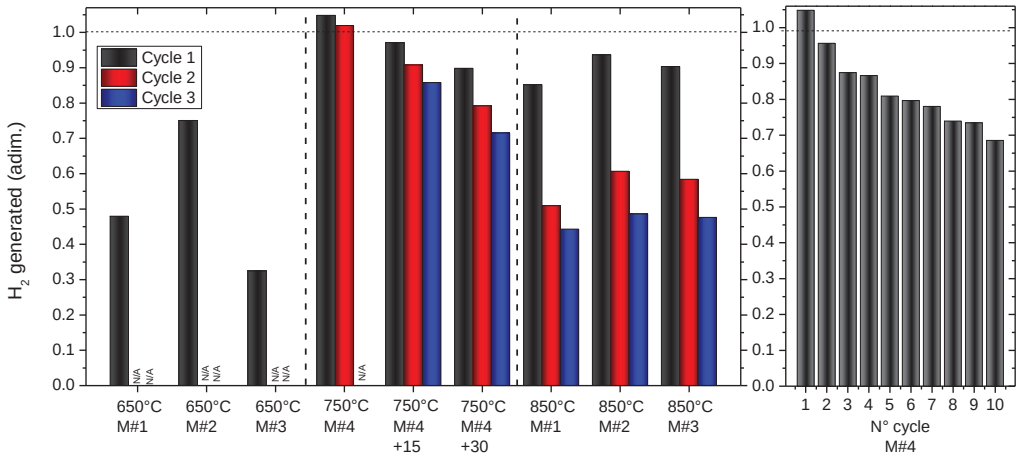

Figure 3.54 – Comparison of the hydrogen yield depending on the temperature, number of cycle and reactant mixture.

To sum up, the optimal working conditions in the reduction stage is a temperature of 750 °C in which the sinterization of the oxygen carrier and the carbon formation are reduced. The best mixture to be used is the low wetness bio-oil in which the water content is around 15%. Using this mixture the carbon formation is totally avoided.

3.3 EXPERIMENTAL SUMMARY

In this chapter the most relevant results from the experimental work are reviewed. The full solid was tested in a packed bed reactor of small size using as reactant gases, individual model compounds and mixtures similar to a real bio-oil according to bibliography. The test temperature was varied from 600 °C to 850 °C. Only the alcohols were tested with oxygen carrier and no catalyst. As they were able to decompose into equilibrium, the final conclusions are applicable also to them.

In the reduction step with every model compound, the three stages were observed in which the iron oxide pass through all the oxidation degrees. The stage A lasts only 5 minutes in all the cases and corresponds to the conversion of Fe_2O_3 into Fe_3O_4. There is no thermodynamic limitation and the conversion is 100% into H_2O and CO_2. It is similar to air combustion but is carried out with the lattice oxygen. An exceptional case was the biogas in which at low temperatures the reaction increases because the catalyst was activated in longer times.

The stage B is the reduction from Fe_3O_4 to metallic iron and is the most important of the process. This is the limiting reaction for hydrogen obtaining. The fact is that the hydrogen generated in the oxidation is proportional to the oxygen carrier conversion in the reduction. The conversion of the iron oxide proceeds in all the cases and the reduction time decreases at higher temperatures. At the beginning of the stage the conversion is the maximum possible and then slowly decreases. This behaviour is compatible with the shrinking core model controlled by the reaction in which the rate is proportional to the reaction surface inside the particle.

Along the cycles, the reduction capacity greatly decreases. The most favourable conditions were at mid temperature, 750 °C, and the mixture M#4 as the reactant. After 10 cycles is possible to obtain a hydrogen yield of 68% with a linear decreasing. The goal of this work is not to optimise the oxygen carrier but an optimization of the solid would enhance the process.

There are two main concepts in the solid-gas reactions involved. The **reaction rate** corresponds to that between reductants (hydrogen and carbon monoxide) and iron oxide. The reaction zone is found in a front in the fixed bed and its size varies depending on the kinetics. At higher rates the front is shortened and vice versa (figure 3.55a). When the gases leave this zone, they

are totally converted into its possible maximum. Due to the dynamic behaviour of the process, it is only possible to see the kinetics when this zone arrives at the final of the bed. The second concept is the **reaction time** that corresponds to that for the total conversion of the solid (figure 3.55b). Due to the thermodynamic limitations, this time depends on the difference between solid-gas and gas-gas equilibriums. So, the oxygen depleted per unit of time is fixed. Thus, it is possible to find a high reaction rate with the highest reaction times. This happens in the reactions at low temperatures in which there is no thermal stress but the difference between the lines in the BG diagram is lower than at high temperatures. In the opposite point, at higher temperatures the reaction rate is lower because of the sinterization but the times are decreased.

Once the iron oxide is totally reduced, the stage C presents the equilibrium composition when only the catalyst is in its active phase. It is assumed that the iron oxide finds this mix of gases from decomposition or reforming at the beginning of the reactor. All the reactants, except the biogas in some conditions, are able to achieve the equilibrium conversion. The controlling step is the decomposition of the methane and is the reason because a reforming catalyst is selected as most suitable. Thus, the catalyst is determinant for the efficiency of the process because it is necessary to produce reductants as fast as possible up to equilibrium conversion. In this sense, the reduction times are shortened.

In an attempt to summarize all the results in one image, the BG diagram is used and the equilibriums points of every liquid reactant are represented in the figure 3.56. The theoretical curve for the solid-gas equilibrium (correspondent to stage B) is constant because the reaction is the same in all the cases: reduction of carbon monoxide (and hydrogen) with iron oxide. But in the gas-gas equilibrium (correspondent to stage C), the curves change depending on the elemental composition of the reactant and its concentration. In the catalytic decomposition, the experimental values are close to the theoretical lines. In the stage B, there is a separation between them with a constant value depending on the reactant. The alcohols differ from the rest and the cause is not clear, but if the figure 3.57 is observed, the amount of carbon monoxide that produces is low. Despite this finding, it is assumed that there is a constant gap along the temperature in which the worst scenario is that the value of separation is 0.1 units of CO ratio.

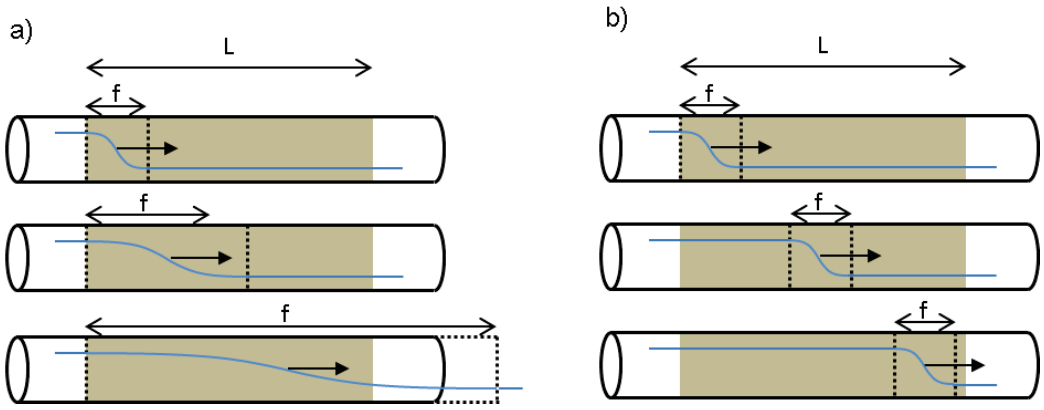

Figure 3.55 – Reactant concentration at different reaction rates (a) and the travelling front (b) (L: length of the packed bed and f: reaction front).

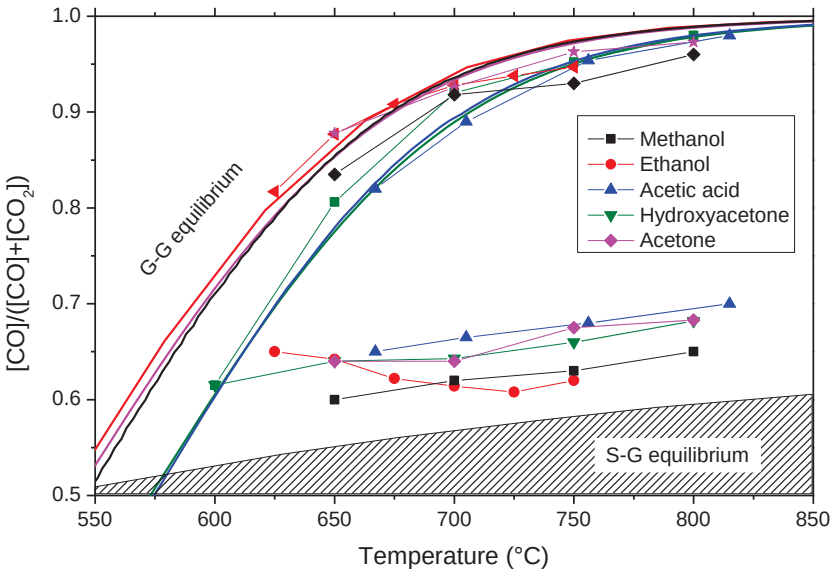

Figure 3.56 –CO ratios in the first cycle with different reactants.

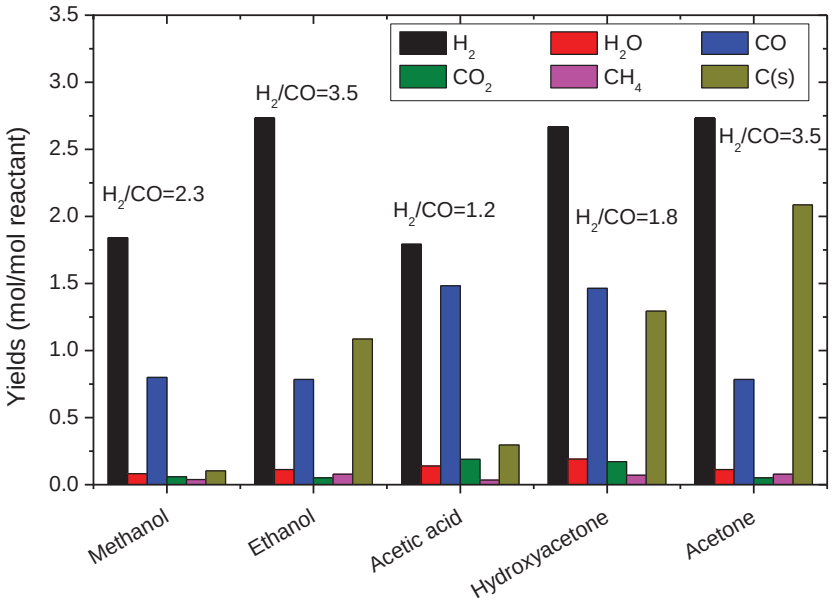

Figure 3.57 – Composition after decomposition reaction of the different model compounds.

There are some hypotheses for the gap presented between the equilibriums and are based on three key points:

- The iron oxides, apart from different oxidation degrees, can present different phases. At working temperature, the iron is in α phase but above 912 °C it could convert into γ phase (Darken and Gurry 1945, 1946). The magnetite does not suffer any change in its structure. The reaction enthalpies only depends on the specie, but the specific heat varies from one phase to another. In the thermodynamic databases, different values for every compound are presented and consequently the Gibbs energy changes. The weak point for this hypothesis is that the oxygen-iron system is extensively studied and the values for the databases are precise.
- Respect to the kinetics, the reaction rate equation is composed of three factors: kinetic constant that depends on the temperature, gas conversion that is limited by the equilibrium constant and solid conversion in which the adopted model is de shrinking core model (eq 3.1). The only factor that depends on the equilibrium is the gas conversion and it should depend on another parameter that is not taken into account. According to the mentioned diffusional restrictions of the gases to pass through the iron oxide layers, there is some evidences that the water is accumulated in the reaction zone

(Gupta 2006). As there is equilibrium between all the present species, the composition is related to the diffusional restriction of the water.

$$(-r_i) = k(T)\cdot\left(P_i - \frac{P_i^*}{K_{obs}(T)}\right)\cdot(1 - X_{sol})^{2/3} \qquad \text{(eq 3.1)}$$

- Another supposition is that the experimental temperature in the bed is slightly lower than the working temperature. In the acetic acid experiments, it is possible to see the difference between the reactor and the oven temperatures. At the beginning of the experiment there is a drop of 30-50 °C and after some minutes achieves the set temperature. Lower CO ratios correspond to a higher oxygen amount in the gases. After the gases pass this cold spots, placed in the reaction zone, they are heated at set temperature at the end of the reactor. In the figure 3.58 is exemplified this pathway: point A is the CO ratio after the decomposition of ethanol, then the iron oxide is reduced and the next point B is at lower temperature in the limit conversion. Finally at the end of the reactor, the point C is at set temperature but the way is through the same elemental composition. This last point is the weakness of the theory because at this zone, the iron oxide could be reduced further. A gap of 0.1 corresponds theoretically to a cold spot 200 °C lower than the working temperature. This is higher than the adiabatic temperature, around 60 °C less (it is not possible less temperature than this).

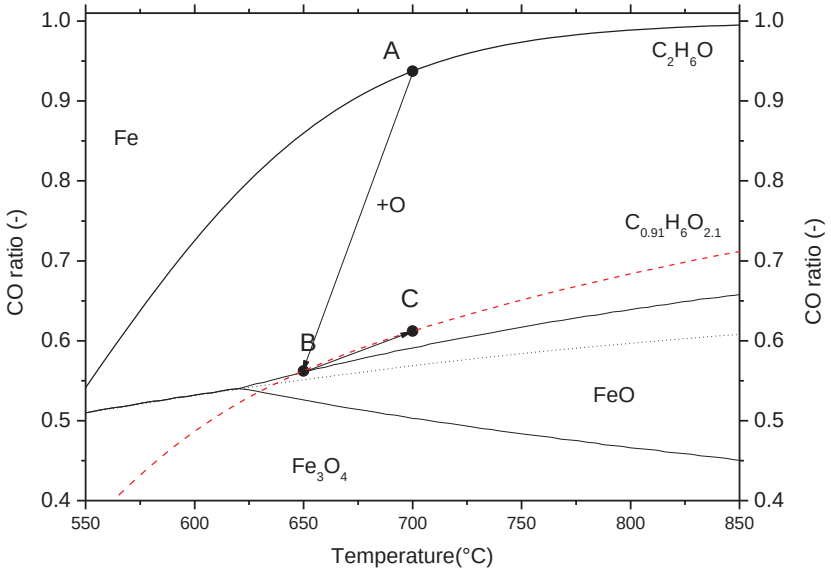

Figure 3.58 – Pathway proposed based on the cold spots theory.

All the hypotheses have its weakness, but the most possible is a combination of them. The cold spots theory and the water accumulation in the reaction zone are facts corroborated by bibliography.

One of the important variables studied was the amount of water in the reactant. Two synthetic bio-oils were prepared with 15% and 30% of water. Longer reduction times are expected because water is an oxidant and is the product of the reactions. For 15% of water the time rises 10 minutes and in 30% achieves 100 minutes of reaction. As it is not possible to eliminate the water from the pyrolytic oils, the time increases but the carbonaceous residue is avoided. According to the accumulation of water hypothesis, these experiments should present higher CO ratios, but the gap was the same as the other reactants in the solid-gas equilibrium (stage B).

After the reduction step is assured, the oxidation is carried out. The operating temperature was in almost all the cases 500 °C, so the kinetic constant should be the same. As it was observed, it varies depending on the temperature and the number of cycle. Both variables are related to the thermal stress suffered by the iron oxide. Thus, the most favourable conditions are a temperature between 700 and 750 °C that ensure low coke deposition and a minimum loss of reactivity. In the oxidation the length of the reaction zone (f) is bigger than the packed bed (L), so the reaction rate is the evolution of the molar flow from the beginning of the reaction (example shown in the third case of the figure 3.55a). In the 10 cycles experiment, the oxidation curve above the 4^{th} cycle is almost identical and this is a sign of constant kinetics. This is a residual reactivity of 60% of the total solid. Future work could be focused on increase the alumina and ceria amount in order to increase the thermal resistance.

The quantity of carbonaceous residue was verified by indirect calculations from the carbon mass balance and agrees with the theoretical. The direct quantification by weighting is not used because the final solid depends on various factors as possible gasification or chaotic accumulation in the reductions. The model compounds with high ratios C/O and C/H favours the deposition of carbon. The most unfavourable case is the acetone (C_3H_6O) in which the 70% of the carbon fed is deposited, corresponding to 28mg/min. In the opposite, the methanol generates 1.4mg/min. The synthetic bio-oil M#4+15 produces 0.26mg/min.

The deposition at the beginning of the packed bed is favoured as it is confirmed by direct observation. Thus, the catalytic decomposition happens

very fast at this point and then the gases (mainly hydrogen and carbon monoxide) pass through the bed. As the carbon is produced as carbon nanofibers, these grow and need more reactant.

In the characterization of the samples, in TEM micrograph two types of structures were observed depending on the metal. The iron oxide after reduction is able to create hollowed carbonaceous structures with a diameter of 20 and 50 nanometres. The nickel catalyst produces carbon nanofibers of 20 nanometres. The difference between them is the size of the crystallite and in the case of iron oxide, the shape is more irregular. In Raman spectroscopy is possible to see the disorder degree of the coke before and after oxidations by comparing the D band (1350 cm^{-1}) and G band (1580 cm^{-1}). In all the cases the spectra are identical and consequently the carbon acts as inert at the oxidation operating conditions.

4 MODELLING

In this section the phenomena that happen during the reduction and oxidation are studied. Two levels of approach are used to analyse the reactions involved in the packed bed. First, a simple model based in the stoichiometry of the process and then a rigorous model implementing the fixed bed equations. From the last one, the kinetic constants are obtained by fitting the molar flows of the gases and the behaviour at different operating conditions could be predicted.

4.1 MODELLING OF FIXED BED REACTORS

Two methods were selected to study the behaviour of the fixed bed reactor in non-steady state:

- Equilibrium and maximum reaction: only the stoichiometry and the thermodynamic equilibriums between species are taken into account. The reaction times and the maximum adiabatic temperatures are calculated approximately. This is explained in the first part of the section.
- Mass balances in fixed bed reactor: Through mathematical modelling, a numerical solution is obtained based on finites differences method. Some simplifications as pressure and temperature constants are supposed due to the dilution of the reactants. This is the rigorous model explained in the second part of the section.

According to the experimental results obtained in thermobalance and in fixed bed reactor, only the mass balances are comparable. For the energy balances, measures along the reactor with thermocouples are needed. Due to the small size of the reactor, this is not possible.

Moreover, the reactions involved are numerous and with the thermogravimetry data is not possible to elucidate the elemental reactions that compose the full reaction pathway. The gases composition is practically controlled by the thermodynamic at operating temperature and also limited by the oxygen transfer rate between solid and gas. The main reactions are the reduction with hydrogen and carbon monoxide of the Fe_3O_4. The fastest

reaction controls the solid conversion and the composition of the gases because both are working in parallel. In this case, the reduction with hydrogen is the fastest (Tokuda et al. 1973; Jozwiak et al. 2007) and both are related by the water gas-shift reaction (r 2.7).

4.2 BASIC MODEL

All the reactions that take place in the packed bed reactor could be included in equilibrium reactors in which minimization of Gibbs energy is assumed. The three stages (two since the second cycle) could be explained as a shock-wave that corresponds to the instant reaction along the reactor in axial direction.

The first assumption in the stoichiometric model is that the reactant is totally decomposed in H_2, H_2O, CO, CO_2, CH_4 y C at the very beginning of the reactor. Due to vapours of unreacted biofuel were not found, even when iron oxide is full converted, the catalyst is active enough for the decomposition before the solid-gas reaction zone (stage B).

In the stage A in which Fe_2O_3 is converted into Fe_3O_4, the reaction is total an irreversible and the reductants (hydrogen, carbon monoxide and methane) are converted into carbon dioxide and water. Due to the conversion is 100% and the oxygen depleted is only 11% of the total, the duration is very short.

The relation between the duration of stage A (t_a) and the duration of stage B (t_b) at a temperature of 750 °C, pure hydrogen fed and conversion equals to that from the experimental equilibrium (theoretical equilibrium plus 0.1), is around 30 times more (eq 4.1).

$$\frac{t_a}{t_b} = \frac{0,89 \cdot n_{O\,total,sol} / \dot{n}_{H_2} \cdot X_{eq,obs,a}}{0,11 \cdot n_{O\,total,sol} / \dot{n}_{H_2} \cdot X_{eq,obs,b}} = \frac{0,89 / 0.258}{0,11} = 31,4 \qquad \text{(eq 4.1)}$$

where

t_i : duration of the stage i

$n_{O\,total,sol}$: moles of oxygen in the solid

$\dot{n}_{H_2}$: molar flow of hydrogen

$X_{eq,obs,i}$: observed equilibrium conversion of the stage i

The stage B is the most important due to it is repeated over the cycles in both reaction senses. In bibliography there are some studies that mark the reduction of FeO into Fe as the limiting step (Tokuda et al. 1973; Gupta 2006; Pineau et al. 2007). Experimentally it was not observed and only the reduction of Fe_3O_4 into Fe is assumed. Consequently, the theoretical curve used is this one. The experimental equilibrium conversion found is the theoretical displaced a value of 0.1. This value is conservative considering that in some case the gap was lower. In this stage, the 89% of the oxygen lattice is consumed and is limited by the thermodynamics regardless of the reactant and the total pressure in the reactor.

The stage C corresponds to the time after the oxygen carrier is converted, so the composition is exactly the catalytic decomposition. In all the cases, except at low temperatures with biogas, the experimental and the theoretical gases concentration agree.

In the figure 4.1, a conceptual example of the evolution of hydrogen ratio along the reactor is represented. Once the unreacted solid and the gas make contact, they react instantly and the steam generated reduces the hydrogen ratio up to the equilibrium. This profile is the reaction front and moves along the reactor with a velocity that depends on the amount of oxygen carrier and the partial pressure of reactant. In the basic model, the reaction rate is supposed maximum and the reaction front is similar to a step that travels in axial direction.

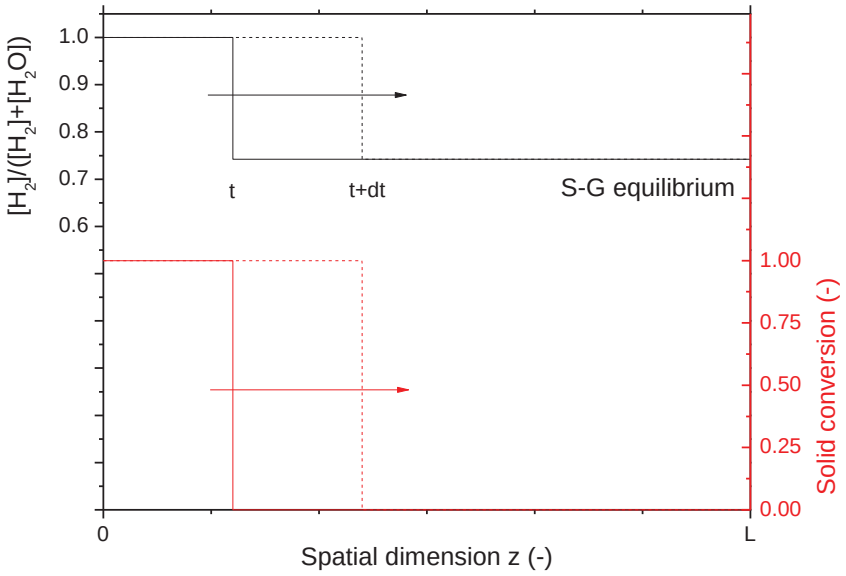

Figure 4.1 – Spatial evolution of the hydrogen ratio (black) and the solid conversion (red) inside the reactor during the reduction with hydrogen.

Feeding biofuel, taking into account only the elemental composition, the behaviour is totally similar but the rate of the oxygen depleted is higher. Therefore the duration of the stages are shortened. Hydrocarbons are able to obtain more oxygen from the solid because they decomposed into more than one mole of hydrogen and carbon monoxide. For example, the amount of oxygen captured with the mixture M#4+15 is 2.3 times higher than with pure hydrogen when is calculated by minimization of Gibbs energy.

In the energy balance of the reactor, some aspects are taken into account: full conversion of Fe_3O_4, gases composition from the catalytic decomposition of M#4+15 at 750 °C and the equilibrium is assigned to the theoretical plus 10%. The calculations are made with the software HSC 5.1. Experimentally, the solid and the gas are diluted in sand and inert gas. With inert species the temperature that corresponds to the gradient of adiabatic maximum temperature is 687 °C, so it decreases because is an endothermic reaction. In a real application in which all the inert is eliminated from the reactor, the temperature is 542 °C. If the energy balances are applied to the reactor and the front zone, the temperature front travels with the same velocity as the reaction front (figure 4.2). The assumptions are that there is no resistance to the heat transfer between solid and gas. Before the reaction zone, the temperature is set by the inlet gas and after this, the energy consumed by the reaction decrease the temperature of the gas and the solid. The progression of the temperature after the reaction zone is that it increases because of the heat provided by the solid and the oven to the gas.

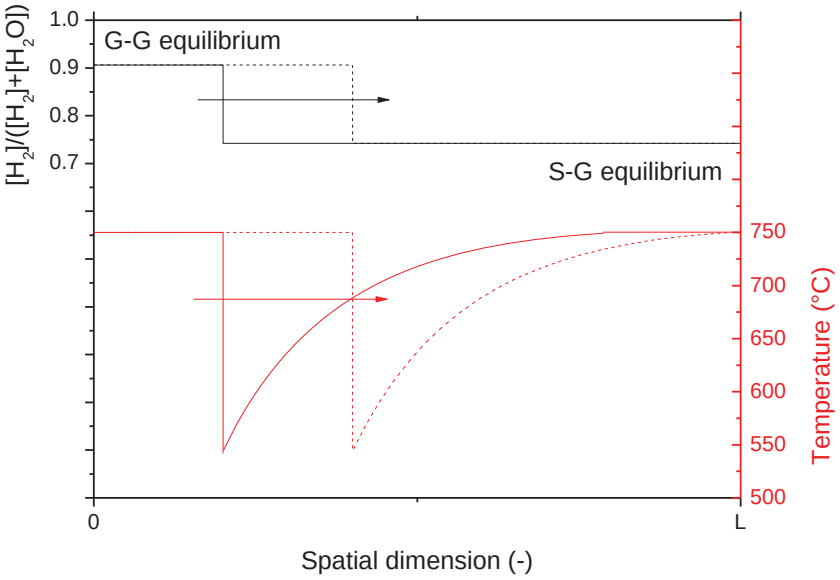

Figure 4.2 – Evolution of the hydrogen ratio (black) and the hypothetical temperature profile (red) during the reduction with synthetic bio-oil (M#4+15)

The oxidation happens in a similar way with both fronts, but due to the reaction is exothermic, the adiabatic temperature is higher than the set temperature, in this case 615 °C with inert solid and gas and 790 °C without them. The hot spots produced by this higher temperature could gasify the coke previously deposited and unfortunately lower the efficiency of the process.

One of the hypotheses for the separation from the equilibrium was the decreasing of temperature during the reaction. This is supported partially because the temperature reached is not enough. Besides this, a kinetic effect that slow down the reaction rate when is near to the equilibrium is needed to explain the behaviour. A diffusional restriction in which the amount of products, water or carbon dioxide, is high agrees with a composition near to equilibrium. So the accumulation of water inside the particle is supported by the combination of the two hypotheses.

4.3 DETAILED MODEL

In a real reactor, the reaction fronts are smoother than the previous section and the shape is similar to a sigmoid. This is because changes from an ideal instant reaction to real kinetics. In an operation a big scale, it is preferable the thinnest reaction zone possible to keep a stable conversion along the time and enhance the control of the process. Moreover, modelling the reactor with higher detail level is possible to obtain more knowledge from the kinetics.

The assumptions are:

- Radial mass dispersion negligible due to small scale.
- Axial mass dispersion included.
- Isothermal reactor since there are low temperature profiles.
- Constant pressure (1 bar) due to the size of the reactor and the dilution of the reactants.

4.3.1 MATHEMATICAL EXPLANATION

The equations that govern the behaviour of the species in a fixed bed reactor with mass dispersion and solid-gas reaction are described in the table 4.1.

To find the solution is necessary to use numerical calculus algorithms in spatial and temporal dimensions. There are two groups to solve the equations in partial derivatives: finite elements and finites differences. From these, it has been used the second one for simplicity in the implementation.

Table 4.1 – Detailed model equations

Mass balances (gas phase)	
$\frac{\partial \dot{n}_i}{\partial t} + u_s \cdot \frac{\partial \dot{n}_i}{\partial z} - D_{eff} \frac{\partial^2 \dot{n}_i}{\partial z^2} = \dot{V} \cdot r_i$	(eq 4.2)
Mass balances (solid phase)	
$\frac{\partial n_{sol}}{\partial t} = V \cdot r_i$	(eq 4.3)
Kinetic equation, SCM	
$r_i = 3 \cdot b \cdot k \cdot \left(C_i - C_i^* / K_{eq} \right) \cdot (1 - X)^{2/3}$	(eq 4.4)
Axial dispersion (Edwards and Richardson 1970)	
$D_{eff} = \left(\frac{0.73}{Re \cdot Sc} + \frac{0.5}{\varepsilon + \frac{9.7 \cdot \varepsilon^2}{Re \cdot Sc}} \right) \cdot u_s \cdot d_p$	(eq 4.5)

where

$\dot{n}_i$: molar flow of specie i (mmol/min)

u_s : superficial velocity (cm/s)

D_{eff} : diffusion coefficient (cm²/s)

$\dot{V}$: volumetric flow of gases (cm³/s)

V : reactor volume (cm³)

r_i : reaction rate (mmol/s·cm³)

n_{sol} : amount of initial solid (mmol)

b : stoichiometric ratio (-)

k : kinetic constant (s^{-1})

C_i : concentration of the specie i (mmol/cm³)

C_i^* : concentration of the specie i in the equilibrium (mmol/cm³)

K_{eq} : equilibrium constant (-)

X : solid conversion (-)

Re : Number of Reynolds (-)

Sc : Number of Schmidt (-)

ε : porosity (-)

d_p : particle diameter (cm)

From the discretization of the equations, the explicit and implicit methods appear. In the explicit method the calculation is iterative along the spatial dimension and direct from previous known values. In the implicit methods, it is necessary to solve the full system of linear equations in every temporal interval. Every method has its strengths and weaknesses. In the explicit method, the implementation is easy and stable but the mesh is very restrictive and the time for obtaining the solution is very high. In the case of the implicit methods, they are harder to implement because of the use of big matrix, but the solutions are more exact and the times to obtain them are much shorter. The selected method is the implicit for solving the system of derivatives partial equations.

The solving method is the Crank-Nicolson (Crank and Nicolson 1947). The precision is of second order respect time and space, while the Euler methods are only of first order precision. The spatial discretization is done from the previous and next point (j in the figure 4.3). The temporal is from the next point because of stability issues (n in the figure 4.3). After the discretization, the boundary conditions are applied. At the beginning there is Dirichlet condition (constant concentration) and at the end Neumann type conditions (constant normal flow). In both conditions order 2 discretization are used.

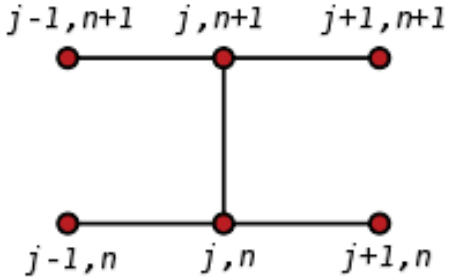

Figure 4.3 – Crank-Nicolson stencil for solving PDE.

Usually, the Courant-Friedrichs-Lewy (CFL=$u_s/(\Delta z/\Delta t)$) condition is checked in order to verify how restrictive is the numeric problem. In the formula, "u_s" is the superficial velocity, "Δz" the spatial mesh size and "Δt" the temporal mesh size. This is a relation between the velocity of the flow in the reactor and the numerical velocity. For an explicit method is mandatory that the velocity of the numerical propagation is higher than the velocity of the flow. In the implicit methods it is not necessary and it is possible to work at higher values. In this case is important because the mesh is stretched in temporal direction.

Another necessary condition in second derivative problems is that the number of spatial intervals must be more than $n_{min}=u_s \cdot L/2 \cdot D$ or Δz less than $2 \cdot D/u$. Assuring this, the mass diffusion is higher than the numerical one and the solution is stable and precise.

Due to the model used for the solid-gas reaction is the shrinking core model (conversion term powered to 2/3), the equations to solve must be linearized. Then, in every temporal iteration, a sub-loop is added to calculate the reaction rate below a fixed error. This loop is very useful in sudden transitions found at the beginning of the reactor or in reaction zones in which the kinetics constant are high. For decreasing even more the time of calculus the Jacobian matrix is included in the algorithm.

4.3.2 KINETIC EXPLANATION

The adopted simplifications in the model are catalytic decomposition at the beginning of the reactor and the shrinking core model as kinetic model for the solid-gas reaction.

For the first one, an energy Gibbs minimization algorithm is build using an iterative solver for a Lagrange multipliers method explained in (Perry and Green 2007). The initial values used are near to the experimental values expected. All the elemental hydrogen found as molecular hydrogen, the CO concentration is equal to the elemental oxygen and the rest is near to zero.

Once the equilibrium composition is calculated, it is introduced into the model as initial composition of the gases. In this way, a pseudo temporal interval "-1" is created in which the catalytic decomposition is total and instantaneous. In the same way, the supposition that the functional groups are not affecting the solution is implemented.

The solid-gas reaction that is selected is the shrinking core model modified in order to obey the equilibrium reactions. The kinetic and the equilibrium term are both based on experimental results. The global kinetic constant depends on the external diffusion of the gases to the particle, the internal diffusion to the reaction zone and the chemical reaction. From these, the external diffusion is neglected but the others are not possible. In the experiments, the equilibrium compositions were displaced a value of 0.1. Thus, an observable equilibrium constant is used in the kinetic equation.

Other kinetic equations discarded were order 1 for the solid, order 1/2 that corresponds to the shrinking model for 2 dimensions and nucleation model as the Avrami or Johnson-Mehl-Avrami-Kolmogorov (JMAK) model. Although the JMAK model fits well the previous work at 500 °C (Plou et al. 2012), it seems not valid for our current packed bed results.

In order to obtain rigorously the kinetic and equilibrium constants, it should be necessary to co-feed different compositions of the 5 gases involved in the reaction in a wide range of temperatures. This experimental work is proposed for future work. The solution carried out was the fitting of the packed bed results.

4.3.3 Model validation

Once the packed bed model is built and checking that there are no numerical problems, it is necessary to check by external results the suitability of the model. The experimental work used is that from P. Hamers (Hamers et al. 2014). Their model is validated from previous works (Smit et al. 2005; Noorman and van Sint Annaland 2007; Tiemersma 2010). The reaction is the cupper oxidation for Chemical Looping Combustion (CLC) in packed bed (r 4.1). This work includes mass and energy balance because in the experimental, the evolution of the temperature profile is measure by thermocouples along the reactor. For the validation, only the mass balance is taken into account.

$$O_2 + 2Cu \rightarrow 2CuO \qquad \text{(r 4.1)}$$

The kinetic is the same as in other works of the same group (Smit et al. 2005; Noorman and van Sint Annaland 2007; Tiemersma 2010). For simplicity, the kinetic and Jacobian functions are obtained by interpolation of discrete points.

In the figure 4.4 the comparison between the models is represented. The difference between both are minimal and the error, calculated as the time to achieve full conversion, is less than 5%. The sources of error are that there is a decreasing in the flow that is not contemplated in the own model and the kinetic varies according to the temperature profile along the reactor, neither implemented into the code.

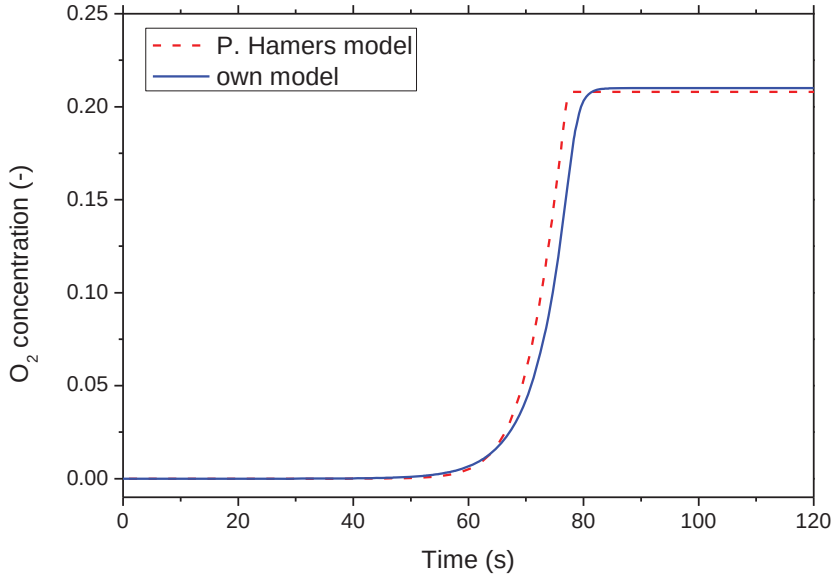

Figure 4.4 – Comparison between the P. Hamers model and own model in the oxidation of cupper in a packed bed.

4.3.4 Integral data fitting

Due to it is not possible to obtain the kinetic constants from the thermogravimetric analysis according to operating conditions in the packed bed, they are calculated from fitting the model and the experimental results with the different liquid reactants.

In this fitting method is inherent that it is only possible to obtain one kinetic constant that corresponds to the most influential reaction, in this case, the reduction with hydrogen because is the fastest (Tokuda et al. 1973; Jozwiak et al. 2007). There is a limit in the reaction in which if the reaction rate is too fast, the mass diffusion controls the evolution of the gases instead of the chemical reaction because is slower. The best advantage of this method is the low number of experiments needed to obtain the kinetic constants because the thermogravimetry analyses are avoided. By this manner, it is crucial to obtain a good numerical resolution that lowers the errors.

In the figure 4.5, an example is represented of how the CO ratio changes according to the value of the kinetic constant. The higher the reaction rate, the more abrupt is the transition between the equilibriums. Experimentally, the

sudden changes were found at low temperatures, so the kinetic constant value is expected to be higher at these temperatures.

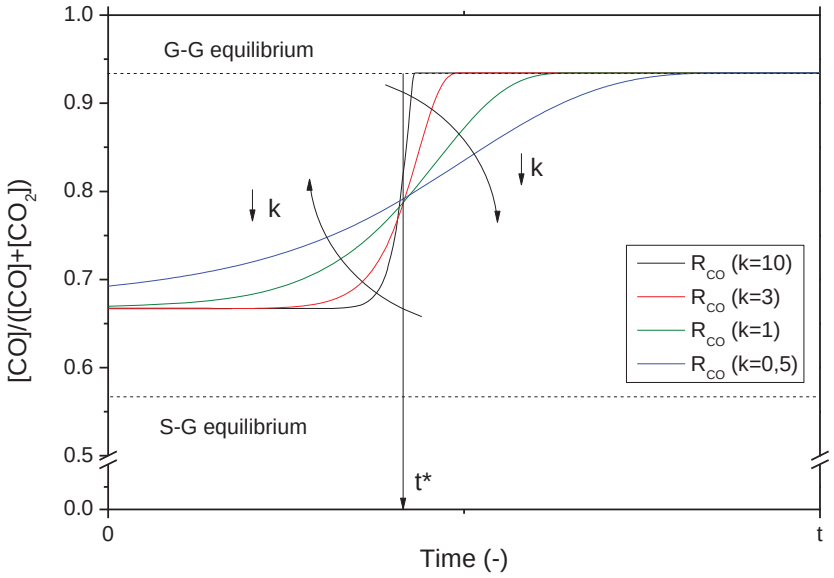

Figure 4.5 – Parametric study of the effect in the kinetic constant in the evolution of the CO ratio in the reduction.

In the fitting method an intermediate step was used that not affect in the final solution. The simulated curves of hydrogen ratio and carbon monoxide ratio were fitted to an accumulated normal distribution. Every kinetic constant from the model has associated a value of a standard deviation and this is compared to the standard deviation obtained in the packed bed results.

In the figure 4.6 there is an example of the comparison between model data and experimental data. The first reduction (stage A) is neglected because only happens during the first cycle and the fitting is focused on the stage B and stage C.

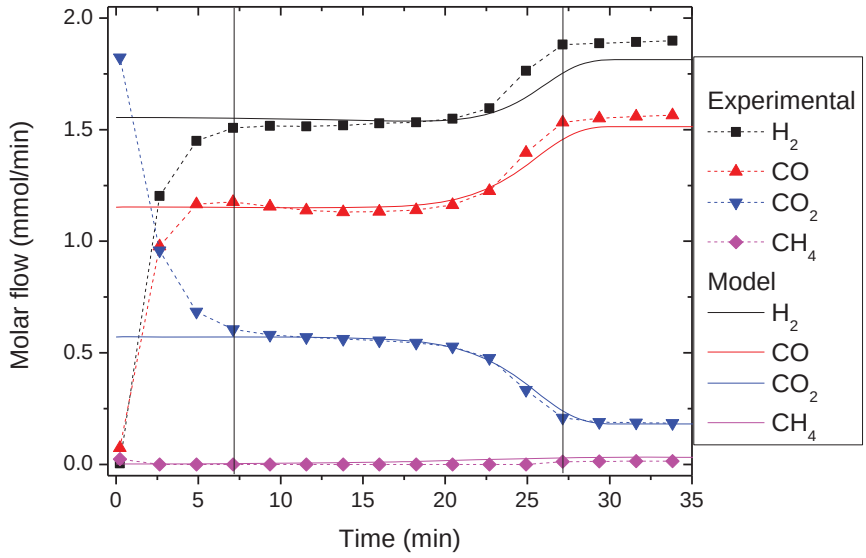

Figure 4.6 – Comparison between experimental and fitted data with acetic acid at 700 °C.

In the figure 4.7, the kinetic constants obtained are represented. Some of these values have a high uncertainty because of the low sampling frequency. The reaction that controls the process is the same for every reactant because every of them suffer the decomposition and then the reduction is done by hydrogen and carbon monoxide. The activation energy obtained from these values is negative, so it is an anti-Arrhenius behaviour. This is caused by the high thermal stress or sinterization that produces a decreasing in the reaction rate. This phenomenon is also viewed in other works (Pineau et al. 2007) (figure 4.8) in which the reduction with hydrogen is tested.

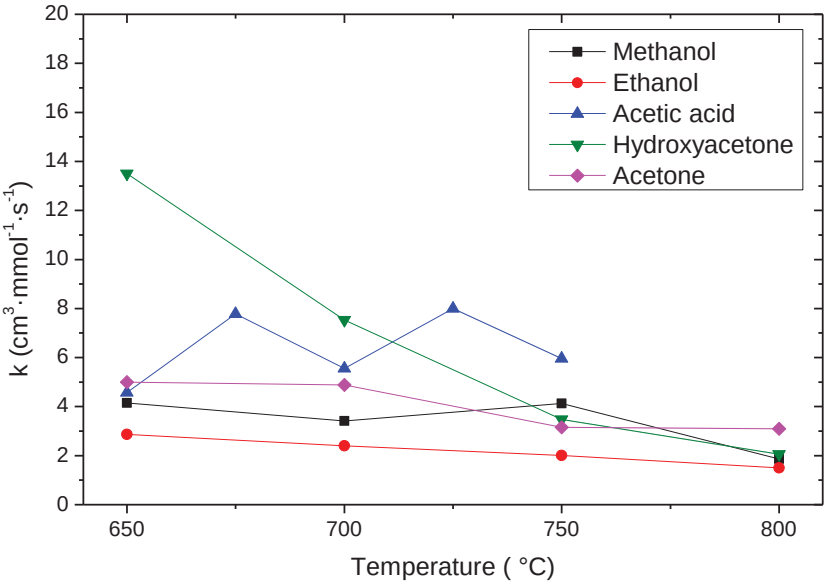

Figure 4.7 – Kinetic constants obtained for different reactants at different temperatures.

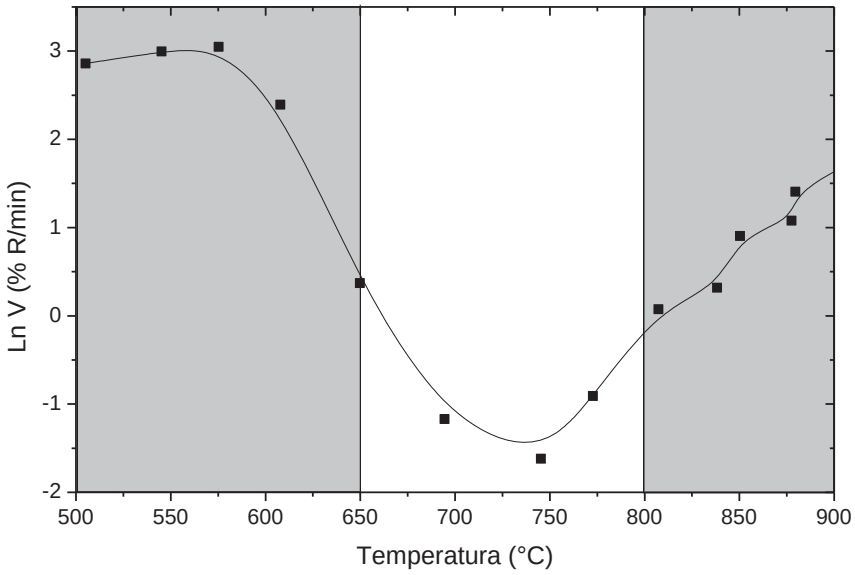

Figure 4.8 – Reaction rate in the reduction at different temperatures (Adapted from (Pineau et al. 2007)).

The observable kinetic constant is affected by two effects in the reactivity loss: one due to the temperature and another due to the time of full conversion. To quantify this loss, the kinetic constants obtained in the oxidation are used because all of them have the same operating conditions and the change in the values is according to thermal stress. The loss reactivity

coefficient of sinterization function S(c,T) is between 0 and 1 and is calculated in base to the reference of 670 °C. For the obtaining of the parameters, the acetic acids experiments are fitted and the 10 cycles with the synthetic bio-oil M#4 (figure 4.9).

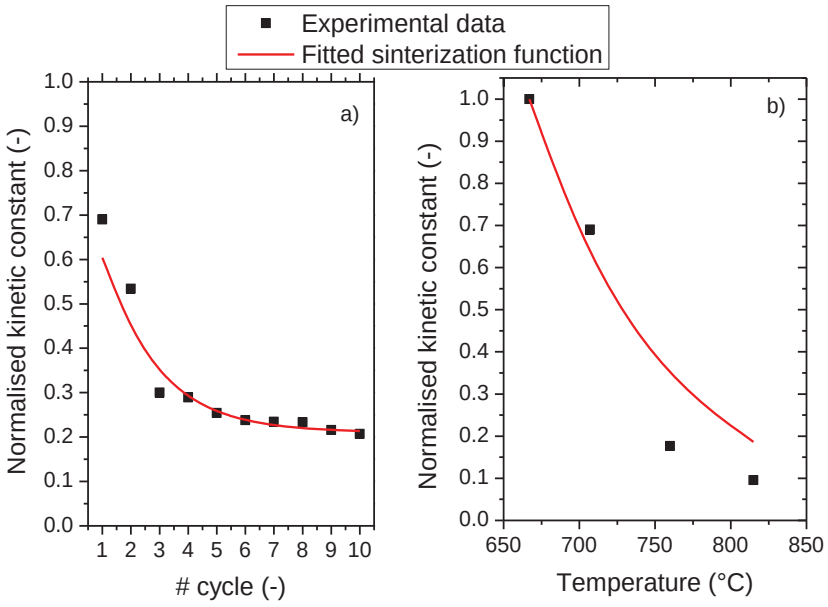

Figure 4.9 – Kinetic constants normalised depending on the temperature and the number of cycle.

The function that describes the effect of the temperature is the product of two factors and both corresponds to exponential decay. In the temperature effect, a deactivation energy is associated and in the cycle a reactivity loss constant σ (eq 4.6). There is also a residual kinetic constant observed in previous works of the group (Lorente et al. 2008; Romero et al. 2012). The values of the function are found in the table 4.2.

$$S(c,T) = \frac{k}{k_{ref}} = \left[k_{\infty} + \left(1 - k_{\infty}\right)\cdot e^{\left(-\sigma\cdot(c-1)\right)}\right]\cdot\left[e^{\frac{E_d}{R}\cdot\left(\frac{1}{T_{ref}} - \frac{1}{T}\right)}\right] \qquad \text{(eq 4.6)}$$

Table 4.2 – Values for the sinterization function.

k_∞ (-)	σ (-)	E_d (kJ/mol)	Adj-R^2
0.348±0.16	0.535±0.49	96.62±23.5	0.922

where,

k_∞ : residual kinetic constant(-)

σ : reactivity loss constant related to the number of cycle (-)

E_d : reactivity loss activation energy (kJ/mol)

4.3.5 PROCESS OPTIMIZATION

Some solutions are proposed to increase the production capacity of the process: working with recycle and optimize the cycle duration of a reduction-oxidation. Moreover, it would be necessary to study the gap found in the solid-gas equilibrium. If this is avoided, this 10% corresponds to a diminution of 35% in time of reaction.

In the basic model is possible to obtain an estimation of the global conversion respect to the reactor conversion. In the figure 4.10, the reactor with recycle scheme is represented. After the reaction, the stream pass through a condenser to eliminate the water of the stream, then the reduction capacity of the stream is recovered partially and mix with the raw material. The temperature of the condenser is a conservative 33 °C in which 5% of the water is not removed. In the figure 4.11, the conversion and the total flow is represented depending on the amount recycled. At no recycle, the base case is a hydrogen ratio difference of 16.4%. With a recycle of 60% of the outlet stream, it is possible to increase the difference to the double, 31.5%, surpassing the thermodynamic limit (recycle equals to 45%). In the other side, at higher recycle, the flow increases and the reactor could be designed under these nominal conditions and consequently the conversion would be lower than the equilibrium. In conclusion, it is necessary to find the mid-point (optimal recirculation) in which is favoured conversion and total flow.

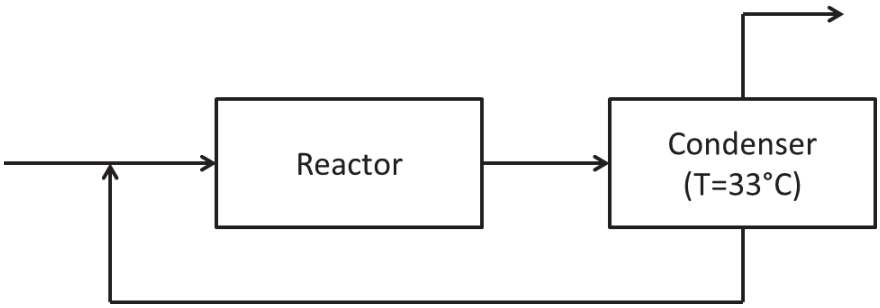

Figure 4.10 – Reactor with recycle scheme.

Other favourable effect with the recycle is that the amount of oxygen at the beginning of the reactor is increased and the carbon deposition is avoided. In this way the purity of the hydrogen is assured.

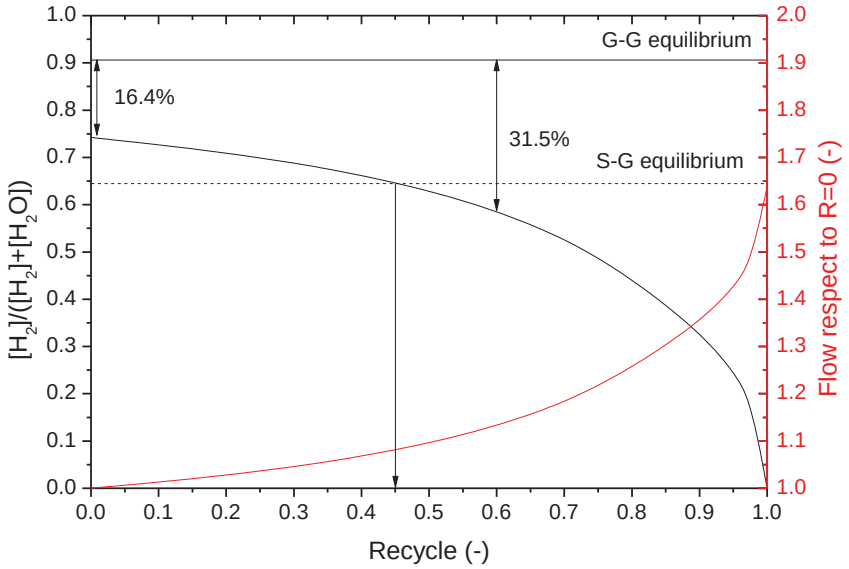

Figure 4.11 – Hydrogen ratio respect to the recycle used (black) and relative increasing in the total flow (red).

In the time cycle optimization, due to the process works in dynamic conditions, it is possible to calculate the best time to maximise the hydrogen production respect to the bio-fuel fed. Considering the basic model, the hydrogen produced is proportional to the solid oxidised and therefore is constant if full conversion is supposed. The reaction time depends on the reactant fed, so in the reduction and in the oxidation the total flow is the same. The time in the reduction is calculated as the oxygen in the sample divided by the rate of oxygen depletion of the stream, calculated as the difference between the equilibriums. The maximum value reached is 3.24 g H_2 / 100 g bio-oil This is constant during a great extension of the conversion because the conversion in the reduction during the stage B is also constant and the oxidation time is fixed at the time needed to convert all solid to Fe_3O_4 again (figure 4.12). Another variable to maximise is the lifetime of the oxygen carrier, so it should be as high as possible. The maximum value is 3.24 g H_2 / 100 g of bio-oil (composition equal to M#4+15) and corresponds to 95% of solid conversion using 87 g of Fe_3O_4. The time is 15% higher than the time obtained in the basic model (dash line in red).

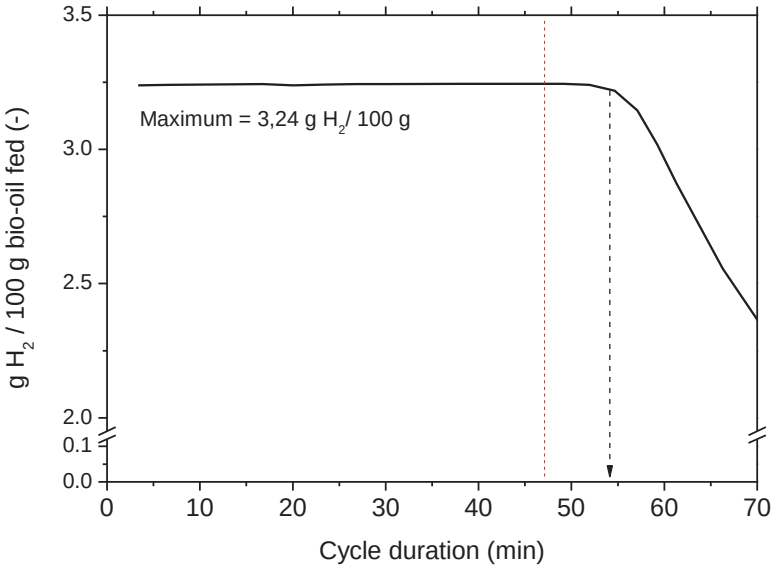

Figure 4.12 – Optimization of the cycle time maximizing the hydrogen produced and the oxygen carrier lifetime.

In the optimization of the working temperature according to the basic model, the target function would be the sum of the difference of ratios between the equilibriums. This only depends on thermodynamics and therefore the temperature. The higher the temperature, the higher the oxygen depleted from the solid and increases monotonously. As conclusion, because there is no optimal point, is preferable to work at high temperatures in which the sinterization does not affect to the reactivity loss.

4.4 MODELLING SUMMARY

There are different types of reactor modelling according to the complexity. From a basic model based on stoichiometry and equilibriums to a model that includes mass and energy balances at reactor and particle level. In this thesis, the behaviour of the reactor according to a basic model and a detailed model is explained.

From the basic model is taken some results as the reduction of Fe_3O_4 to metallic iron (stage B) lasts approximately 30 times more than the stage A, when a synthetic bio-oil is used (M#4+15). Moreover, the energy balances estimate the minimum adiabatic temperature in 542 °C in case of no dilution of solid or gas. Then, the cold spots supposition is correct and together with the water accumulation in the reaction zone could justify the separation from the solid-gas equilibrium.

After the analysis by the basic model, a detailed model build in Matlab® code is used for the study of the kinetics in the reduction and the oxidation. The main reactions are the reduction with hydrogen and carbon monoxide. The model for the kinetic equation is the shrinking core model in which the chemical reaction is the controlling step. The sampling frequency in some cases are not enough for distinguish the correct model but it is the most used equation in bibliography. The effect of the products and the observable equilibrium constants are included in the equation.

The model is validated by comparison with the work of P. Hamers (Hamers et al. 2014). The tested reaction is the oxidation of cupper in a reactor of bigger dimensions than this work. The differences found are minor and the error is less than 5%. The main cause is that the flow is not constant and it is not contemplated in the own model.

Due to the complexity of the reaction pathway and the no possibility of carry out a full study of the kinetics in thermogravimetry analysis, the packed bed results are fitted in order to obtain the kinetic constants. An intermediate step is used with the intention of obtain the values easier and faster. The hydrogen ratio and carbon monoxide ratio is fitted by cumulative normal distribution in the experimental and in the simulated curves. The standard deviations obtained are compared and associated to the kinetic constant value.

The kinetic constants obtained do not follow an Arrhenius behaviour and the reaction rate decrease with the temperature. This is due to the sinterization or thermal stress. In general, the kinetic constant has a constant value along the temperature except in the acetic acid experiments, in which the behaviour is anti-Arrhenius. Moreover, the effect of the thermal stress increases with the cycles verifying that it is cumulative.

In order to quantify the sinterization, a function was proposed from the oxidation results. Due to the experimental conditions are fixed, the variation in the kinetic constant varies according to the thermal stress suffered in the previous reduction. After 10 cycles is possible to see a residual reactivity of 30% of the reference case.

From the basic and detailed model, an optimization of the process based on the recirculation of part of the outlet stream after the condenser and other optimization in order to maximise the hydrogen production and oxygen carrier lifetime. In the recycle, there are two counter effects: at low recirculation the conversion and the total flow slightly increase, but at high recirculation, the total flow increases and there is a risk of the reactor being under nominal conditions. In the other side, the optimal cycle time corresponds to a conversion of 95% of the solid and the hydrogen production is equal to 3.24 g H_2 / 100 g bio-oil fed, using 87 g of Fe_3O_4. This is based on a maximization of hydrogen production and oxygen carrier lifetime.

5 CONCLUSIONS AND FUTURE WORK

The main conclusions according to the goals described in the first section are exposed here.

- **Obtaining of the optimal solid or mix of solids for the reduction stage of the SIP process, focused on the catalyst.**

The ideal solid mix should have a high load of oxygen carrier and the minimum amount of catalyst for the decomposition of the reactant. The most stable species is methane that is fed or appears from the decomposition. So the catalyst selected is related to the methane reforming. In this process the limiting reaction is the gradual dehydrogenation of methane. Nickel aluminate with excess of nickel oxide has been chosen as catalyst. The bulk nickel oxide was tested with unfavourable results due to the sinterization.

Two types of experiments were performed: optimization of the amount of active phase in the catalyst on the one side, and optimization of the proportion of catalyst in the mixture with oxygen carrier on the other. The oxygen carrier had already been optimised in previous works of the group, so its composition was kept "as is". The optimal load of active phase consisted of 10 wt.% of nickel oxide over the stoichiometric nickel aluminate. The proportion of catalyst in the full mixture was 15 wt.%. Despite this finding, in the packed bed reactor, the proportion used was 10 wt.% of catalyst within the solid mixture due to the fact that no loss of activity was found along the experimental runs.

- **Study of the behaviour of the optimal solid in the packed bed for the reduction with biogas**

The synthetic biogas (mixture composed of methane and carbon dioxide) needs the catalyst to carry out the dry reforming of methane. Reduction step exhibits three stages according to the role played by the solid (mix of reactive solid –iron oxide- and catalyst –nickel oxide-): reduction of Fe_2O_3 to Fe_3O_4 (stage A), followed by a reduction of Fe_3O_4 to metallic Fe (stage B) and finally the products coming from the dry reforming of methane (stage C). Along this last stage "C" the former iron oxide has completely been reduced to iron, and

only the catalyst keeps an active role. Along the early stages of the reduction there is an *in situ* activation of the catalyst by combustion of methane by lattice oxygen from nickel oxide that allows metallic nickel to emerge and favours the above mentioned dry reforming between methane and carbon dioxide.

At low temperatures, close to 600 °C, reforming does not achieve equilibrium conversions. In the rest of temperatures tested, the equilibrium is reached. In stage B, corresponding to the reduction of Fe_3O_4 to Fe, the composition of gases exiting the reactor are separated from that predicted theoretically. This deviation, calculated in terms of concentration of hydrogen respecting concentration of hydrogen and water ratio on the one side, and concentration of carbon monoxide vs carbon monoxide plus carbon dioxide ratio on the other, separate of the theoretical values in a proportion of around 10 %, being constant in the whole temperatures range.

Different proportions of CH_4/CO_2 were also tested. Carbon deposition increases at higher methane concentrations. In these cases, the shape of the temporal evolution curves does not change significantly, but the total lengths for full solid conversion decreased. The most probable scenario is that for higher methane partial pressures, methane decomposes in a higher extent producing solid carbon and hydrogen. This last would act as a vigorous reducer of the solid.

The characterization of the carbonaceous residue was measured by Raman spectroscopy. The samples were selected before and after the oxidation step. There is no appreciable change in the structure of the carbon, verifying the inert role of the carbon produced along this step.

- **Study of the behaviour of the oxygen carrier in absence of catalyst for the reduction stage with alcohols as reactant**

In comparison with the rest of reactants used in this thesis, alcohols show a higher capacity to be totally converted into products without using any catalyst. Therefore, the iron oxide works both as oxygen carrier and catalyst.

The reduction proceeds through three concatenated steps: reduction of Fe_2O_3 to Fe_3O_4 (stage A), then from Fe_3O_4 up to metallic iron (stage B). Finally Stage C accounts for products coming from the decomposition of the reactant. The final composition is related to the gas-gas equilibrium and agrees well

with the theoretical at all temperatures tested. Along the solid-gas equilibrium (stage B), the hydrogen and carbon monoxide ratios (i.e. {[H_2]/([H_2]+[H_2O]} and {[CO]/([CO]+[CO_2]}) are separated from their corresponding theoretical values in ca. 5 %.

In ethanol tests, reaction rate decreases at low temperatures because of the high amount of carbon deposited which diminishes the reactivity of the oxygen carrier.

In oxidations it is observed that at high reduction temperatures, the average conversion of steam decreases. The sinterization effect is very pronounced and the iron conversion is restricted. The hydrogen produced is of high purity due to the inert effect of the carbonaceous residue deposited in the previous stage of reduction. The concentration of carbon monoxide is assured by the instrument to be lower than 50 ppm.

The carbonaceous residue observed in TEM micrographs is shaped into carbon nanofibers of 20 and 50 nanometres. Because they are structured carbon, the stability is higher than the amorphous one and the purity of the hydrogen is verified. Structured carbon is not gasified in the oxidation experiments.

- **Study of the behaviour of the optimal solid in the reduction with model compounds and synthetic bio-oil**

The liquid reactants used with the catalyst were acetic acid, hydroxyacetone and acetone. As was the case with synthetic biogas, these need a catalyst for their total decomposition.

In the case of acetic acid, the catalyst was very important because the main product of the thermal decomposition is methane. With the optimal solid mixture, it was possible reaching the usual behaviour with the three marked stages of the reduction of Fe_2O_3. The experimental points in equilibriums correspond to the theoretical values in the gas-gas (stage C), but in the stage B, the solid-gas equilibrium, the values were separated from the theoretical ratio in ca. 9%.

The partial pressure of the reactant was varied from 5% to 15% and the values in the solid-gas equilibrium were coincident. These findings also verify that this gap is independent of the concentration of the reactant. In the gas-gas equilibrium (stage C), every initial composition has its own equilibrium

because it depends on the absolute amount of reactant. They agree against their theoretical in all cases.

The average conversion in oxidations decreases at higher reduction temperatures because of sinterization. Hydrogen produced during this step shows that there is an optimal hydrogen production between 700 and 750 °C.

Thermal decomposition of hydroxyacetone (or acetol) produced a higher number of products than alcohols. The goal of this decomposition was obtaining a high concentration of hydrogen and carbon monoxide able to reduce the oxygen carrier. Times needed for complete reduction diminished respecting to other reactants because the amount of reductants generated per mole of reactant is higher. The three stages are repeated and verified the common behaviour of the solid. In a Baurn Glaessner (BG) diagram it was corroborated that all the experimental points agreed well with previous findings: for gas-gas equilibriums they were fully coincident but for the solid-gas equilibriums, they were separated at an almost constant value of ca. 8% from the theoretically predicted values for each temperature tested.

Respecting oxidations for this reactant, it was observed that the loss of reactivity by sinterization is patent at high temperatures. In the characterization it is observed the apparition of nanofibers and/or nanotubes with both iron and nickel crystallites guiding the filaments.

Acetone followed the same pattern of three stages than the compounds described previously. The gas-gas equilibriums matched with the theoretical ones. Along solid-gas equilibriums, the experimental values were separated away around 10% from those predicted from theory. Using different concentrations in the inlet stream, the effect was identical to the previous experiments: at higher concentration of reactant, the reaction time needed for complete reduction decreases. The subsequent oxidations were identical because sintering only depends on the temperature and not on the concentration of the reactant.

In addition to the model compounds experiments, it was carried out a study with mixtures of the different fractions of the bio-oil. The composition of the synthetic bio-oil was in the range found in bibliography. The species selected were methanol, acetic acid, hydroxyacetone and water. A simple design of experiment was performed in order to minimize the number of experiments. The temperatures tested were 650, 750 and 850 °C and 6 mixtures: 3 extreme points with no water, one average mix from the three

previous mixtures and two mixtures with extra water from the average mix. At low temperatures, the carbon deposited was so high that cloged the reactor before finishing the conversion of the solid. At higher temperatures the behaviour was similar because the elemental compositions of the mixtures were close one to each other. The separation of the experimental ratios from the theoretical (stage B) was around 9% in all the cases. In the mid temperature, 750 °C, the reactant used was the average mixture. Reaction rate was high in all three stages. When the water content was tested, the higher the concentration, the longer the reduction time. This behaviour was expected since water is an oxidant and decreases the reductant capacity of the gas stream. Therefore, the content of water in the bio-oil is preferable to be as low as possible.

A high number of cycles were tested (up to 10 cycles), and the loss of reactivity was observed as quasi-linear with a value of 3% of loss of hydrogen yield per cycle. Respecting the hydrogen in the oxidations, an optimal yield was shown at mid temperature with the mixture M#4+15, that corresponded to the lowest amount of water.

- **Reactor modelling for reductions and oxidations and its dependence with operational variables**

A model has been built to explain the behaviour of reductions and oxidations of the SIP process in a packed bed reactor. It is based on an approximation by finite differences applying the Crank-Nicolson method for solving a system of partial derivative equations. A shrinking core model was selected for the kinetic equation. The model was validated from data taken from literature for the oxidation of cupper in the chemical looping combustion (CLC) process in a packed bed reactor.

The study of kinetics was carried out by fitting of data extracted from experiments performed with the fixed bed reactor. A global kinetic constant was obtained which corresponds to limiting reaction: the reduction of solid with hydrogen. This is because the reactions are in parallel and consequently the fastest reaction is controlling the pathway. The values for kinetics constants decreased along the temperature, showing an anti-Arrhenius behaviour probably related to the sinterization process suffered by the solid at high temperatures. Bibliography describes the same effect attributed to the formation of a layer of FeO that increases the resistance to the transfer of mass

through the particle layers. Sinterization was modelled by a function with double exponential decay: one for the temperature effect and another for the number of cycles. A residual kinetic constant was found that equals 30% of the reference case.

Once the model built and using the kinetics constants fitted from the experimental data, it was performed an optimization of two variables: the degree of recirculation and the length of the cycle. If the outlet stream is recycled after condensing part of the steam, the resultant stream has still a high reductant capacity. The calculations of the optimal values are fuzzy because they strongly depend on matters such as costs of the whole process. At high recycle rates, the global conversion was able to surpass the equilibrium conversion, but the total flow increased greatly and the reaction rate strongly decreased. In the case of cycle length, it was found that the optimal value, in which the hydrogen production and the lifetime of the oxygen carrier are maximised, corresponded to a conversion of the solid of ca. 95%. The production was 3.24 g H_2 per 100 g of bio-oil (M#4+15) using 87 g of Fe_3O_4.

5.1 FUTURE WORK

Different works can be proposed in order to enhance the study in a near future:

The kinetics proposed could enhance the accuracy and the suitable experiments should be carried out by thermogravimetry analysis with a mixture of gases close to that found for the decomposition of the reactants. Moreover, it is possible to extend to a higher concentration of oxidants in order to approach the hypothetical diffusional restrictions. The reaction equation would be fitted to a kinetic equation of the *Langmuir-Hinshelwood-Hougen-Watson* (LHHW) type.

Regarding fitting of data for the packed bed reactor, the operational variables should be varied. For example, the spatial time and the concentration of reactants are crucial. Moreover, it would be mandatory a high sampling frequency in the analysis of gases coming out from the reactor in order to discern the correct model.

The scale used is only few grams and a scaling up provides a vision closer to the real application. Furthermore, it would be necessary a new oxygen carrier based on iron with optimised amounts of dopants that provides higher resistance to thermal stress. Another reactant to be tested should be a real bio-oil. Consequently the configuration of the setup should change in order to feed directly inside the reactor by spraying it. Another variable to test would be the quantity of water in the bio-oil. It is expected that this variable plays an essential role for avoiding carbon deposition and allows working at a higher number of cycles.

Using bigger packed bed reactors, the gradients of temperature and concentration are increased and the model of the reactor is not enough to explain the behaviour of the gases. Additionally, the energy balances should be implemented in the code and experimentally, the temperature profile should be measured by thermocouples along the reactor.

Regarding to the full process (economic scenario), usually the sink of costs and efficiency are the evaporation and the condensation of water. It is recommended to obtain a conversion close to the equilibrium in order to diminish the losses and the price of the hydrogen produced.

REFERENCES

Adanez J, Abad A, Garcia-Labiano F, Gayan P, de Diego LF. "Progress in Chemical-Looping Combustion and Reforming technologies". Prog Energy Combust Sci. (2012);38(2):215–82.

Alifanti M, Baps B, Blangenois N, Naud J, Grange P, Delmon B. "Characterization of CeO_2-ZrO_2 mixed oxides. Comparison of the citrate and sol-gel preparation methods". Chem Mater. ACS Publications; (2003);15(2):395–403.

Al-Ubaid A, Wolf EE. "Steam reforming of methane on reduced non-stoichiometric nickel aluminate catalysts". Appl Catal. (1988);40:73–85.

Ashrafi M, Pfeifer C, Pröll T, Hofbauer H. "Experimental study of model biogas catalytic steam reforming: 2. Impact of sulfur on the deactivation and regeneration of Ni-based catalysts". Energy & Fuels. ACS Publications; (2008);22(6):4190–5.

Bartholomew CH. "Carbon Deposition in Steam Reforming and Methanation". Catal Rev. Taylor & Francis Group; (2007);24(1):67–112.

Baur E, Glaessner A. "Gleichgewicht der Eisenoxide mit Kohlenoxid und Kohlensaure". Z phys Chemie. (1903);43:354–68.

Berenguer J. "Estudio preliminar de la producción de hidrógeno a partir de biogás en reactor de lecho fijo". Universidad de Zaragoza; 2011.

Berndes G, Hoogwijk M, van den Broek R. "The contribution of biomass in the future global energy supply: a review of 17 studies". Biomass and Bioenergy. (2003);25(1):1–28.

Bertero M, de la Puente G, Sedran U. "Fuels from bio-oils: Bio-oil production from different residual sources, characterization and thermal conditioning". Fuel. (2012);95:263–71.

Bimbela F. "Catalytic steam reforming of model compounds of the aqueous fraction of biomass pyrolysis liquids in fixed bed". Universidad de Zaragoza; 2009.

Bleeker MF, Kersten SRA, Veringa HJ. "Pure hydrogen from pyrolysis oil using the steam-iron process". Catal Today. (2007);127(1-4):278–90.

Bleeker MF, Veringa HJ, Kersten SRA. "Deactivation of iron oxide used in the steam-iron process to produce hydrogen". Appl Catal A Gen. (2009);357(1):5–17.

Bridgwater AV. "Review of fast pyrolysis of biomass and product upgrading". Biomass and Bioenergy. (2012);38:68–94.

Campos D. "Producción de hidrógeno a partir de biogás mediante reformado seco de metano y "steam-iron". Influencia de la composición del sólido y

las variables de operación". Universidad de Zaragoza; 2011.

Carazo E. "Obtención de hidrogeno en un reactor de lecho fluidizado con circulación interna (ICFBR) mediante separación de mezclas H_2/CH_4". Universidad de Zaragoza; 2008.

Chen D, Christensen K, Ochoa Fernández E, Yu Z, Totdal B, Latorre N, et al. "Synthesis of carbon nanofibers: effects of Ni crystal size during methane decomposition". J Catal. (2005);229(1):82–96.

Crank J, Nicolson P. "A practical method for numerical evaluation of solutions of partial differential equations of the heat-conduction type". Math Proc Cambridge Philos Soc. Cambridge Univ Press; 1947. p. 50–67.

Czernik S, Bridgwater A V. "Overview of applications of biomass fast pyrolysis oil". Energy & Fuels. ACS Publications; (2004);18(2):590–8.

Darken LS, Gurry RW. "The System Iron-Oxygen. I. The Wüstite Field and Related Equilibria". J Am Chem Soc. American Chemical Society; (1945);67(8):1398–412.

Darken LS, Gurry RW. "The System Iron—Oxygen. II. Equilibrium and Thermodynamics of Liquid Oxide and Other Phases". J Am Chem Soc. American Chemical Society; (1946);68(5):798–816.

Durán P. "Separación y almacenamiento de hidrógeno por procesos redox en reactor de lecho fijo". Universidad de Zaragoza; 2016.

Edwards MF, Richardson JF. "The correlation of axial dispersion data". Can J Chem Eng. Wiley Online Library; (1970);48(4):466–7.

EIA US. "International Energy Outlook 2013 with Projections to 2040". Washington, US. (2013);

Escuer M. "Proceso "steam-iron". Estudio de estabilidad de sólidos redox con capacidades mejoradas". Universidad de Zaragoza; 2008.

Fan M, Abdullah AZ, Bhatia S. "Catalytic technology for carbon dioxide reforming of methane to synthesis gas". ChemCatChem. Wiley Online Library; (2009);1(2):192–208.

Galdámez JR, García L, Bilbao R. "Hydrogen Production by Steam Reforming of Bio-Oil Using Coprecipitated Ni−Al Catalysts. Acetic Acid as a Model Compound". Energy & Fuels. American Chemical Society; (2005);19(3):1133–42.

Gayán P, de Diego LF, García-Labiano F, Adánez J, Abad A, Dueso C. "Effect of support on reactivity and selectivity of Ni-based oxygen carriers for chemical-looping combustion". Fuel. (2008);87(12):2641–50.

Gil M V., Fermoso J, Pevida C, Chen D, Rubiera F. "Production of fuel-cell grade H2 by sorption enhanced steam reforming of acetic acid as a model compound of biomass-derived bio-oil". Appl Catal B Environ. (2015);

Gómez A, Zubizarreta J, Dopazo C, Fueyo N. "Spanish energy roadmap to

2020: Socioeconomic implications of renewable targets". Energy. (2011);36(4):1973–85.

Graça I, Ribeiro FR, Cerqueira HS, Lam YL, de Almeida MBB. "Catalytic cracking of mixtures of model bio-oil compounds and gasoil". Appl Catal B Environ. (2009);90(3-4):556–63.

Gupta CK. "Chemical metallurgy: principles and practice". John Wiley & Sons; 2006.

Hacker V, Fankhauser R, Faleschini G, Fuchs H, Friedrich K, Muhr M, et al. "Hydrogen production by steam–iron process". J Power Sources. (2000);86(1-2):531–5.

Hamers HP, Gallucci F, Cobden PD, Kimball E, Van Sint Annaland M. "CLC in packed beds using syngas and CuO/Al_2O_3: Model description and experimental validation". Appl Energy. Elsevier Ltd; (2014);119:163–72.

Herguido J, Peña JA, Carazo E. "Experimental assessment of hydrogen separation from H_2/CH_4 mixtures by the "steam-iron process" in an interconnected circulating fluidized bed reactor". Int J Hydrogen Energy. (2014);39(26):14050–60.

Hernandez Martinez F. "Efectos del incremento del precio del petróleo en la economía española: Análisis de cointegración y de la política monetaria mediante reglas de Taylor". (2009);

Hock H, Lang S. "Autoxydation von Kohlenwasserstoffen, IX. Mitteil.: Über Peroxyde von Benzol-Derivaten". Berichte der Dtsch Chem Gesellschaft (A B Ser. (1944);77(3-4):257–64.

Hu X, Lu G. "Investigation of steam reforming of acetic acid to hydrogen over Ni–Co metal catalyst". J Mol Catal A Chem. (2007);261(1):43–8.

Ingram L, Mohan D, Bricka M, Steele P, Strobel D, Crocker D, et al. "Pyrolysis of wood and bark in an auger reactor: physical properties and chemical analysis of the produced bio-oils". Energy & Fuels. ACS Publications; (2007);22(1):614–25.

Jerndal E, Mattisson T, Lyngfelt A. "Thermal Analysis of Chemical-Looping Combustion". Chem Eng Res Des. (2006);84(9):795–806.

Jozwiak WK, Kaczmarek E, Maniecki TP, Ignaczak W, Maniukiewicz W. "Reduction behavior of iron oxides in hydrogen and carbon monoxide atmospheres". Appl Catal A Gen. (2007);326(1):17–27.

Kim S, Dale BE. "Global potential bioethanol production from wasted crops and crop residues". Biomass and Bioenergy. (2004);26(4):361–75.

Kirchnerova J, Alifanti M, Delmon B. "Evidence of phase cooperation in the $LaCoO_3$–CeO_2–Co_3O_4 catalytic system in relation to activity in methane combustion". Appl Catal A Gen. (2002);231(1-2):65–80.

Leng S, Wang X, He X, Liu L, Liu Y, Zhong X, et al. "NiFe/γ-Al2O3: A universal catalyst for the hydrodeoxygenation of bio-oil and its model

compounds". Catal Commun. (2013);41:34–7.

Levenspiel O. "Chemical reaction engineering". Ind Eng Chem Res. ACS Publications; (1999);38(11):4140–3.

Li X, Wang S, Zhu Y, Yang G, Zheng P. "DFT study of bio-oil decomposition mechanism on a Co stepped surface: Acetic acid as a model compound". Int J Hydrogen Energy. (2015);40(1):330–9.

Li Y, Li D, Wang G. "Methane decomposition to COx-free hydrogen and nano-carbon material on group 8–10 base metal catalysts: A review". Catal Today. (2011);162(1):1–48.

Lorente E. "Estudio de sólidos con propiedades redox en aplicaciondes de aprovechamiento de hidrógeno". Universidad de Zaragoza; 2008.

Lorente E, Peña JA, Herguido J. "Kinetic study of the redox process for separating and storing hydrogen: Oxidation stage and ageing of solid". Int J Hydrogen Energy. (2008);33(2):615–26.

Lorente E, Peña JA, Herguido J. "Separation and storage of hydrogen by steam-iron process: Effect of added metals upon hydrogen release and solid stability". J Power Sources. (2009);192(1):224–9.

McDowall W. "Technology roadmaps for transition management: The case of hydrogen energy". Technol Forecast Soc Change. Elsevier; (2012);79(3):530–42.

Messerschmitt A. "Process of producing hydrogen". U. S.: Google Patents; 1910.

Mohan D, Pittman CU, Steele PH. "Pyrolysis of wood/biomass for bio-oil: a critical review". Energy & Fuels. ACS Publications; (2006);20(3):848–89.

Moulijn J., van Diepen A., Kapteijn F. "Catalyst deactivation: is it predictable?". Appl Catal A Gen. (2001);212(1-2):3–16.

Nestl S, Voitic G, Lammer M, Marius B, Wagner J, Hacker V. "The production of pure pressurised hydrogen by the reformer-steam iron process in a fixed bed reactor system". J Power Sources. (2015);280:57–65.

Noorman S, van Sint Annaland M. "Packed Bed Reactor Technology for Chemical-Looping Combustion". Ind Eng Chem Res. American Chemical Society; (2007);46(12):4212–20.

Oasmaa A, Meier D. "Norms and standards for fast pyrolysis liquids". J Anal Appl Pyrolysis. (2005);73(2):323–34.

Otsuka K, Kaburagi T, Yamada C, Takenaka S. "Chemical storage of hydrogen by modified iron oxides". J Power Sources. (2003a);122(2):111–21.

Otsuka K, Yamada C, Kaburagi T, Takenaka S. "Hydrogen storage and production by redox of iron oxide for polymer electrolyte fuel cell vehicles". Int J Hydrogen Energy. (2003b);28(3):335–42.

Pans MA, Gayán P, Abad A, García-Labiano F, de Diego LF, Adánez J. "Use of

chemically and physically mixed iron and nickel oxides as oxygen carriers for gas combustion in a CLC process". Fuel Process Technol. (2013);115:152–63.

Perry RH, Green DW. "Chemical engineers' handbook". McGraw-Hill Education; 2007.

Pineau A, Kanari N, Gaballah I. "Kinetics of reduction of iron oxides by H2". Thermochim Acta. (2007);456(2):75–88.

Piotrowski K, Mondal K, Lorethova H, Stonawski L, Szymanski T, Wiltowski T. "Effect of gas composition on the kinetics of iron oxide reduction in a hydrogen production process". Int J Hydrogen Energy. (2005);30(15):1543–54.

Plou J. "Selección de sólidos destinados a la producción de hidrógeno de alta pureza a partir de biogás por combinación de reformado seco y "steam-iron"". Universidad de Zaragoza; 2011.

Plou J, Duran P, Herguido J, Peña JA. "Steam-iron process kinetic model using integral data regression". Int J Hydrogen Energy. (2012);37(8):6995–7004.

Ramachandran R, Dao LH. "Hydration of ethene to form ethanol, adsorption of unreacted ethene then desorption". Google Patents; 1996.

Redl FX, Black CT, Papaefthymiou GC, Sandstrom RL, Yin M, Zeng H, et al. "Magnetic, electronic, and structural characterization of nonstoichiometric iron oxides at the nanoscale.". J Am Chem Soc. American Chemical Society; (2004);126(44):14583–99.

Remón J, Broust F, Volle G, García L, Arauzo J. "Hydrogen production from pine and poplar bio-oils by catalytic steam reforming. Influence of the bio-oil composition on the process". Int J Hydrogen Energy. (2015);40(16):5593–608.

Rioche C, Kulkarni S, Meunier FC, Breen JP, Burch R. "Steam reforming of model compounds and fast pyrolysis bio-oil on supported noble metal catalysts". Appl Catal B Environ. (2005);61(1-2):130–9.

Romero E, Soto R, Durán P, Herguido J, Peña JA. "Molybdenum addition to modified iron oxides for improving hydrogen separation in fixed bed by redox processes". Int J Hydrogen Energy. (2012);37(8):6978–84.

Rydén M, Arjmand M. "Continuous hydrogen production via the steam–iron reaction by chemical looping in a circulating fluidized-bed reactor". Int J Hydrogen Energy. (2012);37(6):4843–54.

Sanz A, Nieva D, Dufour J. "Steam-Iron process as an alternative to Water Gas Shift reaction in biomass gasification". Int J Hydrogen Energy. (2015);

Smit J, van Sint Annaland M, Kuipers JAM. "Grid adaptation with WENO schemes for non-uniform grids to solve convection-dominated partial differential equations". Chem Eng Sci. (2005);60(10):2609–19.

Spivey JJ, Egbebi A. "Heterogeneous catalytic synthesis of ethanol from

biomass-derived syngas.". Chem Soc Rev. Royal Society of Chemistry; (2007);36(9):1514–28.

van Steen E, Claeys M. "Fischer-Tropsch Catalysts for the Biomass-to-Liquid (BTL)-Process". Chem Eng Technol. (2008);31(5):655–66.

Takanabe K, Aika K, Seshan K, Lefferts L. "Sustainable hydrogen from bio-oil—Steam reforming of acetic acid as a model oxygenate". J Catal. (2004);227(1):101–8.

Takenaka S, Kaburagi T, Yamada C, Nomura K, Otsuka K. "Storage and supply of hydrogen by means of the redox of the iron oxides modified with Mo and Rh species". J Catal. (2004);228(1):66–74.

Thaler M, Hacker V. "Storage and separation of hydrogen with the metal steam process". Int J Hydrogen Energy. (2012);37(3):2800–6.

Tiemersma TP. "Integrated autothermal reactor concepts for oxidative coupling and reforming of methane". University of Twente; 2010.

Tijmensen M. "Exploration of the possibilities for production of Fischer Tropsch liquids and power via biomass gasification". Biomass and Bioenergy. (2002);23(2):129–52.

Tokuda M, Yoshikoshi H, Ohtani M. "Kinetics of the Reduction of Fe Ore". Trans Iron Steel Inst Jap. (1973);13(5):350–63.

Trane R, Dahl S, Skjøth-Rasmussen MS, Jensen AD. "Catalytic steam reforming of bio-oil". Int J Hydrogen Energy. (2012);37(8):6447–72.

Turner P, Taylor S, Clarke E, Harwood C, Cooke K, Frampton H. "Calibration effects during natural gas analysis using a quadrupole mass spectrometer". TrAC Trends Anal Chem. (2004);23(4):281–7.

Vagia E, Lemonidou A. "Thermodynamic analysis of hydrogen production via steam reforming of selected components of aqueous bio-oil fraction". Int J Hydrogen Energy. (2007);32(2):212–23.

Vagia EC, Lemonidou AA. "Hydrogen production via steam reforming of bio-oil components over calcium aluminate supported nickel and noble metal catalysts". Appl Catal A Gen. (2008);351(1):111–21.

Vane LM. "A review of pervaporation for product recovery from biomass fermentation processes". J Chem Technol Biotechnol. (2005);80(6):603–29.

Verykios X. "Catalytic dry reforming of natural gas for the production of chemicals and hydrogen". Int J Hydrogen Energy. (2003);28(10):1045–63.

Wang D, Montané D, Chornet E. "Catalytic steam reforming of biomass-derived oxygenates: acetic acid and hydroxyacetaldehyde". Appl Catal A Gen. (1996);143(2):245–70.

Wang S. "A Comprehensive Study on Carbon Dioxide Reforming of Methane over Ni/γ-Al_2O_3 Catalysts". Ind Eng Chem Res. American Chemical Society; (1999);38(7):2615–25.

Wang S, Li X, Zhang F, Cai Q, Wang Y, Luo Z. "Bio-oil catalytic reforming without steam addition: Application to hydrogen production and studies on its mechanism". Int J Hydrogen Energy. (2013);38(36):16038–47.

Wang S, Zhang F, Cai Q, Li X, Zhu L, Wang Q, et al. "Catalytic steam reforming of bio-oil model compounds for hydrogen production over coal ash supported Ni catalyst". Int J Hydrogen Energy. (2014);39(5):2018–25.

Westerhof RJM, Brilman DWF, Garcia-Perez M, Wang Z, Oudenhoven SRG, van Swaaij WPM, et al. "Fractional condensation of biomass pyrolysis vapors". Energy & Fuels. ACS Publications; (2011);25(4):1817–29.

Wu C, Liu R. "Carbon deposition behavior in steam reforming of bio-oil model compound for hydrogen production". Int J Hydrogen Energy. (2010);35(14):7386–98.

Xie J, Su D, Yin X, Wu C, Zhu J. "Thermodynamic analysis of aqueous phase reforming of three model compounds in bio-oil for hydrogen production". Int J Hydrogen Energy. (2011);36(24):15561–72.

Zhang Z-J, Sui S-J, Tan S, Wang Q-W, Pittman CU. "Catalytic conversion of bio-oil to oxygen-containing fuels by simultaneous reactions with 1-butanol and 1-octene over solid acids: Model compound studies and reaction pathways.". Bioresour Technol. (2013);130:789–92.

WEB REFERENCES

[web 1] Energy Department of USA

(http://www.energy.gov/)

[web 2] Seventh Framework Programme for Research

(http://ec.europa.eu/programmes/horizon2020/)

[web 3] Promoting the production and utilization of energy crops at European level (ENCROP)

(http://ec.europa.eu/energy/intelligent/projects/en/projects/encrop)

APPENDIX

This PhD. dissertation is presented as paper compendium. The articles that comprise the study are:

I. J. Plou, P. Durán, J. Herguido, J.A. Peña. "Purified hydrogen from synthetic biogas by joint methane dry reforming and steam-iron process: Behaviour of metallic oxides and coke formation". Fuel, 118 (2014) 100-106.
II. J. Plou, P. Durán, J. Herguido, J.A. Peña. "Hydrogen from synthetic biogas by catalyzed MDR and SIP: Screening of catalyst and iron oxide mixtures". Fuel, 140 (2015) 470-476.
III. M. Herrer, J. Plou, P. Durán, J. Herguido, J.A. Peña. "Hydrogen from synthetic biogas via SIP using $NiAl_2O_4$ catalyst: Reduction stage". International Journal of Hydrogen Energy, 40 (2015) 5244-5250.
IV. R. Campo, J. Plou, P. Durán, J. Herguido, J.A. Peña. "Combined production and purification of hydrogen from methanol using steam iron process in fixed bed reactor". Journal of Power Sources, 242 (2013) 520-526.
V. E. Hormilleja, J. Plou, P. Durán, J. Herguido, J.A. Peña. "Hydrogen from ethanol by steam iron process in fixed bed reactor". International Journal of Hydrogen Energy, 39 (2014) 5267-5273.
VI. J. Plou, P. Durán, J. Herguido, J.A. Peña. "Steam-iron process kinetic model using integral data regression". International Journal of Hydrogen Energy, 37 (2012) 6995-7004.

Moreover, congress communications have been included in order to complete the details that the papers do not cover. The full abstracts presented are:

I. J. Lachén, J. Plou, P. Durán, J. Herguido, J. A. Peña. "High-purity hydrogen from acidic fractions of bio-oil by "steam-iron". European Hydrogen Energy Conference 2014 (EHEC 2014), Sevilla (España).

II. J. Plou, P. Durán, J. Herguido, J. A. Peña. "Producción de hidrógeno a partir de bio-oil sintético mediante el proceso "steam-iron". Congreso Iberoamericano de Hidrógeno y Pilas de Combustible 2014 (Iberconappice 2014), Barcelona (España).

III. J. Plou, P. Durán, J. Herguido, J. A. Peña. "Hydrogen production from bio-fuel using the "steam-iron" process: Model and kinetics". Hydrogen Power Theoretical and Engineering Solutions International Symposium 2015 (Hypothesis 2015), Toledo (España).